



The University of
Nottingham

**School of Pharmacy - Centre for Doctoral Training in Targeted
Therapeutics**

**Kinetics of Inhaled Antibodies
by Gamma Scintigraphy**

Catherine Pereira

**Thesis submitted to the University of Nottingham for the degree of
Doctor of Philosophy**

September 2012

ABSTRACT

Inhalation represents a potentially attractive delivery route for biologics, especially those designed to treat pulmonary diseases such as asthma, cystic fibrosis or lung cancer. Delivery directly to the site of action should increase local concentrations of drug, whilst reducing systemic side effects. However, there is limited knowledge regarding the mechanisms of pulmonary clearance, with gaps in understanding; where molecules are absorbed, the mechanisms involved, regional variability throughout the lung, and how to control pulmonary retention and/or facilitate cellular uptake.

The work presented in this thesis details the development of a SPECT/CT imaging protocol to determine the pulmonary retention and tissue redistribution of technetium labelled antibodies and their fragments *in vivo*, in mice, to begin to address these knowledge gaps.

The SPECT/CT imaging method was applied to a whole monoclonal murine immunoglobulin G1 (mIgG1), as well as its Fab and scFv fragments and a small protein (FN3) in order to determine whether diffusion controlled pathways were important in pulmonary antibody clearance. Additionally, the pulmonary retention of mutant mIgG1 with differing binding affinities to the murine neonatal Fc receptor (mFcRn)

were assessed in order to determine whether antibody transport across the epithelium occurred via active transcytosis.

It was determined that 54.4 ± 0.63 % of the total instilled dose of a whole monoclonal antibody remains in the lung over 24 hrs, with Fab and scFv fragments cleared significantly quicker with 28.7 ± 0.73 % and 34.9 ± 0.85 % respectively of the total instilled dose remaining in the lung at 24hrs. The pulmonary retention of the 11 kDa FN3 protein was also assessed with 21.0 ± 0.65 % remaining in the lungs after 24 hrs. No evidence of build up of any protein was detected in the oesophagus/stomach, suggesting little contribution by mucociliary clearance. Very little build up of whole antibody, Fab or scFv was observed in the liver or kidneys. However, very clear evidence of renal filtration of the 11 kDa fragment was observed. There was no difference in the pulmonary retention of wild type IgG and any of the mFcRn binding mutants.

Additional investigation of antibody retention rates in the murine house dustmite (HDM) model of asthma, although not making use of the SPECT/CT method, showed that antibody is cleared more rapidly from the diseased lung than the normal lung. It was also shown that the expression pattern of the mFcRn receptor is the same in the normal and HDM exposed lung and so this increase in clearance rate occurs via passive diffusion controlled processes. This is most likely a result of

increased paracellular transport due to disrupted mucosal barrier function.

The SPECT/CT imaging method developed has proven to be a simple and reliable method to assess, non-invasively, pulmonary antibody retention *in vivo*. Overall it appears that antibody transport across the pulmonary epithelium occurs predominantly via diffusion controlled mechanisms, which include both paracellular transport and non-specific transcytosis by pinocytotic routes. Additionally, in the mouse, neither receptor mediated transport by mFcRn nor mucocillary clearance is important in the pulmonary clearance of antibodies.

ACKNOWLEDGEMENTS

I would like to thank my supervisors Prof. David Pritchard, Dr Simon Young and Dr Carl Webster for their support and guidance throughout this project.

I also wish to acknowledge the University of Nottingham Centre for Doctoral Training in Targeted Therapeutics, AstraZeneca, MedImmune and the EPSRC for providing the funding for this work.

I would like to extend special thanks to the AstraZeneca and MedImmune based groups with which I worked to complete this research. My thanks especially go out to Susan Fowler, Susanne Witt, Ian Wilkinson, Nicki Davies and Matt Bell from MedImmune; as well as Steve Jordan, Katharine Wiley, Annie Clark, Sally-Ann Rickets, Juliana Maynard, Gary Parker, Neil Gingles and Heather Keen from AZ.

Finally I would like to thank my friends and family, especially my husband Igor, for their support and patience during the whole of this PhD, particularly during the write-up period.

CONTENTS

ABSTRACT	I
ACKNOWLEDGEMENTS	IV
CONTENTS	V
LIST OF FIGURES	XII
LIST OF ABBREVIATIONS	XXI
CHAPTER 1: GENERAL INTRODUCTION AND LITERATURE REVIEW	1
1. Project Overview	1
1.1 Delivery of Biologics	1
1.2 Research into non-invasive delivery of biologics	3
1.3 The lung	6
1.3.1 Structure of the human lung	6
1.3.2 Pulmonary epithelium	8
1.3.3 Tight junctions	10
1.4 Pulmonary delivery of biologics	12
1.5 Crossing pulmonary epithelium	14
1.5.1 Paracellular transport	16
1.5.2 Non-specific transcytosis	19
1.5.3 Receptor mediated transcytosis	21
1.5.4 FcRn Expression and activity in the lung	25

1.5.5 Importance of the location of the site of action	26
1.6 Conclusions from the literature regarding pulmonary clearance of proteins	27
1.7 Investigating inhalation as a potential delivery route for antibodies	28
1.8 Animal models of lung disease	29
1.8.1 Mouse models of asthma	30
1.8.2 Acute mouse models.	30
1.8.3 Chronic mouse models	32
1.8.4 Strain differences	33
1.9 Imaging pulmonary antibody clearance <i>in vivo</i>	34
1.9.1 SPECT/CT	34
1.9.2 SPECT imaging	36
1.9.3 CT Imaging in small animal models of asthma	38
1.10 Aims and Objectives	40
1.11 Thesis structure	42
CHAPTER 2: PRODUCTION OF REAGENTS FOR USE IN THE <i>IN VIVO</i> IMAGING EXPERIMENTS	43
2. Overview	43
2.1 Introduction	44
2.1.1 Investigation of passive diffusion as a transport mechanism for the pulmonary clearance of antibodies	44
2.1.2 Investigation of transcytosis by mFcRn as a mechanism for the pulmonary clearance of antibodies	46

2.2	Materials and methods	48
2.2.1	Materials	48
2.2.2	Methods	49
2.2.2.1	Preparation of DNA for transfection and/or SDM	49
2.2.2.2	Site directed mutagenesis	51
2.2.2.3	CHO cell expression of proteins	52
2.2.2.4	Bacterial expression of the FN3 protein	54
2.2.3	Purification	55
2.2.3.1	Protein A affinity chromatography	55
2.2.3.2	Nickel affinity Chromatography	56
2.2.3.3	Size exclusion chromatography	56
2.2.4	SDS-PAGE	57
2.2.5	Endotoxin removal using a polymixin B – agarose column	57
2.2.6	Endotoxin testing	57
2.2.7	Octet experiments to determine binding affinities of whole IgG mutants to mFcRn	59
2.3	Results and Discussion	60
2.3.1	Protein expression	61
2.3.1.1	Expression and purification of the Fab fragment	61
2.3.1.2	Expression of the scFv fragment	66
2.3.1.3	Expression and purification of FN3 protein	70
2.3.2	Production and testing of mutant IgG with differing binding affinities to the mFcRn receptor.	74
2.3.2.1	Expression and purification of the H435A mutant	74
2.3.2.2	Expression and purification of the IgG V250Q mutant	78

2.3.2.3 Expression and purification of the H435A_I253A double mutant	81
2.3.3 Assessment of the levels of mFcRn binding of the whole IgG mutants	84
2.4 Conclusion	88
CHAPTER 3: SET UP AND VALIDATION OF <i>IN VIVO</i> IMAGING EXPERIMENTS	89
3. Overview	89
3.1 Introduction	89
3.2 Materials and Methods	91
3.2.1 Materials	91
3.2.2 Methods	91
3.2.2.1 Reduction of antibody and fragments	91
3.2.2.2 Ellman's Assay	91
3.2.2.3 Production of the final conjugate	92
3.2.2.4 Thin layer chromatography	93
3.2.2.5 Measurement of sample activity in the well counter	95
3.2.2.6 ELISA – to detect mIgG1	95
3.2.2.7 Imaging on the planar gamma camera	97
3.2.2.8 Comparison of pulmonary transport of labelled vs. unlabelled antibody after intratracheal instillation.	98
3.3 Results and Discussion	99
3.3.1 Validation of labelling chemistry with Ellman's reagent and TLC	99

3.3.2 Experiments to validate the stability of the labelled antibody <i>in vivo</i>	102
3.3.3 Comparison of detection of construct in same plasma samples by ELISA or radioactivity measurements.	108
3.3.4 Detection of known concentrations of IgG and ^{99m} Tc labelled IgG by ELISA to determine whether presence of label affects conformation	110
3.3.5 Experiments to confirm whether the presence of the technetium label affects antibody transport out of the lung	112
3.4 Conclusions	114
CHAPTER 4: IMAGING PULMONARY ANTIBODY CLEARANCE	115
4. Overview	115
4.1 Introduction	115
4.1.1 SPECT/CT imaging	116
4.2 Materials and Methods	117
4.2.1 Materials	117
4.2.2 Methods	118
4.2.2.1 Statement of ethics for <i>in vivo</i> studies	118
4.2.2.2 SPECT/CT imaging protocol	118
4.2.2.3 Image processing and fusion	119
4.2.2.4 Histopathological measurement of mFcRn expression in healthy BALB/c mouse lung	120
4.3 Results and Discussion	122
4.3.1 Pulmonary clearance of a whole IgG	122

4.3.2 Pulmonary clearance of antibody fragments and the FN3 protein	128
4.3.3 Pulmonary retention of mutant mIgG with differing binding affinities to mFcRn	135
4.3.4 Immunohistochemical analysis of the expression of mFcRn in the normal mouse lung	138
4.4 Conclusion	140
CHAPTER 5: FURTHER CHARACTERISATION OF AND INVESTIGATION OF PULMONARY ANTIBODY CLEARANCE IN A MURINE HOUSE DUST MITE MODEL OF ASTHMA	141
5. Overview	141
5.1 Introduction	141
5.1.1 _ Affect of the diseased lung on antibody transport	143
5.2 Materials and methods	143
5.2.1.1 Statement of ethics for <i>in vivo</i> studies	143
5.2.2 _ HDM dosing protocol used in CT imaging experiments	144
5.2.3 CT Imaging	145
5.2.4 Assessment of antibody transport out of HDM exposed lung	146
5.2.5 mIgG1 ELISA	147
5.2.6 Immunohistochemistry	148
5.3 Results	149
5.3.1 Model development/characterisation	149
5.3.1.1 Lung inflammatory cell influx	149
5.3.1.2 CT Imaging results	151

5.3.2 Histology _____	155
5.3.2.1 Disease progression and mFcRn expression _____	155
5.3.2.2 mFcRn expression in the HDM exposed lung _____	157
5.3.3 Antibody transport of out diseased lung _____	159
5.4 Conclusion _____	160
CHAPTER 6: SUMMARY, FINAL CONCLUSIONS AND SUGGESTIONS FOR FUTURE WORK _____	161
6. Summary and final conclusions _____	161
6.1 Suggestions for future work _____	165
REFERENCES _____	167

LIST OF FIGURES

Figure 1.1 - Table summarising biologics currently marketed or in clinical trials for pulmonary disease. Data from (1) Pelaia, et al. 2012 (2) Rafii, et al. 2013 (3) Aaron, et al. 2013 (4) Morjaria, et al. 2012. ___ 3

Figure 1.2 - Image depicting the structure of the lung, from the trachea to the alveolar sacs, showing the branching nature of the airways. Picture from (Patton & Byron, 2007) _____ 7

Figure 1.3 - Images showing the structures of the tracheal, small bronchial and alveolar epithelia, from (Patton & Byron, 2007) _____ 8

Figure 1.4 - Images showing the structure of the tight junction in the pulmonary epithelium. _____ 11

Figure 1.5 - A diagram showing the possible pathways for IgG to cross the pulmonary epithelium and enter the systemic circulation. In paracellular diffusion (blue arrow) the IgG would pass between the epithelial cells through the tight junctions. In transcytosis the IgG would pass through the epithelial cells, either non-specifically (green arrow), or via binding to the FcRn receptor (purple arrow). _____ 15

Figure 1.6 - Table showing relationship between Diffusion constant D and molecular weight of a series of common biological species in water. Data from: (Fall, et al., 2005) _____ 17

Figure 1.7 - A summary of available data for the *in vivo* pulmonary clearance of proteins after inhalation in rats, expressed as the time to reach maximum concentration in the blood vs. the molecular weight of the protein (data from: (Byron & Patton, 1994)). _____ 18

Figure 1.8 - Location of the key residues on IgG which facilitate binding of IgG to FcRn. From: (Ward & Ober, 2009) _____ 23

Figure 1.9 - Diagram showing effect of pinhole collimator in SPECT imaging. _____ 38

Figure 2.1 - Pictures showing the structures and relative sizes of the proteins which will be investigated in the SPECT/CT imaging studies. Blue colour signifies antibody constant regions, green colour signifies antibody variable regions and red colour signifies Fibronectin III regions. _____ 46

Figure 2.2 - Nickel affinity column elution trace for the Fab fragment (50 kDa), showing the elution of product from Fractions C1-C12 as well as the corresponding SDS-PAGE gel of the protein containing fractions, concentrated cell culture supernatant, diafilter flow through and column flow through. _____ 62

Figure 2.3 - Size exclusion purification elution trace for the Fab fragment (50 kDa), showing elution of product from Fractions D1-D12 as well as the corresponding SDS-PAGE gel of the protein containing fractions and the original Nickel affinity purified protein load. _____ 64

Figure 2.4 - QC gel for Fab fragment (50 kDa). Both non reduced lanes show bands at the correct Mw of 50 kDa, reduced lanes show two bands of approx 25 kDa (one for Fab heavy chain and one for Fab light chain) _____ 65

Figure 2.5 - Nickel affinity purification elution trace for the scFv fragment (28 kDa), showing elution of product from Fractions C7-D5 as well as the corresponding SDS-PAGE gel of the protein containing fractions, concentrated cell culture supernatant, diafilter flowthrough and column flow through. _____ 67

Figure 2.6 - Size exclusion purification elution trace for the scFv fragment (28 kDa), showing the elution of product from fractions C6-D5 as well as the corresponding SDS-PAGE gel of the protein containing fractions, column flow through and the original nickel affinity purified protein loaded. _____ 68

Figure 2.7 - QC gel for the scFv fragment (28 kDa). All lanes show a band at the correct Mw of 28 kDa. The non-recued lanes show an additional band at approx 55 kDa, suggested to be dimer formation. _69

Figure 2.8 - Nickel affinity purification elution trace for the FN3 protein (11 kDa), showing elution of product from Fractions C6-D4 as well as the corresponding SDS-PAGE gel of the protein containing fractions, concentrated cell culture supernatant and column and diafilter flowthroughs. _____ 71

Figure 2.9 - Size exclusion purification elution trace for the FN3 protein (11 kDa), showing the elution of the product from fractions D12-E9 as well as the corresponding SDS-PAGE gel of the protein containing fractions. _____ 72

Figure 2.10 - QC gel for the FN3 protein (11 kDa), showing a single band at 11 kDa in all lanes. _____ 73

Figure 2.11 - Protein A purification elution trace for the H435A mutant (150 kDa), showing elution of product from Fractions A3-A10 as well as the corresponding SDS-PAGE gel of the protein containing fractions, concentrated cell culture supernatant and diafilter and column flow through. _____ 75

Figure 2.12 - Repeat protein A affinity purification elution trace for the H435A mutant (150 kDa), showing elution of product from Fractions A2-A10 as well as the corresponding SDS-PAGE gel of the protein

containing fractions, the flow through from the 1st pass and column flow through. _____ 76

Figure 2.13 - QC gel for the IgG_H435A mutant (150 kDa). Non reduced lanes show a band at the correct Mw of 150 kDa. Reduced lanes show two bands, one at approx 50 kDa corresponding to the heavy chains and one at approx 20 kDa corresponding to the light chains. _____ 78

Figure 2.14 - Protein A purification elution trace for the V250Q mutant (150 kDa), showing elution of product from Fractions A1-A11 as well as the corresponding SDS-PAGE gel of the protein containing fractions, and column load and flow through. _____ 79

Figure 2.15 - QC gel for the IgG_V250Q mutant (150 kDa). Reduced lanes show two bands, one at approx 50 kDa corresponding to the heavy chains and one at approx 20 kDa corresponding to the light chains. _____ 80

Figure 2.16 - Protein A purification elution trace for the H435A_I243A mutant (150 kDa), showing elution of product from Fractions 1-9 as well as the corresponding SDS-PAGE gel of the protein containing fractions, and column load and flow through _____ 81

Figure 2.17 - Repeat protein A purification elution trace for the H435A_I253A mutant (150 kDa), showing elution of product from Fractions 1-A8 as well as the corresponding SDS-PAGE gel of the protein containing fractions, the flow through from the 1st pass and column flow through _____ 83

Figure 2.18 - QC gel for the H435A_I253A mutant (150 kDa). Reduced lanes show two bands, one at approx 50 kDa corresponding to the

heavy chains and one at approx 20 kDa corresponding to the light chains. _____ 84

Figure 2.19 - Graph showing association/dissociation of WT IgG to Octet streptavidin sensors coated with mFcRn over the full range of IgG concentrations at pH 7.4. Each green line represents the response recorded for an individual sensor. The red line represents removal of the sensor from IgG containing solution and immersion in fresh buffer. _____ 86

Figure 2.20 - Pooled results from Octet analysis of binding affinity for WT IgG and mutants to mFcRn, at pH 6 and 7.4. Data shows the relative binding affinities to mFcRn as a percentage of the WT binding. Error bars represent \pm sem (n=12 per bar) _____ 87

Figure 3.1 - Diagram showing principles of thin layer chromatography (TLC) _____ 95

Figure 3.2 - Data for IgG at 1.79 mg/mL, Mw of 148125. Table showing the values obtained from Ellman's assay of both reduced and unreduced antibody in triplicate, as well as a re-test of the same batch of reduced IgG after 1 month storage at -80°C. _____ 100

Figure 3.3 - Activities of bottom and top halves of TLC plates as determined by the well counter. Calculated RCP (%) are 100 % at all time points. _____ 102

Figure 3.4 - A series of gamma camera images showing a) the redistribution of free ^{99m}Tc within one mouse over 46 minutes, with b) a graph quantifying the activity observed in different organs over 46 minutes. Activity is initially highest in the lung, dropping rapidly to a plateau at approx background levels after 30 mins. Activity in the thyroid and stomach is initially very low increasing over the course of

the scan. Activity in the bladder remains roughly constant at low levels throughout the scan. _____ 104

Figure 3.5 - Graph showing the quantification of levels of activity within the lung, bladder, stomach and thyroid over the course of a 46 min scan. High levels of initial activity persist within the lung over the course of the scan. Very low levels of activity are recorded in the thyroid, stomach and bladder, which do not increase over 46 minutes. _____ 107

Figure 3.6 - Comparison of detection of ^{99m}Tc -IgG by ELISA (detecting antibody) or by total activity of the sample as determined in the well counter (detecting the label). Expressed as % relative increase from $t=0$ with error bars of \pm sem ($n=6$). The graph indicates that the level of radiolabelled antibody reported by either detection method is highly similar. _____ 110

Figure 3.7 - Results of experiment comparing analysis of known concentrations of labelled and unlabelled antibody determined by ELISA. Graph shows that the ELISA reports correct concentrations of both labelled and unlabelled antibody, within experimental error. Error bars are \pm sem ($n=6$). _____ 112

Figure 3.8 - Graph showing that the concentration of labelled and unlabelled antibody detected by ELISA in plasma samples taken up to 4 hours post dose are highly similar. Error bars are \pm sem ($n=6$). ___ 113

Figure 4.1 - Representative SPECT/CT images showing pulmonary retention of IgG at a) 0, b) 2, c) 4 and d) 24 hrs. Areas of lung activity are shaded green and areas of activity outside the lung shaded yellow. The images show decreasing levels of activity in the lung over 24 hrs, with activity visible within the bladder and intestines at some timepoints. _____ 123

Figure 4.2 - Graph showing the pulmonary retention of intratracheally instilled antibody over 24 hrs. Error bars are \pm sem (n=6). _____ 126

Figure 4.3 - Table showing the best fit values for non-linear regression analysis (biphasic exponential decay model) for pulmonary clearance of WT whole mIgG. _____ 127

Figure 4.4 - Representative SPECT/CT images showing pulmonary retention of A) Fab and B) scFv at i) 0, ii) 2, iii) 4 and iv) 24 hrs. Areas of lung activity are shaded green and areas of activity outside the lung shaded yellow. The images show decreasing levels of activity in the lung over 24 hrs, with activity visible within the bladder and intestines at some timepoints. _____ 129

Figure 4.5 - Graph showing the pulmonary retention profiles of intratracheally instilled antibody, fragments and the FN3 protein over 24 hrs. Error bars are \pm sem (n=6 per point). _____ 130

Figure 4.6 - Representative SPECT/CT images showing: _____ 133

A) pulmonary retention of FN3 protein at i) 0, ii) 2, iii) 4 and iv) 24 hrs. Areas of lung activity are shaded green and areas of activity outside the lung shaded yellow. The images show decreasing levels of activity in the lung over 24 hrs, with activity visible within the bladder and intestines at some timepoints. In addition, there is activity visible in the kidneys between 2 and 4 hours post dose _____ 133

B) Rotated FN3 2 hr image with views from original SPECT scan showing activity in kidney and lungs. Black represents low activity and white represents high activity. _____ 133

Figure 4.7 - Graph showing pulmonary retention of IgG, Fab, scFv and FN3 protein 24 hrs post i.t instillation as a function of molecular weight. _____ 134

Figure 4.8 - Graph showing the pulmonary retention of intratracheally instilled antibody and FcRn binding mutants over 24 hrs. Error bars are \pm sem (n=6 per point). _____ 136

Figure 4.9 - Image of mouse lung stained with anti-mFcRn antibody at x20 magnification. Brown areas represent mFcRn expression, visible in the epithelium, endothelium and on alveolar macrophages. _____ 139

Figure 5.1 - Graph showing cell numbers in BALF from saline control, HDM exposed and HDM exposed budesonide treated mice after 7 weeks HDM exposure and 2 week budesonide treatment. HDM exposure results in statistically significant increases in total cell numbers, Eos, Neuts and Lymphs. Numbers of Monos do not change. Budesonide treatment results in a statistically significant decrease in numbers of total cells, Eos and Lymphs. Analysis is with one tailed Student's unpaired t-test, * is $p < 0.05$, ** is $p < 0.01$ and *** is $p < 0.005$. Error bars are \pm sem (n=6 per group). _____ 151

Figure 5.2 - Representative CT slices through mouse lungs exposed to a) saline or b) HDM over 7 weeks including c) an image comparing lungs of HDM exposed animals with or without budesonide treatment. Images show black as low density and white areas as higher density. Vehicle images showed no density changes over 7 weeks. HDM images showed a large area of increased density in week 5, which persists into week 7 if left untreated. Treatment with budesonide, results in a reduction in high density areas in week 7. _____ 152

Figure 5.3 - Graph showing modal lung densities determined by CT imaging over 7 weeks for saline, HDM and HDM + budesonide exposed animals. HDM exposure results in increased lung density after 1 week, which persists over 7 weeks if no treatment is given. Treatment with budesonide reverts lung density to baseline levels . * statistically significant changes in density between HDM and vehicle

groups, $p < 0.05$, # statistically significant change in lung density between HDM and HDM + budesonide groups, at ## = $p < 0.01$ and ### = $p < 0.005$. Error bars are \pm sem (n=6 per group). _____ 154

Figure 5.4 - Images showing extent of inflammation in histological samples of a) saline and b) and c) HDM exposed lungs at x20 magnification. Image a) shows healthy lung. Image b) shows massive inflammation localised around airways and vessels. Image c) shows giant multinuclear macrophages in HDM exposed alveoli and inflammation around small vessels. _____ 156

Figure 5.5 - Images showing extent of mFcRn expression in histological samples of a) saline and b) HDM exposed lungs at x20 magnification. Brown colour indicates mFcRn expression or non-specific binding and in healthy lung (a) is visible on macrophages and epithelium. In HDM exposed lung (b) there is significant non-specific binding to mucus in the airways and in inflamed areas directly beneath the airways. _____ 158

Figure 5.6 - Graph showing levels of antibody recoverable from the BALF over 24hrs post intratracheal instillation in either HDM or saline control animals. Error bars are \pm sem (n=6). _____ 160

LIST OF ABBREVIATIONS

α	Alpha
AHR	Airway hyper-reactivity
A	Alanine
BALF	Bronchoalveolar lavage fluid
CHO	Chinese hamster ovary
COPD	Chronic obstructive pulmonary disease
cm	Centimetre
CT	Computed tomography
Cys	Cystine
Da	Dalton
DPBS	Dulbecco's Phosphate buffered saline
<i>E.coli</i>	<i>Escherichia coli</i> bacteria
EDTA	Ethylenediaminetetraacetic acid
ELISA	Enzyme linked immuosorbent assay
EPO	Erythropoietin
Eu	Endotoxin units
Fab	Fragment antigen-binding (of an antibody)
Fc	Fragment crystallisable (of an antibody)
FcRn	Neonatal Fc receptor
FN3	Fibronectin III domain
g	Gram
g	Gravity
GM-CSF	Granulocyte macrophage colony stimulating factor
H	Histidine
HDM	House dust mite
His	Histidine
HRP	Horseradish peroxidase
hrs	Hours
HU	Hounsfield units
I	Isoleucine

IgE	Immunoglobulin E
IgG	Immunoglobulin G
IHC	Immunohistochemistry
IL	Interleukin
kDa	Kilodalton
kVP	Peak kilovoltage
mA	Milliampere
mIgG	Murine immunoglobulin G
mFcRn	Murine neonatal Fc receptor
mg	Milligram
mL	Millilitre
mm	Millimeter
mM	Millimolar
MW	Molecular weight
NBF	Neutral buffered formalin
NFW	Nuclease free water
nm	Nanometer
°C	Degrees Celsius
PBS-T	Phosphate buffered saline with Tween 20
PCR	Polymerase chain reaction
PEI	Polyethylenimine
Q	Glutamine
QC	Quality control
RCP	Radiochemical purity
ROI	Region of interest
RPM	Revolutions per minute
s	Seconds
scFv	Single chain variable region
SDM	Site directed mutagenesis
SDS-PAGE	Sodium dodecyl sulphate polyacrylamide gel electrophoresis
SEC	Size exclusion chromatography
SPECT	Single photon emission computed tomography

TCEP	Tris(2-carboxyethyl)phosphine
TLC	Thin layer chromatography
Tmax	Time to maximum plasma concentration
μl	Microlitre
μm	Micrometer
V	Volts
V	Valine
WT	Wild type

CHAPTER 1: General Introduction and Literature Review

1. Project Overview

The overall aim of the work detailed in this thesis was to investigate inhalation as a potential delivery route for therapeutic antibodies. It is hoped that exploitation of currently unused delivery routes for biologics will lead to an increased number of therapies reaching the market, helping to reduce unmet patient need.

1.1 Delivery of Biologics

Research into the development of biologic based drugs such as monoclonal antibodies, recombinant proteins and growth factors is a rapidly expanding sector of the pharmaceutical industry. The first biologic drug approved for delivery to patients was recombinant human insulin in 1982, with the first monoclonal antibody, muromonab, FDA approved in 1986 (Reichert, et al., 2005). Since then the FDA has approved over 130 biological based drugs and as of May 2011 there are 26 monoclonal antibody therapies approved for delivery to patients in the USA. (Reichert, 2012)

Protein based therapies, such as monoclonal antibodies, are generally high molecular weight, hydrophilic and rapidly denatured in the gastrointestinal tract. These factors make oral formulation of biologics difficult and result in poor oral bioavailabilities for the vast majority of biologic based therapies (Antosova, et al., 2009). Consequently parenteral delivery is the most common delivery route for biologics, with numerous formulations available on the market formulated for subcutaneous, intravenous or intramuscular injection.

Parenteral delivery avoids denaturation of the therapeutic protein in the gastrointestinal tract and provides rapid systemic delivery with bioavailabilities approaching 100%. However, there are drawbacks to parental delivery including patient discomfort, high cost of goods; related to the strict asepsis required in the final formulation and poor safety of parenteral delivery in countries which lack reliable access to sterile needles and syringes (Chames, et al., 2009).

Intravenous dosing of antibodies, for example Herceptin® (trastuzumab) and Avastin® (bevacizumab), generally involves infusion, which necessitates that therapy is provided in a clinical setting by a trained medical professional. Intramuscular or subcutaneous injection is less time consuming and inconvenient for patients than intravenous dosing. Humira® (adalimumab) an anti-TNF α monoclonal antibody used to treat rheumatoid arthritis is a monoclonal antibody that is currently FDA approved for subcutaneous injection (Eisenstein,

2011) and a subcutaneous formulation of Herceptin© currently in phase III clinical trials. (Eisenstein, 2011).

One biologic, Xolair© is currently marketed for the treatment of asthma. Figure 1.1 lists a selection of biologics currently in clinical trials for asthma, COPD or pulmonary fibrosis treatment.

Biologic	Description	Disease	Status
Omalizumab ⁽¹⁾	Anti-IgE antibody	Asthma	Approved
Mepolizumab ⁽¹⁾	Anti-IL5 antibody	Asthma	Phase II/III
Tralokinumab ⁽¹⁾	Anti-IL13 antibody	Asthma	Phase II
MEDI-528 ⁽¹⁾	Anti-IL-9 antibody	Asthma	Phase II
STX-100 ⁽²⁾	Anti- α v β 6 Integrin antibody	Pulmonary Fibrosis	Phase II
CNTO888 ⁽²⁾	Anti-CCL2 antibody	Pulmonary Fibrosis	Phase II
QAX576 ⁽²⁾	Anti-IL13 antibody	Pulmonary Fibrosis	Phase II
Etanercept ⁽³⁾	Anti-TNF α fusion protein	COPD	Phase II
ACZ-885 ⁽⁴⁾	IL-1 β agonist	COPD	Phase II
SB-681323 ⁽⁴⁾	P38 MAPK inhibitor	COPD	Phase II

Figure 1.1 - Table summarising biologics currently marketed or in clinical trials for pulmonary disease. Data from (1) Pelaia, et al. 2012 (2) Rafii, et al. 2013 (3) Aaron, et al. 2013 (4) Morjaria, et al. 2012.

1.2 Research into non-invasive delivery of biologics

There has been a significant level of research into the development of non-invasive protein delivery systems, including nasal, buccal, transdermal, pulmonary and oral delivery (Brown, 2005). The most well known example of a non-invasively formulated biologic is the pulmonary delivery of insulin for the treatment of diabetes. The

development of inhaled insulin formulations was a very active area of research until the withdrawal of Pfizer's FDA approved inhaled insulin product Exubera© from the market in 2008, citing poor sales. Other inhaled insulin projects in late phase clinical trials, such as the Novo Nordisk AERx1 formulation (insulin Diabetes Management System, iDMS), were then stopped due to the perceived lack of commercial potential (Bailey & Barnett, 2007).

There is a small number of biologics currently marketed in non-invasive formulations, these include: Miacalin© a nasal formulation of the polypeptide hormone calcitonin from Novartis to treat postmenopausal osteoporosis and Minirin© an oral formulation of demopressin (a synthetic form of antidiuretic hormone) from Ferring that is used to treat nocturnal enuresis (Moeller & Jorgensen, 2008). In terms of pulmonary delivery the most successful biologic based drug currently on the market is Pulmozyme© a recombinant human DNAse delivered by nebulisation to relieve the symptoms of cystic fibrosis. There are also numerous inhaled biologic projects currently in late stage development/early clinical trials, for example Ablynx is currently running a Phase 1 trial to test the safety of an inhaled nano-body based drug to treat respiratory syncytial viral infections (Schepens, et al., 2011).

Pulmonary delivery of antibody formulations could be achieved using nebulisation for liquid based formulations or dry powder inhalers for

solid formulations. A significant amount of research has been undertaken to allow the formulation of proteins, including therapeutic antibodies, for both nebulisation and in inhalers.

In terms of the suitability of nebulisation for antibody delivery to the lung, a study by Maillet (Maillet, et al., 2008) investigated Cetuximab, a monoclonal antibody against EGFR with approval for use in the treatment of metastatic cancer. It was demonstrated that the antibody was both resistant to formulation for nebulisation and able to retain functionality following nebulisation.

In terms of antibody formulation for dry powder inhalation, numerous studies have determined suitable excipients to promote the successful freeze or spray drying of the protein. The major challenges in producing a suitable dry powder antibody formulation are maintenance of protein stability, minimising aggregation, glycation and lactosylation (Constantino, et al., 1998). Additionally, excipients are required to tailor the bulk flow properties of the powder formulation so that a suitable aerosol can be formed for delivery to the lung. In general antibody stability is improved with the addition of carbohydrate excipients such as mannitol and lactose (Constantino, et al., 1998b) which, provided that the protein to excipient ratio is optimised, are also capable of producing formulations which are amenable to aerosolisation (J D Andya, et al., 1999).

1.3 The lung

There are numerous reasons to believe that inhalation is an attractive delivery route for biologics, generally due to the large, highly perfused surface area for absorption within the lung. Pulmonary delivery is also commonly utilised for small molecules, particularly in the delivery of glucocorticosteroids and bronchodilators in the maintenance and treatment of asthma. Additionally, the antibiotic tobramycin is formulated as an aqueous nebulization for the treatment of “Pseudomonas” infections in cystic fibrosis patients.

Additionally, delivery of biologics to treat lung disease, for example in lung cancer, cystic fibrosis or asthma, is also possible and in such cases it is anticipated that delivery direct to the site of action would reduce systemic side effects and increase local drug concentrations when compared to parenteral delivery routes.

1.3.1 Structure of the human lung

The primary functions of the lungs are to deliver oxygen to the bloodstream and remove carbon dioxide from the body. In general the lung is split into two anatomical regions, the conducting regions which transmit air through the lungs and the respiratory regions where gas exchange occurs. The structure of the human lung, from the trachea to the alveoli, is shown in Figure 1.2

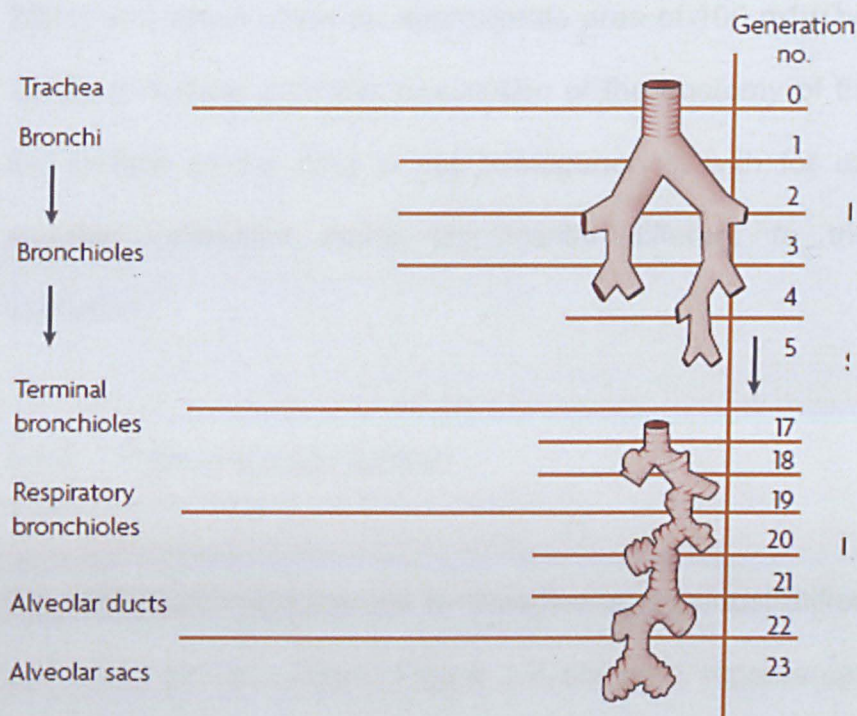


Figure 1.2 - Image depicting the structure of the lung, from the trachea to the alveolar sacs, showing the branching nature of the airways. Picture from (Patton & Byron, 2007)

The conducting regions of the lung consist of the trachea, bronchi and bronchioles. The trachea is the largest conducting airway, with an average diameter of 2-2.5 cm in humans and which divides into two smaller bronchi after an approximate length of 9 – 12 cm. Each of these bronchi then further branches into two smaller bronchi as shown in Figure 1.2 and this pattern of bifurcation repeats 15 times until the first level of the respiratory regions of the lung is reached (Weibel and Gomez, 1962). The diameter and length of the bronchi decrease with each progressive bifurcation, until the terminal respiratory bronchioles, at 0.5 mm in diameter, further divide into the alveolar ducts and sacs, which are the main site of gas exchange within the lungs (Itoh, et al.,

2004) and which cover an approximate area of 100 m² (Owens, et al., 2003). It is clear from this description of the anatomy of the lung that the surface of the lung is not homogeneous, with for example the alveolar epithelium being significantly different to the tracheal epithelium.

1.3.2 Pulmonary epithelium

The epithelium in the trachea is classified as pseudostratified columnar epithelium and is ciliated. Figure 1.3 shows a representation of the tracheal epithelium.

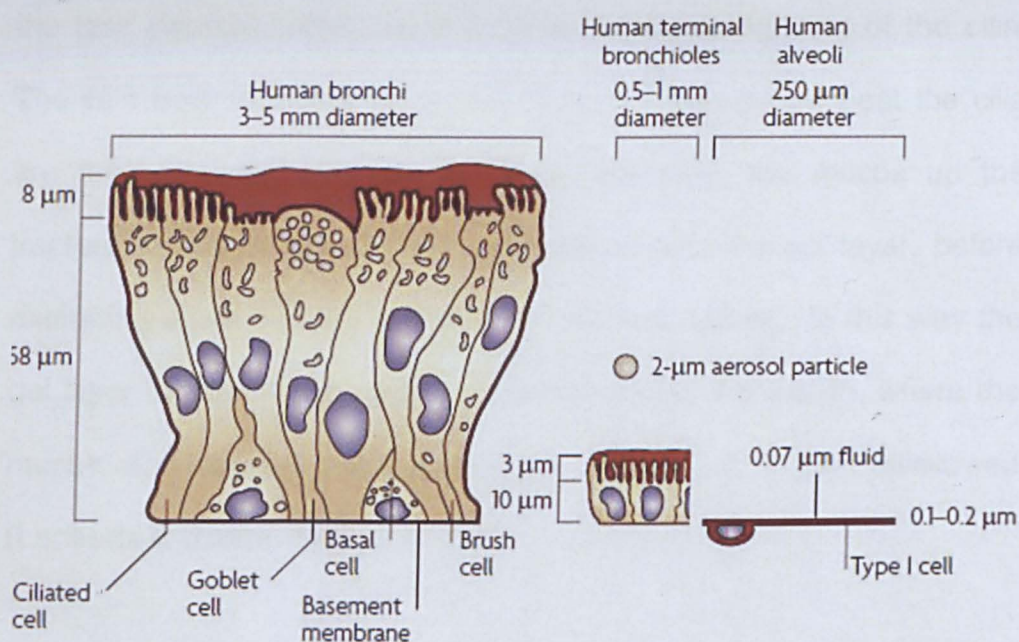


Figure 1.3 - Images showing the structures of the tracheal, small bronchial and alveolar epithelia, from (Patton & Byron, 2007)

There are 3 major cells types present, ciliated cells, basal cells and goblet cells. The ciliated cells extend from the basal lamina to the

luminal surface, forming tight junctions with each other. There are between 200-300 cilia on the surface of each ciliated cell, which are 0.25 μm in diameter and 6 μm in length (Proud, 2008). Basal cells attach to the basement membrane and support the ciliated cells. Goblet cells secrete the mucins which form part of the mucus layer which covers the epithelium. The mucus layer in the trachea and largest airways is around 8 μm deep and functions to trap inhaled particulates such as dust and allow for their removal from the lungs (Patton, 1996). The mucus layer is in fact made up from two distinct layers, a highly viscous gel layer lying on top of a less viscous sol layer. The more viscous top layer traps inhaled particulates whereas the less viscous bottom layer facilitates effective beating of the cilia. The cilia beat to move the mucus layer, on the upward beat the cilia are fully extended into the gel layer and push the mucus up the trachea, on the downbeat the cilia contract into the sol layer, before extending again into the gel layer for the next upbeat. In this way the gel layer is moved continually up the trachea to the mouth, where the mucus and any inhaled particulates trapped in it are swallowed (Lenaerts & Gurny, 1990).

The larger bronchi possess an epithelium that is very similar to the trachea, however, as the bronchi become progressively shorter and smaller in diameter the nature of the epithelium changes with less ciliated cells present and a gradual transition to a thinner, more

squamous, organisation. This changing epithelium is represented in Figure 1.3.

The alveolar epithelium (again represented in Figure 1.3) is 0.1 - 0.4 μm thick and made up of two cell types. The large flat squamous Type I cells cover 90 % of the alveoli surface with the remaining 10 % covered with cuboidal Type II cells which secrete the alveoli lining fluid, which is 70 nm in depth (Crapo, et al., 1983). Tight junctions are formed between neighbouring cells. The alveol are suited to gas exchange primarily due to the very short diffusion path between the airspaces and bloodstream. The partial pressure of oxygen is also higher in the alveolar regions than the bloodstream, with the opposite true for the partial pressure of carbon dioxide. This provides a gradient to drive oxygen incorporation into the blood and carbon dioxide removal from the blood (Smyth & Hickey, 2011).

1.3.3 Tight junctions

All sections of the airways from the trachea to the alveolar sacs are characterised by epithelial barriers where cells are joined by tight junctions. Tight junctions provide points of contact between adjacent cells and are located just below the apical surface. The junction is composed of predominantly claudin and occludin protein strands which are anchored to the cytoskeleton, extend through the cell membrane and directly interact with the extracellular domains of protein strands

extending from neighbouring cells (Tsukita & Itoh, 2001) (Martin-Padura, et al., 1998) (Furuse, et al., 1993). The structure of the tight junction is shown in Figure 1.4.

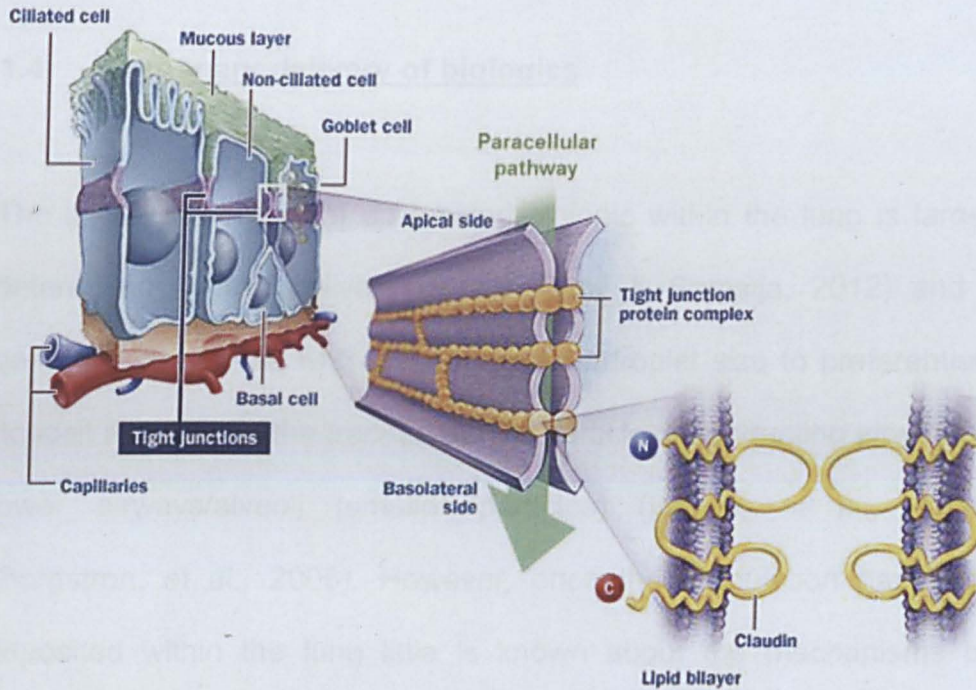


Figure 1.4 - Images showing the structure of the tight junction in the pulmonary epithelium.

The junctions function to structurally link adjacent cells, providing a barrier to the free diffusion of molecules between the epithelial cells (Chen-Quay, et al., 2009). This allows the epithelium to function correctly as a barrier and prevents any excessive build-up of fluid in the lungs. The junctions are selectively permeable, regulating the passage of water, ions and other solutes (Rubas, et al., 1996) and are considered to result in a paracellular space of between 0.1 and 5 nm (Madara, 1998).

In terms of the pulmonary delivery of biologics, tight junctions will prevent the free diffusion of any inhaled product between the cells of the pulmonary epithelium and as such the rate of paracellular transport of larger biologics is expected to be very slow.

1.4 Pulmonary delivery of biologics

The initial distribution of an inhaled biologic within the lung is largely determined by the delivery device, (Patil & Sarasija, 2012) and is generally concerned with tailoring particle/droplet size to preferentially deposit the dose in the trachea (larger particles), conducting airways or lower airways/alveoli (smaller particles) (Isaacs, et al., 2004), (Borgstron, et al., 2006). However, once the formulation has been deposited within the lung little is known about the mechanisms by which it redistributes within the lung tissue and how ultimately it is transported out of the lung. Our understanding of the pulmonary distribution of inhaled biologics is further complicated by different local permeability and clearance mechanisms in the alveolar vs. bronchial regions.

Any biologic deposited in the trachea will initially make contact with the mucus layer, a sol-gel layer which is moved slowly towards the larynx by the beating of the cilia on the surface of the underlying epithelial cells (Cuand & Saltzmann, 2009). An inhaled biological must be able to diffuse through the mucus layer before it is moved up the trachea to the

larynx and swallowed, or the biologic will not successfully reach the lung. The factors which influence diffusion through the mucus layer include the size of inhaled molecule and any interaction between the inhaled molecule and the components of mucus (Khanvilkar, et al., 2001) (Thornton & Sheehan, 2004). It has been demonstrated that neutrally charged particles are more easily able to diffuse in the mucus and reach the underlying epithelium, whereas charged particles interact more strongly with mucus and diffuse more slowly (Weers, et al., 2010). A study by (Saltzmann, et al., 1994) found that antibody transport through cervical mucus was rapid, with the diffusion in mucus comparable to that in water. As such, diffusion through the mucus layer is not anticipated to be the rate limiting step in pulmonary antibody clearance.

A biologic deposited in the alveoli will initially make contact with the alveolar lining fluid. In contrast to the trachea, there is no mucus layer to diffuse through and the alveolar lining fluid layer is particularly thin. However, the alveoli have two defence mechanisms which are not present in the trachea/upper airways, which can greatly influence the amount of an inhaled drug which is able to reach the pulmonary epithelium. First the lining fluid contains proteases which will quickly degrade inhaled peptides, although larger proteins such as IgG are degraded much more slowly and can persist in the lung for several days (Byron & Patton, 1994). Secondly, alveoli are patrolled by macrophages with the human lung estimated to contain around 500

million alveolar macrophages, with approximately 12-14 macrophages per alveolus (Chrystal, et al., 1997). Any inhaled biologic will be phagocytosed if it does not quickly dissolve in the alveolar lining fluid.

Strategies such as containing inhaled drugs in polymer nano- or micro-particles have been shown to be able to reduce their susceptibility to macrophage clearance (Jones, et al., 2002). Additionally, the PEGylation of such encapsulated formulations has been suggested as a route to both avoid macrophage detection and promote pulmonary retention. PEGylated micro-particles have been shown to be retained in the lung longer than unmodified microparticles, although it is not clear where exactly within the lungs the particles were located (Kutscher, et al., 2010).

Once an inhaled biologic diffuses through the fluid lining the lung and reaches either the bronchial or alveolar epithelial cells even less is known about how biological molecules are internalised or transported out of the lung.

1.5 Crossing pulmonary epithelium

In general there are two main pathways by which an inhaled biologic could cross the pulmonary epithelium. Firstly by paracellular transport, that is transport by diffusion between the epithelial cells. Secondly by transcytosis, that is transport through the epithelial cells. This transport

through the epithelial cells can be subdivided into two different pathways, active and passive transport. Passive transport is non-specific transport through the cell and active transport is the selective uptake and delivery of a molecule through the cell by a dedicated receptor. The neonatal Fc receptor (FcRn) is known to bind and transport IgG and has been shown to be capable of actively transporting IgG through pulmonary epithelial cells (Roopenian & Akilesh, 2007). The three different transport routes across the pulmonary epithelium are represented pictorially in Figure 1.5

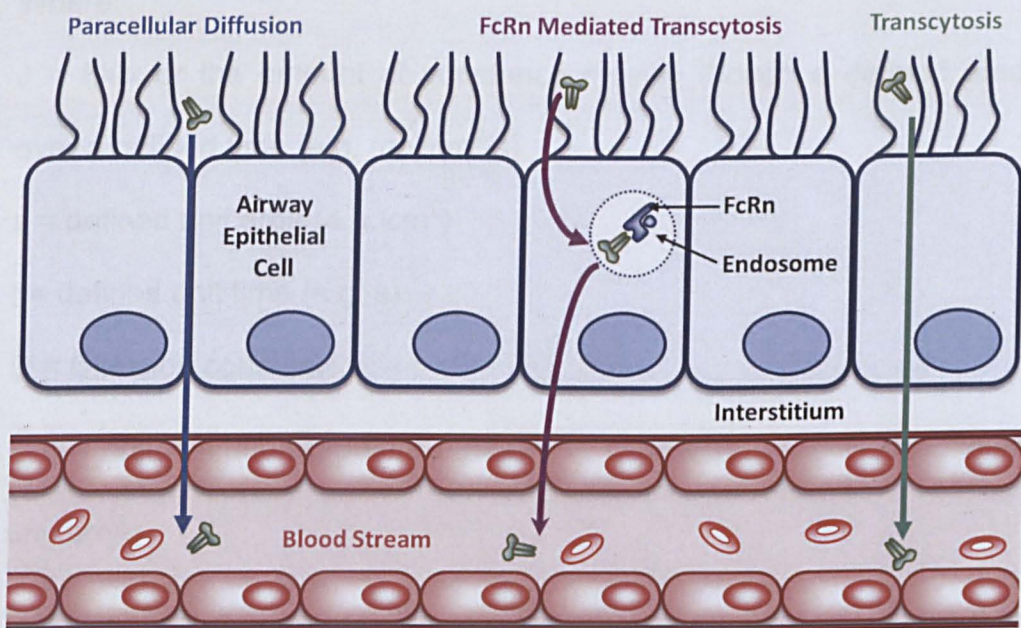


Figure 1.5 - A diagram showing the possible pathways for IgG to cross the pulmonary epithelium and enter the systemic circulation. In paracellular diffusion (blue arrow) the IgG would pass between the epithelial cells through the tight junctions. In transcytosis the IgG would pass through the epithelial cells, either non-specifically (green arrow), or via binding to the FcRn receptor (purple arrow).

1.5.1 Paracellular transport

Paracellular diffusion is non-specific and is diffusion controlled. Diffusion is governed by Fick's Law, which defines the movement of a substance (J) as being directly proportional to the concentration gradient ($\frac{\partial c}{\partial x}$), according to the following equation:

$$J(x, t) = -D \frac{\partial}{\partial x} c(x, t)$$

Where:

J = Flux or the amount of substance moving through a defined area over a defined time (e.g. mol/cm²/s)

x = defined unit area (e.g. cm²)

t = defined unit time (e.g. s)

D = Diffusion constant

$\frac{\partial}{\partial x} c$ = concentration gradient (change in concentration over a defined unit area)

The magnitude of the diffusion constant (D) is related to both the size of a given substance and the properties of the medium that it is diffusing in. Figure 1.5 relates molecular weight and D for a variety of substances in water.

The data in Figure 1.6 show that the magnitude of D is inversely related to molecular weight, in a given diffusion medium, meaning that larger molecules have smaller diffusion constants. Using the equation for Fick's Law, a smaller diffusion constant always results in a lower rate of diffusion, indicating that molecular weight is inversely related to the rate of diffusion. In terms of paracellular transport between cells this relationship indicates that smaller molecules ought to pass more quickly between the cells in the pulmonary epithelium than larger molecules.

Substance	Molecular weight (Da)	D ($\times 10^7$ cm ² /s)
Glucose	192	660
Insulin	5734	210
Cytochrome c	13370	11.4
Serum albumin	68500	6.1
Catalase	247500	4.1
Fibrinogen	339700	2.0

Figure 1.6 - Table showing relationship between Diffusion constant D and molecular weight of a series of common biological species in water. Data from: (Fall, et al., 2005)

IgG is very large at 150 kDa and as such would be expected to slowly diffuse out of the lung. The results of various studies into transport of proteins/peptides out of the rat lung are shown in Figure 1.7 with the time taken to reach maximum concentration in the plasma (Tmax)

compared to the molecular weight of the protein. The graph shows a correlation between molecular weight and T_{max}, with smaller peptides more quickly transferred out of the lung and into the blood than larger proteins such as albumin and IgG.

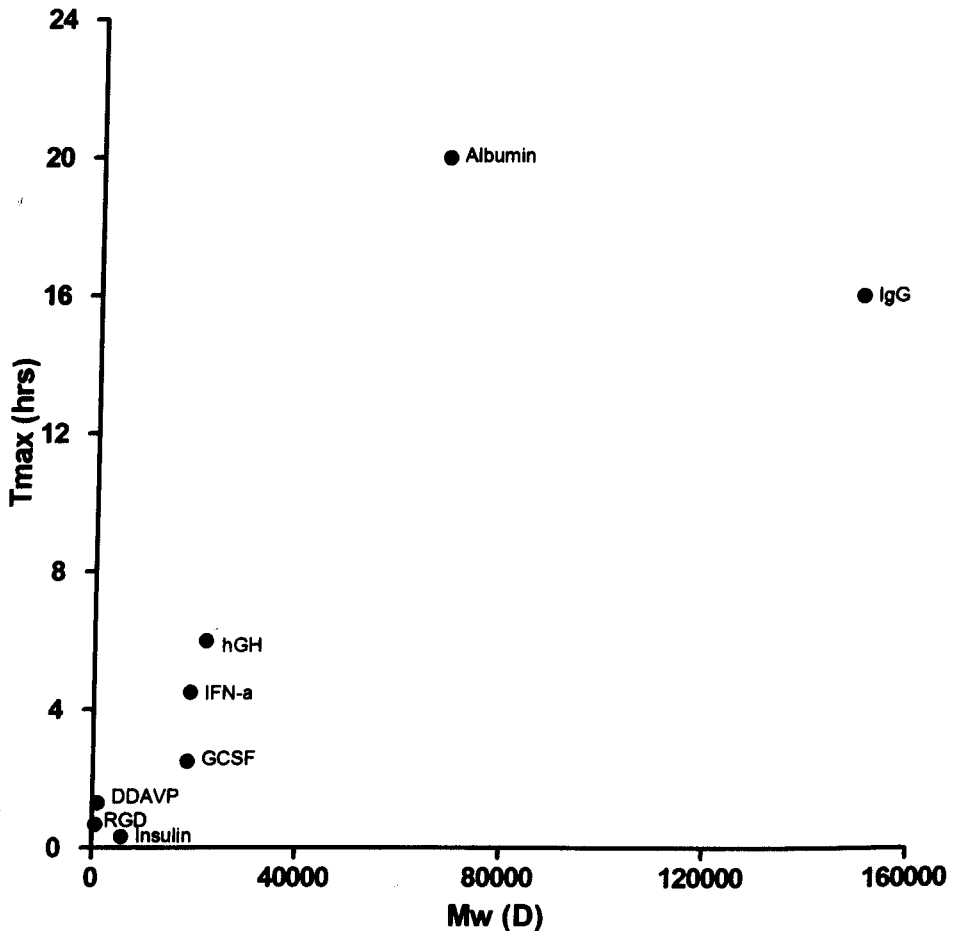


Figure 1.7 - A summary of available data for the *in vivo* pulmonary clearance of proteins after inhalation in rats, expressed as the time to reach maximum concentration in the blood vs. the molecular weight of the protein (data from: (Byron & Patton, 1994)).

There are many other factors than simple molecular weight which could influence the rate of paracellular transport such as hydrophobicity, hydrodynamic radius and overall charge (Patton, 1996). In general the smaller and more hydrophilic a molecule, the quicker it has been

shown to cross the epithelium (Kobayashi, et al., 1995) (Effros & Mason, 1983) .

Numerous studies have shown that the effective pore size in the pulmonary epithelium is predominantly 1-5 nm (Patton, 1996), with molecules having a hydrodynamic radius under 5nm being transported rapidly out of the lung (Wangensteen, et al., 1993). It is thought that this represents paracellular transport through the tight junctions, although this has never been visualised.

1.5.2 Non-specific transcytosis

Non-specific transcytosis involves the uptake of fluid, and any solutes present, into vesicles and their transportation through the cell. This process is entirely non-specific and as such all molecules will be transported though the pulmonary epithelium in this manner, however the likelihood that a molecule will be taken up into the vesicles is controlled by diffusion. As for paracellular transport this non-specific transcytotic pathway will be related to molecular weight with larger molecules being transcytosed more slowly than smaller molecules. In actuality, non-specific transcytosis is not a single pathway, with numerous possible routes to uptake and transport molecules through the cell (Royand & Wrana, 2007) (Mayorand & Pagano, 2005).

The simplest non-specific transcytotic route is adsorptive pinocytosis where invaginations in the plasma membrane trap a random sample of the luminal fluid, which is then transported into the early endosome, from where it can be transferred to the degradative lysosomal pathway, recycled back to the apical surface or transferred to the basolateral surface resulting in transcytosis (Alberts, et al., 1994).

Another route for non-specific transcytosis is via uptake into caveolae, which are invaginations of the plasma membrane, approximately 50-100 nm in diameter, which contain proteins from the caveolin family and cholesterol (Gumbleton, 2001). As caveolae form, fluid is entrapped by pinocytosis, the contents of the caveolae can then either be delivered to the endosome or trafficked across the cell, where the caveolae fuse with the plasma membrane at the opposite cell surface and the cargo is released. There are two proposed mechanisms for the transcytotic pathway, either a single caveola crosses from one plasma membrane to the other or multiple caveolae fuse, passing the cargo across the cell (Gumbleton, et al., 2003). There is some evidence that caveolar transport involves rapid shuttling, which can bypass transfer of cargo to the endosome and promote transcytosis (Plant, et al., 2012).

Transcytosis can also occur following endocytosis in vesicles coated in clathrin (Pucadyil & Schmid, 2009). The vesicle's transport through the cell is mediated by actin, with the vesicle ultimately fusing with the early

endosome (Sahay, et al., 2010a). Clathrin dependent endocytosis is specific for certain required nutrients, such as iron via the transferrin receptor and cholesterol via attachment to the low density lipoprotein (LDL) receptor (Plant, et al., 2012), however numerous studies have shown that the process can transport other cargo, predominantly nanoparticles, both into and through the cell (Sahay, et al., 2010b).

As the rates of both non-specific transcytosis and paracellular transport are diffusion controlled it is difficult to differentiate between these two pathways *in vivo*. However, it should be possible to determine whether passive transport by either paracellular transport or non-specific transcytosis, is important in pulmonary antibody clearance.

1.5.3 Receptor mediated transcytosis

The neonatal Fc receptor (FcRn) was first identified in rodents as the receptor responsible for transferring IgG from mother's milk across the neonatal intestine (Brambell, 1970). Later work has identified numerous roles for FcRn throughout the body, with FcRn expressed in the placenta functioning to transfer IgG from mother to offspring in humans (Leach, et al., 1996). Additionally, FcRn is important in IgG homeostasis (Roopenian & Akilesh, 2007), with FcRn knockout mice having abnormally low IgG serum levels and increased IgG catabolism rates (Roopenian, et al., 2003) (Ghetie, et al., 1996) .

FcRn expression is common in many tissues including the lung, kidney, intestine, liver, eye, at the blood-brain barrier and in antigen presenting cells (Kim, et al., 2008) (Spiekermann, et al., 2002) (Zhu, et al., 2001) (Roopenian & Akilesh, 2007). Additionally, FcRn expression has been confirmed in all mammalian species so far tested (Ward & Ober, 2009). There is limited interspecies FcRn cross-reactivity with mouse FcRn binding IgG from most species including human, rabbit, bovine, rat and sheep (Ober, et al., 2001). However, human FcRn is far more specific, with very poor binding to non human IgG.

Numerous studies have demonstrated the capacity of FcRn to transcytose IgG across polarized epithelial cells (Tzaban, et al., 2009). It is important to note that FcRn is not expressed on the apical cell surface, but is located within the endosome. As such transport by FcRn does not involve an active uptake of IgG into the cell. However, once the IgG reaches the endosome, FcRn facilitates active transport of the IgG away from degradative pathways and out of the cell.

In more detail, the receptor mediated transcytosis of IgG by FcRn begins, as for non-specific transcytosis, with plasma membrane invagination forming a fluid filled transport vesicle, which contains the IgG (Abrahmason & Rodewald, 1981). The vesicle transports the IgG to the endosome, where binding of IgG to FcRn occurs at the lowered pH of 6.0-6.5 (Praetor, et al., 1999). The IgG, which is bound to FcRn, avoids transfer to the degradative lysosomes and instead is

exocytosed from the cell when its transport vesicles fuse with the plasma membrane at the basolateral side of the cell (Deng, et al., 2010). The increase in pH to 7.0-7.5 in the interstitial space causes disassociation of IgG from FcRn, with the net result being transport of IgG from the epithelial surface fluids to the interstitial space (Datta-Mannan, et al., 2007).

The interaction of IgG to mFcRn has been studied extensively and the crystal structure of the FcRn-IgG complex has been solved (Martin, et al., 2001). This enabled key residues, which facilitate the interaction, to be identified, these can be seen in Figure 1.8.

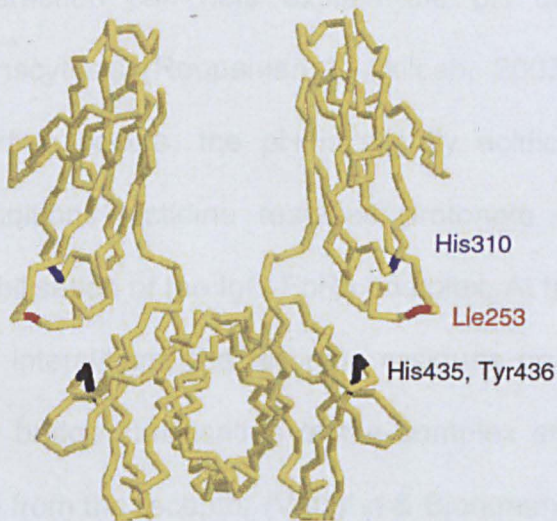


Figure 1.8 - Location of the key residues on IgG which facilitate binding of IgG to FcRn. From: (Ward & Ober, 2009)

The binding of human IgG with human FcRn is stabilised by two salt bridges, one between IgG Histidine_310 and FcRn Glutamine_117 and

the second between IgG Histidine₄₃₅ and FcRn Glutamine₁₃₂. In addition there is a strong hydrophobic interaction between IgG Isoleucine₂₅₃ and FcRn Tryptophan₂₅₃ (Ghishan, et al., 2006). Modification of Histidine 310, Histidine 435 or Isoleucine 253 to alanine in IgG results in dramatically reduced or completely ablated binding of FcRn (Dall'Acqua, et al., 2002) (Kabat, et al., 1991). The same residues are conserved in mouse IgG1 and their mutation again results in decreased binding to mouse FcRn, additionally mutation of Valine 250 to Glutamine has been shown to result in increased binding of mIgG1 to mFcRn (Raghavan, et al., 1995) (Dall'Acqua, et al., 2002).

The importance of histidine residues in the FcRn-IgG binding interaction can help explain the pH dependence involved in IgG transcytosis (Roopenian & Akilesh, 2007). In the endosome, where binding occurs, the pH is slightly acidic at 6.0 - 6.5. Under these conditions histidine residues protonate and permit the salt bridge stabilisation of the IgG-FcRn complex. At the neutral pH encountered in the interstitium, the histidine residues on IgG re-protonate, removing salt bridge stabilisation of the complex and promoting dissociation of IgG from the receptor (Vaughn & Bjorkman, 1998).

In summary, a mechanism exists by which IgG can be actively transported across the pulmonary epithelium, therefore the pulmonary clearance of IgG should occur at a faster rate than would be expected from diffusion controlled pathways alone. However, the relative

contributions of both diffusion and transcytosis in terms of IgG crossing the pulmonary epithelium are not known.

1.5.4 FcRn Expression and activity in the lung

FcRn is expressed in a wide range of tissues and on the majority of cell types. There has been some research into the expression of FcRn in the lung although the results are contradictory. A study by (Spiekermann, et al., 2002) provides the best evidence for FcRn expression within the human and cynomolgus monkey lungs, with immunohistochemical staining for FcRn showing expression in the bronchial epithelia. There was also evidence of weaker bronchial expression of FcRn in mouse lungs. However, another study (Akilesh, et al., 2007) found no evidence of FcRn expression in either the bronchial epithelium or endothelium of the pulmonary arteries. Other reports of FcRn expression in the mouse lung are also contradictory, with some reporting expression over the entire lung and others reporting no pulmonary expression (Kuo & Avensen, 2011). There is however very strong evidence for the presence of FcRn on alveolar macrophages (Spiekermann, et al., 2002).

It is therefore not certain whether the active transcytosis pathway for IgG is present in the mouse lung. However, work by (Bitonti & Dumont, 2006) has shown decreased transport of inhaled Fc conjugated molecules out of the lung when the IgG-FcRn interaction is disrupted

by mutation of histidine 435 to alanine. This suggests that the active transport pathway is present, however the capacity of the pathway is not currently known.

1.5.5 Importance of the location of the site of action

One further area of complication in determining the ideal distribution of an inhaled antibody is that different biologics will require different final distribution within the lung, which is ultimately dependent on the location of the target. For example, an antibody inhaled for lung cancer treatment would need to be preferentially taken up into the tumour. (Maillet, et al., 2011) have shown that inhaled cetuximab is able to penetrate tumours in the lung *in vivo* and has strong anti-tumour activity. Another example is inhaled granulocyte-macrophage colony-stimulating factor (GM-CSF) a potential treatment for patients with cystic fibrosis, which is expected to act in the alveoli. GM-CSF cannot be dosed via the IV route, due to its high water solubility and large size severely limiting the percentage of the dosed drug able to cross from the bloodstream into the alveoli (L Heslet & Nepper-Christensen, 2012). Inhalation is a convenient way to deposit the desired dose directly into the alveoli, avoiding this problem.

1.6 Conclusions from the literature regarding pulmonary clearance of proteins

The factors determining the distribution of inhaled biologics within the respiratory system are not currently clearly defined and understood (Patton, et al., 2010). At present, very few biologics are formulated for inhalational delivery and their distribution within the lung has tended to be determined on a case by case basis rather than by investigation of the underlying mechanisms. Often formulations are optimised for inhalational delivery based upon desired PK/PD parameters, with no investigation into distribution mechanisms being undertaken.

The surface area of the respiratory tract is very large and antibodies ought to be able to cross the mucosal lining and enter systemic circulation, avoiding first pass degradation in the liver. However, inhalation would also be an ideal delivery route for antibodies against pulmonary targets, where delivery would be directly to the local site of action. This could reduce the dose of antibody required and therefore the cost of the treatment as, with systemic administration of antibody, only a small fraction of the total dose would reach the lining of the respiratory tract. In turn this ought to reduce the levels of systemic toxicity and side effects seen with some current antibody therapeutics.

1.7 Investigating inhalation as a potential delivery route for antibodies

In general it can be considered that there are two different conditions under which antibodies could be delivered by inhalation:

1 – In a situation where it is desirable for the antibody to be retained in the lung at high concentrations, for example, when the antibodies are directed against pulmonary targets, for instance in asthma or chronic obstructive pulmonary disease (COPD) treatment.

2 - In a situation where it is desirable for the antibody to be rapidly absorbed into systemic circulation, as was the case for inhaled insulin.

In order to determine whether inhalation is a feasible delivery route, in either of the conditions discussed above, it is necessary to obtain information about the fate of an antibody following inhalation. Specifically, knowledge is required regarding the rates of antibody transport out of the lung, and the mechanisms by which this transport occurs. Once this information is available then it should become possible to determine the major factors influencing pulmonary antibody clearance and provide strategies to manipulate pulmonary retention time.

1.8 Animal models of lung disease

In the situation where therapeutic antibodies are delivered by inhalation to treat pulmonary disease, the lung encountered by the antibody is expected to differ from the normal healthy lung. As such one of the aims of this work is to investigate the pulmonary transport of antibodies in the diseased lung. This can be achieved *in vivo* using mouse models of lung disease. The most commonly used models of the diseased lung are those models designed to mimic the airway inflammatory and remodelling changes observed in human asthma (Zosky & Sly, 2007).

Asthma is an allergic, chronic inflammatory airway disease with several characteristics including, airway inflammation which is eosinophilic in nature, airway hyperresponsiveness (excessive constriction of the airway smooth muscle in response to spasmogens), acute sudden onset airway obstruction that can be fatal if not reversed and underlying structural changes within the lung (Fish & Peters, 1999) (Fanta, 2009). These structural changes are termed airway remodeling and involve fibrosis in the airway walls, goblet cell hyperplasia, smooth muscle thickening and increased collagen deposition (Bousquet, et al., 2000). Asthma is generally considered to be Th2 driven, with the immune response being driven by IL-4, IL-5, IL-9 and IL-13 and leading to both increased serum IgE levels and to the production of allergen specific IgE (Barnes, 2001).

There are numerous animal models of asthma available across a variety of species, including the mouse (Bates, et al., 2009), rat (Martin & Tamaoka, 2006), guinea pig (Ricciardolo, et al., 2008), dog (Chapman, 2008) and monkey (Coffman & Hessel, 2005); However, no current animal model reflects all the hallmarks of human asthma.

1.8.1 Mouse models of asthma

The mouse is a convenient species for the study of asthma, as there are a wide variety of mouse specific reagents available, which aids in the analysis of ex-vivo samples and there is also detailed knowledge available of both mouse physiology and genetics (Busse & Holgate, 2008). Mice do not spontaneously develop asthma, however numerous studies have shown that mice can be sensitised to a wide range of antigens, including ovalbumin (Kumar, et al., 2008), LPS (Smith & Herschman, 2004), house dust mite extract (Johnson, et al., 2004) and ragweed (Yadav, et al., 2009). Protocols generally involve sensitisation of animals to allergen, followed by allergen challenge and can be split into either acute or chronic models.

1.8.2 Acute mouse models

Acute mouse models of asthma generally last over 7-14 days. Sensitisation is usually achieved in the presence of an adjuvant, which reduces both the time and dose required for sensitisation (Blyth, et al.,

1996). Additionally, adjuvants such as aluminium hydroxide have been shown to drive the formation of a Th2 based immune response, which is characteristic of human asthma (Fuchs & Braun, 2008). The allergen (usually ovalbumin) and adjuvant are usually given via the intraperitoneal route as systemic sensitisation has been shown to be more rapid and robust than for example inhalational sensitisation. Following sensitisation the animal is challenged by inhalation of the allergen.

Acute mouse models do result in some of the changes observed in human asthma, including airway inflammation, goblet cell hyperplasia, airway hyper-responsiveness (AHR) and high levels of IgE. However, the airway remodeling observed in asthmatic patients is not present and both airway inflammation and hyper-responsiveness can resolve following the final challenge (McMillan & Lloyd, 2004). Acute models have been used to successfully probe the underlying cell signaling mechanisms involved in asthma, identifying numerous targets for research into novel asthma treatments. However, several treatments which function in the acute mouse model have proven ineffective in clinical trials. For example acute mouse models highlighted IL-5 as a key factor in the development of AHR, with IL-5 knock out mice not developing AHR or allergic airway inflammation (Foster, et al., 1996) (Cho, et al., 2004), however IL-5 antagonists had less clinical benefit than expected, with no effect observed on the forced expiratory volume in patients (Kips, et al., 2003).

1.8.3 Chronic mouse models

Chronic exposure protocols were developed as an attempt to overcome the limitations of the acute mouse models. The chronic exposure protocols aimed to reproduce the airway remodeling observed in human disease in the hope that this would result in models that were more predictive of efficacy in the clinic (Lloyd, 2007). Ovalbumin (Wegmann, 2008) and HDM (Kim, et al., 2009) are the most commonly used allergens in the chronic mouse models, with ovalbumin given intraperitoneally, subcutaneously or intranasally with aluminium hydroxide three times per week over an average of 2 - 3 months (Nials & Uddin, 2008).

In these chronic ovalbumin models, protocols have been carefully fine tuned to minimise tolerance to the allergen developing, which generally involves careful control of the dose of allergen received, especially via the intranasal route (Kumar, et al., 2008). HDM extract is generally given intranasally, 3 - 5 times per week over 5 - 10 weeks (Rydell-Tormanen, et al., 2008). There has been no evidence of tolerance to HDM developing, perhaps due to HDM being an allergen to which animals would ordinarily be exposed. This also makes HDM extract a more clinically relevant allergen and it is important in the development of human asthma (Saglani, et al., 2009). However, the fact that HDM is a clinically relevant allergen is of less importance than developing a clinically predictive mouse model of asthma.

Both the ovalbumin and HDM chronic models result in the development of some of the features of human asthma. There is a predominantly Th2-dependent allergic response, with marked eosinophilia in the airways and robust AHR (Nials & Uddin, 2008). Importantly there is significant evidence of airway remodeling with goblet cell hyperplasia, smooth muscle hypertrophy and epithelial metaplasia (McMillan & Lloyd, 2004). In contrast to the acute models, the inflammatory and airway remodeling changes observed in the chronic models have been shown to persist following delivery of the final dose of allergen (Kumar, et al., 2004). As yet no novel compounds tested in the chronic mouse models have been tested in the clinic, however the response to corticosteroids (McMillan & Lloyd, 2004), leukotriene antagonists (Henderson, et al., 2002) and phosphodiesterase 4 inhibitors (Herbert, et al., 2008) is in line with what is observed in the clinic.

1.8.4 Strain differences

One complication in the development and implication of mouse models of asthma is variation in response to allergen between strains (Boyce & Austen, 2005). Ultimately the optimal protocol for sensitisation and challenge must be determined independently for each strain (Shinagawa & Kojima, 2003). BALB/c mice have been shown to develop increased levels of AHR than C57BL/6 mice in response to the same ovalbumin sensitization and challenge protocol (Takeda, et al., 2001). In contrast, levels of eosinophils and neutrophils recoverable in

bronchoalveolar lavage fluid (BALF) are greater in C57BL/6 mice than BALB/c (Gueders, et al., 2009). Additionally, there are differences observed in the cytokine expression levels between the two strains with BALB/c showing increased IL-4, IL-5, IL-13, and CCL11 expression levels and C57BL/6 showing higher CCL11 and CCL5 expression (Gueders, et al., 2009).

1.9 Imaging pulmonary antibody clearance *in vivo*

There are a number of imaging techniques currently available, which can provide a great deal of information about the structure and function of organs and systems within the body. In this project, the focus is on delivery to the lung, therefore information regarding lung structure, function and both the pulmonary and systemic distribution of inhaled antibodies over time is desirable. This can be achieved by making use of both Computed Tomography (CT) and Single Photon Emission Computed Tomography (SPECT) imaging to provide structural information regarding the lung and information regarding the spread of inhaled antibodies after instillation.

1.9.1 SPECT/CT

A CT scan is in essence a 3D X-ray, determining the X-ray density of each specific point and creating a 3D representation of these density differences. Areas of high density, such as bones, show up bright white

and areas of low density, such as the air filled lungs, show up black. CT scans provide very high levels of detail regarding the anatomy of a test subject, either human or animal (Delbeke & Isreal, 2009).

A SPECT scan produces a result similar to a CT scan, in that SPECT measures the density of radiation at specific points and builds up a 3D representation of the distribution of radiation within a subject. In most cases a gamma emitting isotope, such as ^{99m}Tc or ^{123}I is introduced into a subject and its progress followed over time using SPECT (Chatziioannou, 2005). SPECT is used extensively in the pre-clinical testing of pharmaceuticals (Franc, et al., 2008) and in clinical settings to image myocardial perfusion, tumours and brain activity (Mariani, et al., 2010).

By combining the anatomical detail of a CT scan with the radioactivity map from a SPECT image, the radioactivity within a subject can be localised. The two images (CT and SPECT) must be generated with the subject in a fixed position, so that the images can be fused. The CT image is in essence a 3D X-ray of the animal and provides anatomical information, which is overlaid with the 3D radioactivity map provided by the SPECT image. This results in an easily interpretable qualitative picture of the 3D distribution of the radiolabel within the animal, the results of which can be quantified in terms of levels of radioactivity within a given region of interest.

In this project a combination of CT/SPECT will be used to provide both structural data regarding the anatomy of the animal from CT and functional data of pulmonary antibody clearance from SPECT, using radiolabelled antibodies. By overlaying the CT and SPECT images the distribution of the radiolabelled antibody can be determined within the animal over time.

A radiolabel will need to be introduced to the antibodies investigated in order to facilitate SPECT imaging. The chemistry to introduce the radioactive isotope ^{99m}Tc onto various proteins, including antibodies is well established (Mather & Ellison, 1990). The reaction is a two step process where disulphide bridges in the antibody hinge region are reduced to give free thiol (-SH) groups, which are then reacted with technetium to give the radiolabelled antibody.

1.9.2 SPECT imaging

SPECT imaging is based on the detection of gamma radiation which is emitted from the nucleus of radioactive isotopes during radioactive decay. Gamma rays are detected by scintigraphy and the detector in the SPECT imager is a single thallium doped sodium iodide crystal (DePuey, et al., 2000). When a gamma ray hits the crystal the energy is sufficient to excite an electron from the valence band to the conductance band. When the excited electron returns to the ground state a photon is released. This causes the generation of a flash of light

when a gamma ray hits the crystal and is termed scintigraphy (Knoll, 2010). Detection of the emitted photons results in current generation and the magnitude of the current generated at each point over the surface of the detector produces a map of intensity proportional to the intensity of gamma ray emission in the subject being imaged.

One drawback of using scintillation as a detection method is that any incident gamma ray hitting the detector results in current generation, in reality it is necessary to constrain the incident radiation in order to produce a clear image. In order to accurately relate the current generated to a specific location within the subject it is necessary to limit the gamma rays hitting the detector to those which are emitted perpendicular to the detector. This is achieved using a collimator. In SPECT imaging, a collimator generally consists of a sheet of lead drilled with small (3-5 mm) holes, which covers the entire detector. Lead effectively blocks gamma rays, so only radiation parallel to the holes (perpendicular to the detector) reaches the crystal (Knoll, 2010).

In small animal imaging, where the subject is small compared to the size of the detector, a pinhole collimator is generally employed. This limits the detectable gamma rays as described above, but also acts to magnify the detected image in a similar way to how a pinhole camera projects an optical image. A schematic of a pinhole collimator can be seen in Figure 1.9.

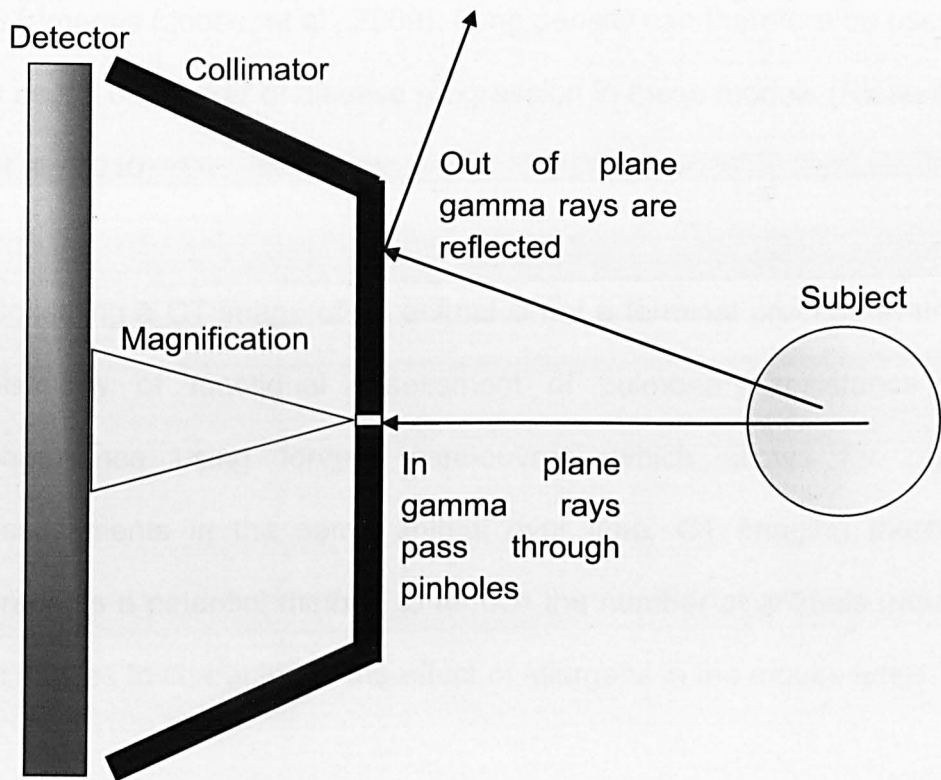


Figure 1.9 - Diagram showing effect of pinhole collimator in SPECT imaging.

In order to build up a 3D image the detector is rotated around the subject. Usually two detectors are held parallel on opposite sides of the subject and rotated around 180° , this results in a 360° image generated in half the time taken for one detector to travel 360° .

1.9.3 CT Imaging in small animal models of asthma

CT imaging presents a non-invasive method to assess the extent of the structural and functional changes that occur in rodent models of lung disease. The inflammatory changes in the lung observed in small animal models of asthma have the effect of increasing airway thickness, which has been shown to result in changes in lung density in

CT images (Jobse, et al., 2009). Lung density can therefore be used as a useful biomarker of disease progression in these models (Riesenfeld, et al., 2010).

Collecting a CT image of an animal is not a terminal procedure, unlike histology or functional assessment of pulmonary resistance and compliance using forced manoeuvres, which allows for repeat assessments in the same animal over time. CT imaging therefore presents a potential method to reduce the number of animals required in studies to characterise the effect of allergens in the mouse lung.

1.10 Aims and Objectives

The overall aim of this project is to determine whether inhalation is a feasible route of delivery for therapeutic antibodies, particularly antibodies against pulmonary targets.

More specifically, the aim is to produce a reliable experimental and data analysis procedure to accurately determine the redistribution pattern of an inhaled antibody *in vivo*, which can be applied to any antibody and in models of diseased lungs.

This principal aim can be further broken down into the following objectives:

- To establish a set of techniques which, when combined, can be used to analyse the pulmonary clearance of any antibody
- To establish a method for radio-labeling antibodies, which is simple, fast and stable *in vivo* over at least 24 hours.
- To collect baseline transport data for an inhaled, whole, monoclonal antibody, in the healthy lung
- To investigate the mechanisms by which antibodies cross the lung epithelium by:

- Investigating passive diffusion by comparing the pulmonary retention of antibody fragments and small proteins of differing molecular weights and
 - Exploring the role of transcytosis of antibodies by FcRn by comparison of transport data for studies using mutant antibodies with different binding affinities to FcRn.
- To determine the effect of disease on antibody retention in the lung, determining if lung residency is expected to be sufficiently long to allow successful treatment of asthma/COPD.

1.11 Thesis structure

Chapter 1 – General introduction, review of the relevant literature and statement of aims and objectives

Chapter 2 – Expression and purification of the proteins required for the SPECT/CT imaging experiments – including mutant IgG, antibody fragments and the FN3 protein

Chapter 3 - Set-up and validation of the chemistry to introduce a radiolabel into the antibody, followed by preliminary imaging experiments to assess the stability of the radiolabelled antibody over 24 hrs.

Chapter 4 - SPECT/CT imaging results for the pulmonary clearance rate of a whole monoclonal IgG. Investigation of the mechanism of pulmonary antibody clearance using antibody fragments and mutant IgG with different binding affinities to mFcRn.

Chapter 5 - Further characterisation of the murine HDM model of asthma with CT imaging and assessment of antibody clearance from the diseased lung.

Chapter 6 – Summary of the data generated, overall conclusions and suggestions for future work.

CHAPTER 2: Production of reagents for use in the *in vivo* imaging experiments

2. Overview

This chapter details the work undertaken to produce the reagents required for the *in vivo* imaging experiments designed to determine antibody retention in the lung following intratracheal instillation.

A whole mouse IgG1 was provided by MedImmune, UK. In addition to this two sets of reagents were produced:

For the studies designed to determine the importance of passive diffusion as a pulmonary clearance method two antibody fragments were produced. These were the Fab and scFv fragments of the IgG1 provided by MedImmune as well as the FN3 protein, a single 11 kDa domain of the protein fibronectin with a structure similar to an Ig like β -sandwich fold.

For the studies to determine the importance of the mFcRn receptor in pulmonary antibody clearance three mutant versions of the mouse IgG1 were expressed. The three mutants produced were: (1) an improved mFcRn binder (2) a decreased mFcRn binder and (3) a null binder.

2.1 Introduction

As described in the general introduction in Chapter 1, there are two main pathways by which an inhaled antibody would be expected to cross the pulmonary epithelium. The first pathway is via passive diffusion, the second is transport through the epithelial cells via receptor mediated transcytosis by FcRn. One of the major aims of this work was to determine the relative contributions of these pathways to antibody transport out of the lung.

2.1.1 Investigation of passive diffusion as a transport mechanism for the pulmonary clearance of antibodies

The pulmonary epithelium is not heterogeneous; for example, the epithelium lining in the trachea is ciliated pseudostratified columnar epithelium and is approximately 60 μm thick. In contrast the main cell type lining the alveoli, the type I cell is roughly 0.2 μm deep (Ehrhardt, et al., 2008). Practically it is not possible to investigate passive diffusion across discrete areas of the pulmonary epithelium *in vivo* and as a result the imaging studies will only determine an average contribution for passive diffusion to antibody transport out of the lung. This will be an average value covering transport across the tracheal, conducting airway and alveolar epithelia.

Passive diffusion in general is faster for smaller molecules and slower for larger molecules, with the rate of passive diffusion inversely proportional to the molecular weight. The basis for this dependence on molecular weight, as determined by Fick's Law, is described in more detail in section 1.5.1.

In order to determine whether passive diffusion is an important mechanism in the pulmonary clearance of antibodies, the transport of the whole antibody will be compared to the transport of antibody fragments. The Fab (50 kDa) and scFv (28 kDa) fragments of the whole IgG (150 kDa) model antibody were expressed, the structures of which are shown in Figure 2.1.

The FN3 protein, an 11 kDa single domain of fibronectin will also be tested, in order to provide clearance data for a species smaller than an scFv. The FN3 protein is a single domain of fibronectin type III, which contains the same Ig-like beta sandwich fold, as the antibody fragments, although the number and arrangement of the outer strands differs from those found in the antibody variable domains (Clarke, et al., 1999).

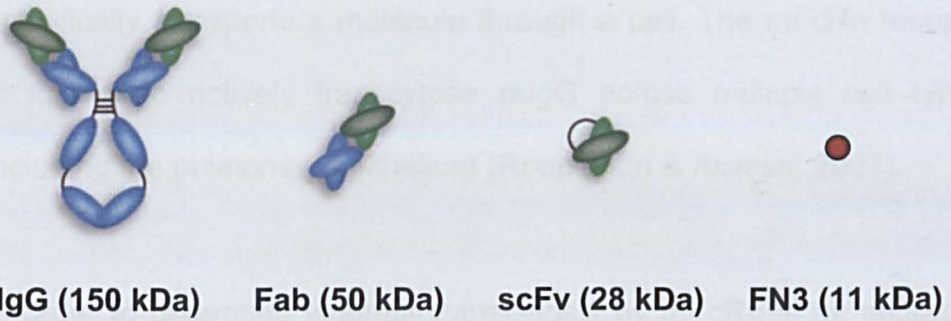


Figure 2.1 - Pictures showing the structures and relative sizes of the proteins which will be investigated in the SPECT/CT imaging studies. Blue colour signifies antibody constant regions, green colour signifies antibody variable regions and red colour signifies Fibronectin III regions.

If the whole IgG is transported out of the lung by diffusion controlled processes then comparison of the results for these two fragments and the whole IgG are expected to show linear trends. One complication is that there are two possible passively diffusion controlled pathways that an antibody could be transported out of the lung by (Patton, 1996). Firstly there is diffusion between the epithelial cells and secondly there is non-specific transcytosis through the epithelial cells. Although it will not be possible to differentiate between these two pathways, the extent to which passive transport is important in pulmonary antibody clearance, is obtainable.

2.1.2 Investigation of transcytosis by mFcRn as a mechanism for the pulmonary clearance of antibodies

In contrast to passive diffusion controlled transport, receptor mediated transcytosis is an active uptake mechanism where a receptor

specifically transports a molecule through a cell. The mFcRn receptor is known to actively transcytose mIgG across multiple cell types, including the pulmonary epithelium (Roopenian & Akilesh, 2007).

In order to determine whether transcytosis by mFcRn is an important pathway in the pulmonary clearance of antibodies, mutant versions of the original whole IgG are required. Several single amino acid point mutations to the heavy chain of mIgG1 antibodies have been shown to alter binding to mFcRn and based upon mutations detailed in the literature three useful mutations were identified (Dall'Acqua, et al., 2002). The V250Q mutant where valine 250 is mutated to glutamine is known to improve binding of mIgG1 to mFcRn. The H435A mutant where histidine 435 is mutated to alanine shows either completely ablated or significantly reduced binding to mFcRn. The double mutant H435A_I235A where both the histidine 435 and isoleucine 253 residues have been mutated to alanine has been shown to completely ablate binding to mFcRn.

As these mutants would have differing binding affinities to mFcRn if transcytosis by mFcRn is important in pulmonary antibody clearance, then transport out of the lung ought to be faster for improved mFcRn binders (V250Q) and slower for reduced or null mFcRn binding mutants (H435A and H435A_I253A), when compared to wild type (WT). As a minimum, if active transcytosis by mFcRn is involved in

pulmonary antibody clearance, then the clearance profiles of these mutant mIgG would be expected to differ.

2.2 Materials and methods

2.2.1 Materials

The following were provided by MedImmune, UK

- Whole IgG heavy chain in the expression vector pEU 23.3.
- Whole IgG light chain in the expression vector pEU 22.2.
- Purified Fab-HIS10 heavy chain DNA in nuclease free water.
- Purified scFv-HIS10 DNA in nuclease free water.
- FN3cys2-HIS10 protein in pET expression vector.
- Forward and reverse oligonucleotides of the correct sequence to introduce the desired point mutations (H435A, I253A and V250Q) into the whole mIgG1 heavy chain.
- M20A feed – proprietary CHO cell medium containing FBS and glucose, designed to provide optimal protein expression in CHO cells.
- Biotinylated mouse FcRn complexed with mouse beta-2-microglobulin (the stable *in vivo* form of the receptor).

For expression the following media were used:

- 2TY media (per litre):
10 g yeast extract, 16 g tryptone, 5 g NaCl in distilled water.

- Super broth (per liter):
24 g yeast extract, 12 g bacto-tryptone, 5 mL glycerol, 72 mM potassium phosphate dibasic, 17 mM potassium phosphate monobasic, 100 mL 20% glucose.

2.2.2 Methods

2.2.2.1 Preparation of DNA for transfection and/or SDM

Whole IgG heavy chain in the expression vector pEU 23.3 and whole IgG light chain in the pEU 22.2 expression vector were provided by MedImmune UK. 1 μ L of each was transformed into z competent DH5 α *E.coli* cells as follows:

2TY agar plates were dried at 37 °C and a single aliquot of DH5 α z-competent cells were thawed on ice. A total of 100 μ L DH5 α cells per transformation were transferred to pre-chilled microfuge tubes on ice and 2 μ L DNA was added to each aliquot of cells. The cells were mixed gently before incubation on ice for 10 min. Then 50 μ L cells from each transformation were plated and grown overnight at 37 °C. A single colony was picked from each 2TY agar plate and grown for 8 hours in 5 mL 2TY medium plus 100 μ g/mL ampicillin.

The DNA was harvested using a Qiagen mini-prep kit according to the following protocol (Qiagen, 2006). The cells were pelleted for 10 min at

2000 g in a bench top centrifuge and the supernatant discarded. The pellet was re-suspended in 0.5 mL 2TY medium and transferred to a 1.5 mL microfuge tube. The cells were re-pelleted at 3500 g for 5 min in a table-top microfuge and the media removed. The cells were re-suspended in 250 μ L buffer P1 and 250 μ L buffer P2 and the tube inverted 4 times to mix thoroughly. 350 μ L buffer N3 was added, the tube inverted 4 times until a homogenous colourless suspension was achieved, then the tube was centrifuged at 3500 g for 10 min in a table top microfuge. The supernatant was transferred to a Qiagen mini-prep column, centrifuged for 1 min and the flow through discarded. The column was washed with 0.5 mL buffer PB, centrifuged for 1 min and the flow through discarded. The column was washed with 0.75 mL buffer PE, centrifuged for 1 min and the flow through discarded. The column was centrifuged for a further 1 min, to remove any residual wash buffer and the flow through discarded. The column was transferred to a fresh microfuge tube and 50 μ L nuclease free water added to the centre of the column, allowed to stand for one min, then centrifuged for 1 min.

DNA concentrations were then measured by absorbance at 260 nm. The absorbance of a 50 μ g/ml double stranded DNA solution at 260 nm is 1.0 and this relationship can be used to determine the concentration of the unknown DNA sample.

2.2.2.2 Site directed mutagenesis

Site directed mutagenesis (SDM) was used to introduce point mutations to the IgG WT heavy chain DNA. The SDM was achieved using a polymerase chain reaction (PCR) method. In general, a PCR mix was set up with 1 μL heavy chain DNA template at 50 $\mu\text{g}/\text{ml}$, 2.5 μL DMSO (5%), 25 μL , 2x Phusion mastermix (New England BioLabs Inc.), 17.5 μL NFW and 2 μL each of the appropriate forward and reverse oligonucleotides at 100 ng/ml . A negative control of PCR mix using 4 μL NFW instead of oligonucleotides was also used. Optimum conditions used in the PCR reactions varied for each mutation.

For the PCR to generate the H435A mutant, the conditions were as follows: initial denaturation at 98 $^{\circ}\text{C}$ for 30 s, followed by 30 cycles of denaturation at 98 $^{\circ}\text{C}$ for 10 s, annealing at 60 $^{\circ}\text{C}$ for 20 s and elongation at 72 $^{\circ}\text{C}$ for 5 min, final elongation was then at 72 $^{\circ}\text{C}$ for 10 min.

For the V250Q mutant, the conditions used in the PCR reaction to correctly produce the mutant were: initial denaturation at 98 $^{\circ}\text{C}$ for 30 s, followed by 30 cycles of denaturation at 98 $^{\circ}\text{C}$ for 10 s, annealing at 55 $^{\circ}\text{C}$ for 20 s and elongation at 72 $^{\circ}\text{C}$ for 5 min, final elongation was then at 72 $^{\circ}\text{C}$ for 10 min.

To give the double mutant, the I253A mutation was introduced into the H435A mutated heavy chain DNA. The PCR mix was prepared as before, using the H453A heavy chain DNA as the template and the PCR reaction run using the same conditions as for the original introduction of the H435A mutation into the WT heavy chain DNA.

Following the PCR reaction 1 μ L DpnI was added to each reaction to facilitate digestion of the template plasmid and digestion allowed to proceed at 37 °C for 1 hour. Then 5 μ L of each reaction was transformed into z competent DH5 α cells, plated onto 2TY agar plates and grown overnight at 37 °C (as described in detail in section 2.1.1)

Provided that no colonies had grown on the negative control plate, single colonies from the reaction plates were picked and grown overnight in 5 mL 2TY media, plus 100 μ g/mL ampicillin. Mini-preps of the DNA from each clone were completed as described in section 2.1.1 and sequenced. Sequencing results were analysed in Sequencher 4.0.

2.2.2.3 CHO cell expression of proteins

All of the mutant antibodies and antibody fragments produced were expressed in a Chinese hamster ovary (CHO) cell line. For all protein expressions 500 mL CHO cells in CD-CHO medium (Invitrogen), at a density of 1×10^6 cells/mL were prepared in roller bottle culture vessels with 0.05 mM penicillin and 0.05 mM streptomycin antibiotics.

For the scFv fragment, purified DNA was diluted to a concentration of 62.5 µg/mL in 8.2 mL CD-CHO medium (Sigma Aldrich). 8.2 mL of the transfection promoter poly(ethylenimine) (PEI) (Sigma Aldrich) at 720 µg/ml) was added to the diluted DNA, vortexed for 10 s and added to the 500 mL of CHO cells after a one minute incubation at room temperature.

For expression of the mutant IgG heavy chain DNA encoding the desired mutation, was diluted to 30 µg/mL in 8.2mL CD-CHO medium. Wild type light chain DNA was also prepared at 30µg/mL in 8.2mL CD-CHO medium. 8.2 mL PEI at 360 µg/mL was added to both the heavy and light chain DNA. The DNA/PEI mixes were vortexed for 10 s before being added directly to the same 500 ml CHO cells following a one minute incubation period at room temperature.

For the Fab fragment, the above procedure for whole IgG mutants was repeated using Fab heavy chain DNA, as provided by MedImmune UK.

Both the cultures for the fragments and mutants were then fed with M20A medium (as described in section 1.1) according to the following schedule: 100 mL per 500 mL culture 4 hrs post transfection, 50 mL per 500 mL culture 3 days post transfection and 100 mL per 500 mL culture 7 days post transfection. After 10 days, the cell culture supernatants were harvested by centrifugation at 2000 g for 30 min. The supernatants were then clarified by filtration through a 0.2 µm filter

to sterilise and to remove any cell debris. Finally supernatants were then concentrated to approx 1200 mL using a 10,000 Da diafiltration unit, then diluted to 4000 mL with DPBS and concentrated back to 200 mL.

2.2.2.4 Bacterial expression of the FN3 protein

1 μ L of the FN3cys2 protein in pET vector provided by MedImmune UK was added to 50 μ L BL21(DE3)star *E.coli*, incubated for 30 min at room temperature then heat shocked at 42 °C for 45 seconds. 0.45 mL 2TY media was added and the transformation incubated at 37 °C for 1 hour with shaking at 300 rpm, before 2 μ L of the transformation was plated onto 2TY+100 μ g/ml ampicillin agar plates and incubated overnight at 37 °C.

A scraping of cells from the transformation plate was added to 100 mL 2TY+100 μ g/mL ampicillin media to form a starter culture and grown overnight at 37 °C with shaking at 250 rpm. The final expression was completed in 4 x 400 mL flasks containing superbrotch medium (as described in section 3.1) with 100 μ g/mL ampicillin. 10 mL of the starter culture was added, then grown at 37 °C with shaking at 250 rpm for 2 hours. The optical density was read and if between 0.6 and 1, then IPTG was added to a final concentration of 0.2 mM. Cells were incubated at 28 °C for a further 4 hours with shaking at 250 rpm before centrifugation at 2000 g for 10 minutes. The supernatant was discarded

and 30 mL BugBuster (Novagen) plus 20 μ L lysonase and 10 μ L benzonase was added to each of the 4 cell pellets. The cells were re-suspended in the lysis mixture and centrifuged at 10,000 g for 30 minutes to pellet insoluble debris. Finally, the lysed cell solution was clarified by filtration through a 0.2 μ m filter.

2.2.3 Purification

2.2.3.1 Protein A affinity chromatography

A 5ml MabSelectSure (GE Healthcare) column was equilibrated with 25 mL cold DPBS (Sigma-Aldrich). The column was then connected to an AKTA explorer FPLC chromatography system (GE healthcare). The concentrated cell culture supernatant was loaded onto the column at a flow rate of 4 mL/min. The loaded column was then washed with 25 mL DPBS at 4 mL/min in order to remove any unbound proteins. The column was then washed with 5 column volumes of PBS, followed by 5 column volumes of 50 mM sodium acetate buffer at pH 5.4. This higher pH wash removes bound impurities from the column, leaving behind bound antibody which was then eluted with 5 column volumes of 50 mM sodium acetate buffer at pH 3.65. 2 ml elution fractions were collected and neutralised with addition of 100 μ L 0.05 M Tris buffered saline at pH 9.0, to increase the pH of the eluted fractions to approximately pH 7.0. This increase in pH improves antibody stability and decreases the risk of protein precipitation.

2.2.3.2 Nickel affinity Chromatography

Two Hi-trap columns (GE Healthcare) were connected in series. The concentrated cell culture supernatant was loaded onto the columns at a flow rate of 4 mL/min. The columns were washed with 5 column volumes 2xDPBS and connected to an AKTA explorer FPLC chromatography system (GE healthcare) The following buffers were prepared: Buffer A = 2xDPBS and Buffer B = 2xDPBS + 400 mM imidazole. Columns were washed with 2 column volumes 0% buffer B, followed by 10 column volumes 10% Buffer B. A gradient elution was performed over 10 column volumes from 10-100% buffer B. Finally the columns were washed with 2 column volumes 100% buffer B.

2.2.3.3 Size exclusion chromatography

A Superdex 75 16/60 gel filtration column (GE Healthcare), was loaded onto an AKTA explorer FPLC chromatography system (GE healthcare) washed with 1.5 column volume milliQ water and equilibrated with 1.5 column volumes DPBS. The protein-containing fractions from the protein A purification were pooled and concentrated to 7 mL in centrifugal concentrators with a 50 kDa molecular weight cut off and mixed with 1 mL 1M TCEP solution. The concentrated, TCEP incubated solution was then loaded onto the gel filtration column in a 10 mL loop and an isocratic elution over 1 column volume was performed in DPBS, at 2.5 ml/min, collecting 3mL elution fractions.

2.2.4 SDS-PAGE

Fractions eluted from the columns during the protein purifications were screened by SDS-PAGE to determine whether they contained the protein of interest. 15 μ L of each protein containing fraction, plus samples of the concentrated media initially loaded onto the column and of the column flow-through, were mixed with 5 μ L 4xLDS loading buffer (Invitrogen) and boiled for 2 minutes. Samples were run on a 4-12% bis-tris NuPAGE gel (Invitrogen), in 1x NuPAGE MES SDS running buffer (Invitrogen) for 40 min at 200 V and 400 mA with the SeeBlue ladder (Invitrogen) as a reference. The gel was stained with instant blue (Invitrogen) and destained in MilliQ water.

2.2.5 Endotoxin removal using a polymixin B – agarose column

10 mL Polymixin B agarose resin (Sigma Aldrich) was manually packed into a disposable plastic column (Sigma Aldrich) and the column washed with 100 mL DPBS. 2.5 mL concentrated FN3 protein in DPBS was loaded onto the column, before elution with 5ml cold DPBS.

2.2.6 Endotoxin testing

The endotoxin levels within the final protein samples were tested using an Endosafe Endotoxin Quantifier and Endosafe Endotoxin Test Cartridges (both Charles River). The quantification of the levels of

endotoxin present in the samples is based upon the reaction of endotoxin with Limulus Amoebocyte Lysate (LAL), the reaction is colourimetric with the colour intensity proportional to the amount of endotoxin present in the sample and calibrated to a standard curve. The test reports the total Eu/mL sample and performs a spike control test which compares an aliquot of test sample to a known endotoxin standard. This test is included to ensure that the test sample does not react unexpectedly with the LAL substrate giving artificially high or low endotoxin level readings. This is important as several common additives, such as EDTA, can affect the accuracy of the test (Charles-River, 2003).

The protein sample was diluted 1:2 in endotoxin free water and 50 µL loaded into each of the four lanes in the endotoxin testing cartridge. The results displayed are the endotoxin level in the sample in Eu/mL and sample %CV. In addition, for the control test, the results are displayed as Spike Eu/LI, Spike %CV and Spike Recovery%.

To be suitable for *in vivo* use the endotoxin test for the sample must report: %CV less than 25%, spike %CV less than 25%, % spike recovery between 50-200% and a final Eu/mg less than 50.

2.2.7 Octet experiments to determine binding affinities of whole IgG mutants to mFcRn

Whole IgG mutants were prepared at 400, 200, 100, 50, 25, 12.5 ng/mL in DPBS + 0.002% Tween 20 at either pH 6.0 or pH 7.4. Biotinylated mFcRn was prepared at 10 µg/mL again in DPBS + 0.002% Tween 20 at either pH 6.0 or pH 7.4. Two different protocols were run: association at pH 6 with dissociation at pH 6 and association at pH 7.4 with dissociation at pH 7.4.

The assay is fully automated, and involves: hydrating the streptavidin biosensors in assay buffer (DPBS at the desired pH) followed by loading of the biotinylated mFcRn onto the streptavidin sensors and gathering of a corresponding baseline for the coated sensors by immersion in fresh assay buffer. The coated sensors are then immersed in sample solution and the association of the two proteins measured, finally the coated sensors are immersed into fresh assay buffer and the dissociation of the two proteins measured. Measurements are based on biolayer interferometry (see section 4.4 for details).

Results for protein association and dissociation for each sensor are background corrected and the mean total of IgG bound to the sensors is plotted for each mutant, expressed as a percentage of the binding of WT IgG to mFcRn.

2.3 Results and Discussion

The Fab and scFv fragments as well as the whole IgG mutants were expressed in CHO cell culture and purified by column chromatography from the concentrated cell culture supernatants. Antibody fragments were purified by nickel affinity chromatography. Whole IgG were purified with Protein A affinity chromatography. Size exclusion chromatography was used as a secondary purification step if the protein product from the initial purification was not sufficiently pure.

The basic principle behind the column purifications is the same in both the protein A and nickel affinity columns, however the chemical make-up of the columns differs to take into account the nature of the protein to be purified. In brief the columns contain a matrix designed to bind to the target protein in a specified buffer but to disassociate in a different buffer. This allows for selective binding of the target protein, followed by controlled elution of the protein from the column (Kastner, 2000).

Protein A affinity columns were used to purify the whole IgG mutants. The columns are packed with beads coated in protein A, which binds to the Fc region of whole IgG at pH5.4 but disassociates at pH3.65. The antibody containing solution is loaded onto the column at pH5.4, and binds to the protein A coated beads. The column is washed with buffer at pH5.4 to remove any unbound proteins from inside the column and the purified antibody is then eluted from the column at pH 3.65.

The Fab and scFv fragments were expressed with a 10-HIS tag in order to allow purification by nickel affinity chromatography. In a nickel affinity or HIS-trap column, gel beads are coated with NiSO₄. In the presence of water this results in free Ni²⁺ ions on the surface of the beads. The nickel ions strongly bind histidine in aqueous conditions, however in the presence of imidazole the binding is disrupted and the bound protein desorbs from the column (GE-Healthcare, 2005).

Size exclusion chromatography was used as a secondary purification step if the initial purification did not result in sufficiently pure protein. In a size exclusion or gel filtration column, the column is packed with small gel beads, which do not bind to the target protein. Instead separation is based on molecular weight. Smaller molecules are more easily caught in the pores between the gel beads, with larger molecules diffusing more easily through the column (Kastner, 2000).

2.3.1 Protein expression

2.3.1.1 Expression and purification of the Fab fragment

The Fab fragment (50 kDa) was expressed with a 10-His tag in CHO cells and purified by nickel affinity chromatography as described in the methods section. The elution trace from the nickel affinity column is shown in Figure 2.2 and shows removal of impurities in fractions A1-A12 before elution of the Fab fragment from fractions C1 to C12,

together with the SDS-PAGE gel showing the protein concentrations of the fractions of interest as well as initial load and column flowthrough.

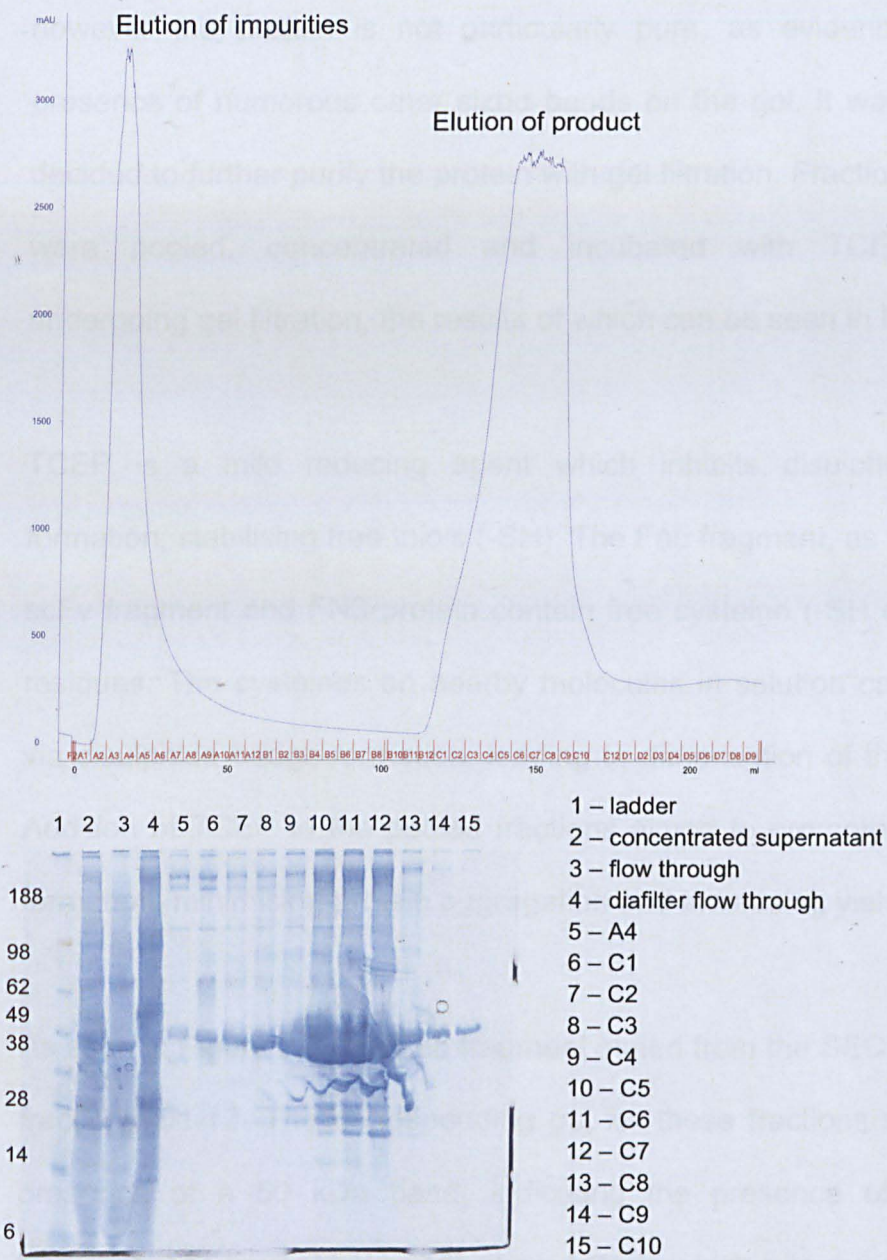


Figure 2.2 - Nickel affinity column elution trace for the Fab fragment (50 kDa), showing the elution of product from Fractions C1-C12 as well as the corresponding SDS-PAGE gel of the protein containing fractions, concentrated cell culture supernatant, diafilter flow through and column flow through.

It can be seen in the gel, in figure 2.2, that the eluted fractions are significantly cleaner than the initial load and column flow through. The strong bands at 50 kDa show the presence of the Fab fragment, however the protein is not particularly pure, as evidenced by the presence of numerous other sized bands on the gel. It was therefore decided to further purify the protein with gel filtration. Fractions C3-C10 were pooled, concentrated and incubated with TCEP, before undergoing gel filtration, the results of which can be seen in Figure 2.3.

TCEP is a mild reducing agent which inhibits disulphide bridge formation, stabilising free thiols (-SH). The Fab fragment, as well as the scFv fragment and FN3 protein contain free cysteine (-SH containing) residues. The cysteines on nearby molecules in solution can interact, via disulphide bridge formation, leading to dimerisation of the product. Addition of TCEP to the pooled fractions aimed to promote monomer formation, minimising protein aggregation and increasing yield.

As seen in Figure 2.3, the Fab fragment eluted from the SEC column in fractions D1-12. The corresponding gel for these fractions shows the presence of a 50 kDa band, indicating the presence of the Fab fragment. The lower MW bands show protein which has reduced in the gel. It was assumed that this is due to boiling the samples before loading onto the gel. Fractions D4-D11 were pooled and concentrated to 7 ml in a 10 kDa cut off centrifugal concentrator. The final yield was determined by A_{280} to be 75mg.

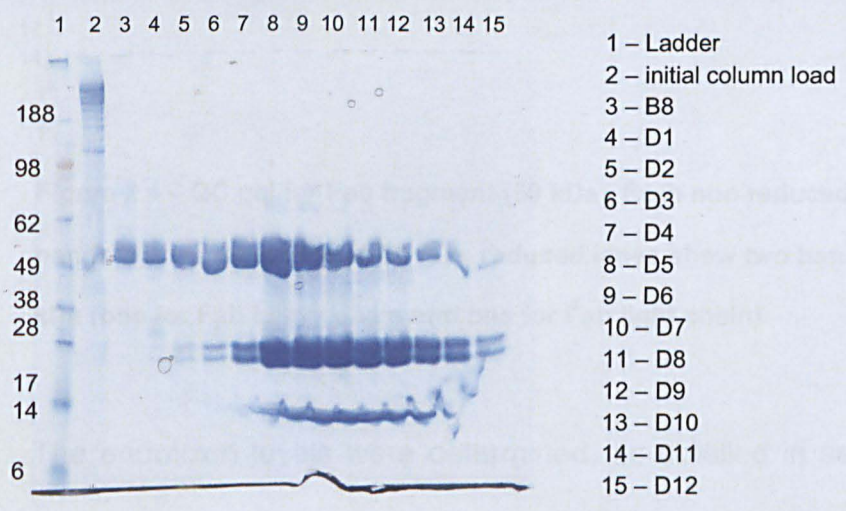
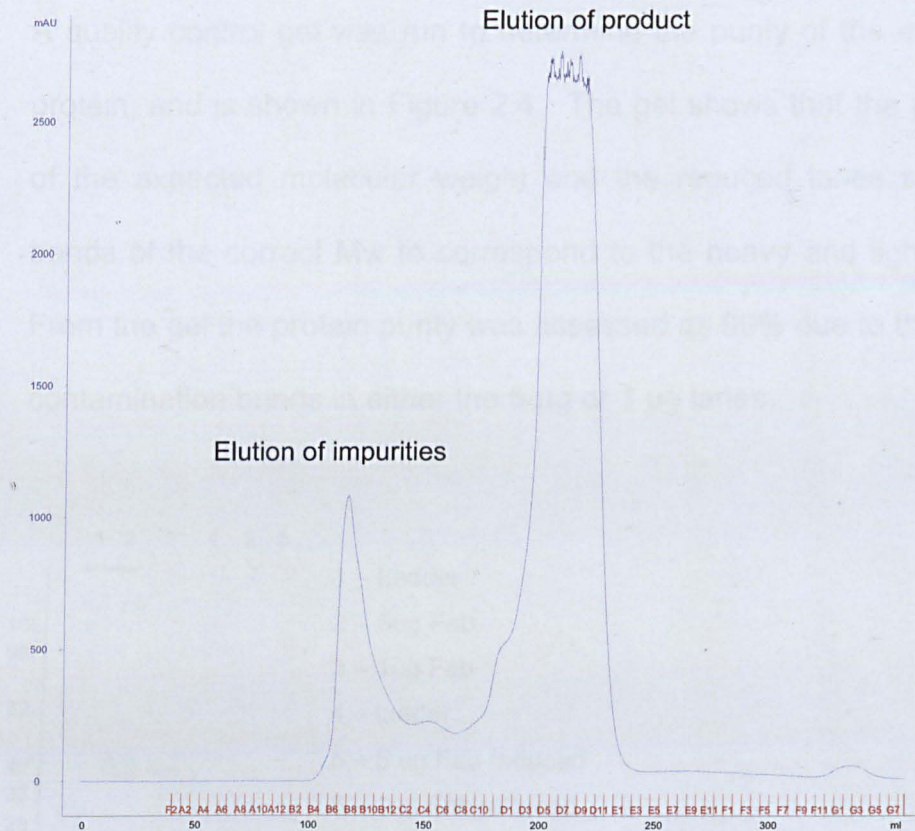


Figure 2.3 - Size exclusion purification elution trace for the Fab fragment (50 kDa), showing elution of product from Fractions D1-D12 as well as the corresponding SDS-PAGE gel of the protein containing fractions and the original Nickel affinity purified protein load.

A quality control gel was run to determine the purity of the expressed protein, and is shown in Figure 2.4. The gel shows that the protein is of the expected molecular weight and the reduced lanes show two bands of the correct Mw to correspond to the heavy and light chains. From the gel the protein purity was assessed as 99% due to the lack of contamination bands in either the 5 μ g or 1 μ g lanes.

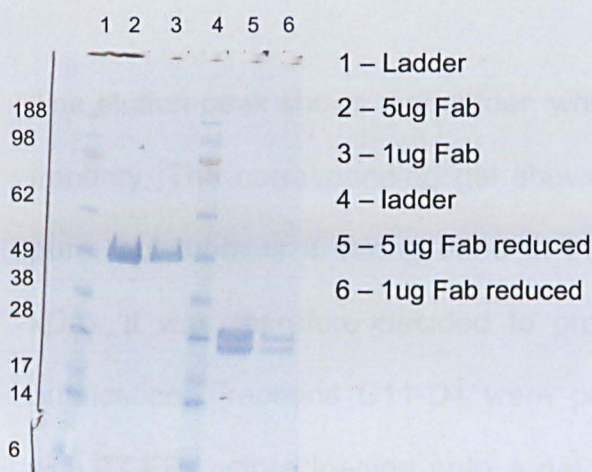


Figure 2.4 - QC gel for Fab fragment (50 kDa). Both non reduced lanes show bands at the correct Mw of 50 kDa, reduced lanes show two bands of approx 25 kDa (one for Fab heavy chain and one for Fab light chain)

The endotoxin levels were determined, as detailed in section 2.2.6 to be 1.028 Eu/mg. The maximum permitted endotoxin level in a product designed to be used *in vivo* is 50 Eu/mg therefore this very low level of endotoxin means that the Fab fragment is safe to use in the *in vivo* images studies.

In conclusion the purity, endotoxin levels and yield of the Fab fragment are all sufficient for the imaging studies.

2.3.1.2 Expression of the scFv fragment

The protein was expressed with a 10-His tag in CHO cells and purified by nickel affinity chromatography and SEC, as described in the methods section. Figure 2.5 shows the elution trace from the His trap column, showing impurity removal in fractions A8-12 and scFv elution in fractions C7-D5.

The elution peak shows a shoulder, which indicates the presence of an impurity. The corresponding gel shows that the eluted protein is not pure, but there is a strong band at the correct molecular weight (28 kDa). It was therefore decided to proceed with further gel filtration purification. Fractions C11-D4 were pooled, concentrated, incubated with TCEP, before loading onto a gel filtration column, the results of which are shown in Figure 2.6.

The elution trace in Figure 2.6 shows two peaks, a large elution peak, with a second shoulder. Fractions covering both peaks were run on the gel shown in figure 2.6. The gel shows the presence of the scFv in fractions C6-D5, these were concentrated to 5ml in a 10kda cut off centrifugal concentrator. The final yield was determined by A_{280} to be 42mg.

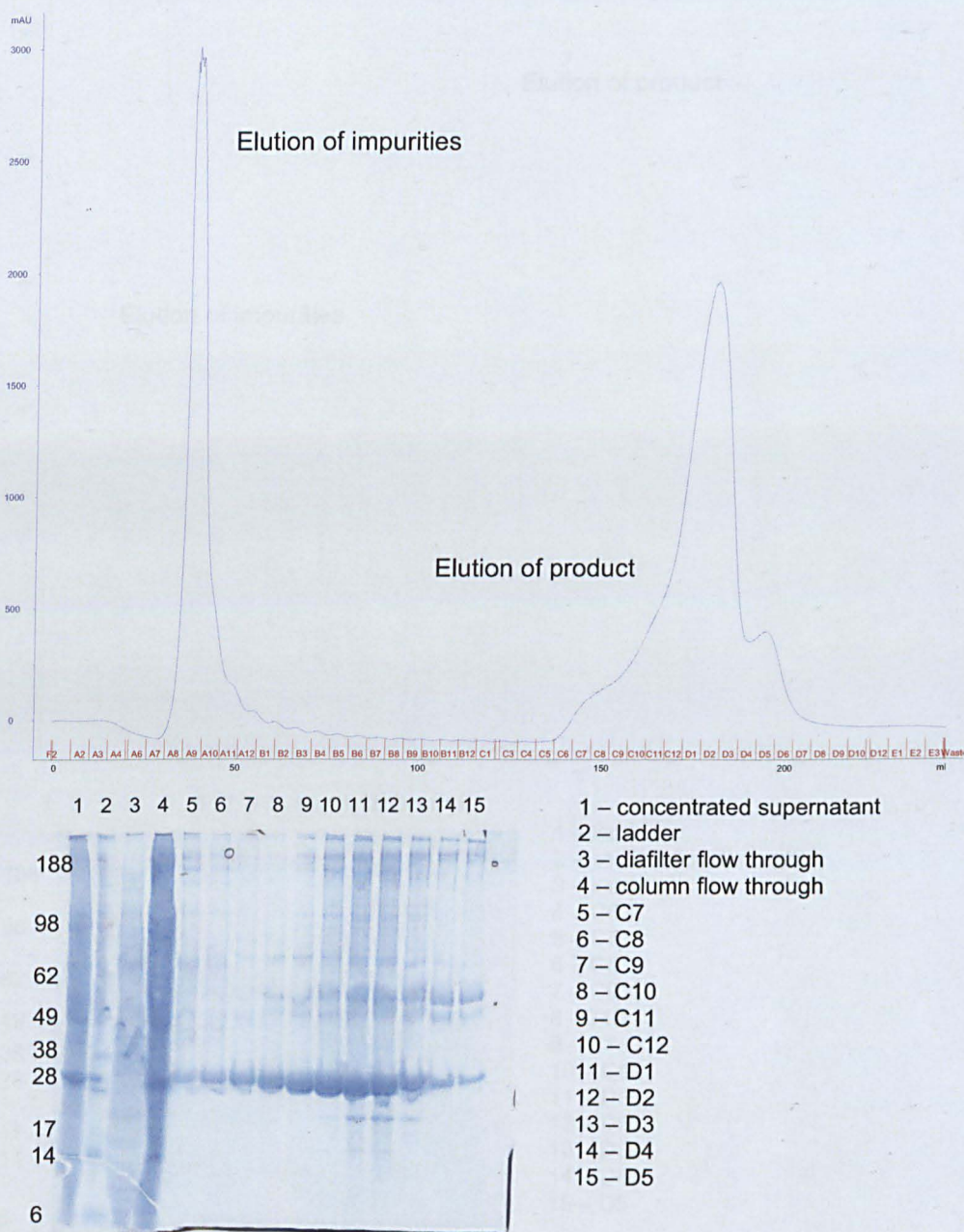


Figure 2.5 - Nickel affinity purification elution trace for the scFv fragment (28 kDa), showing elution of product from Fractions C7-D5 as well as the corresponding SDS-PAGE gel of the protein containing fractions, concentrated cell culture supernatant, diafilter flowthrough and column flow through.

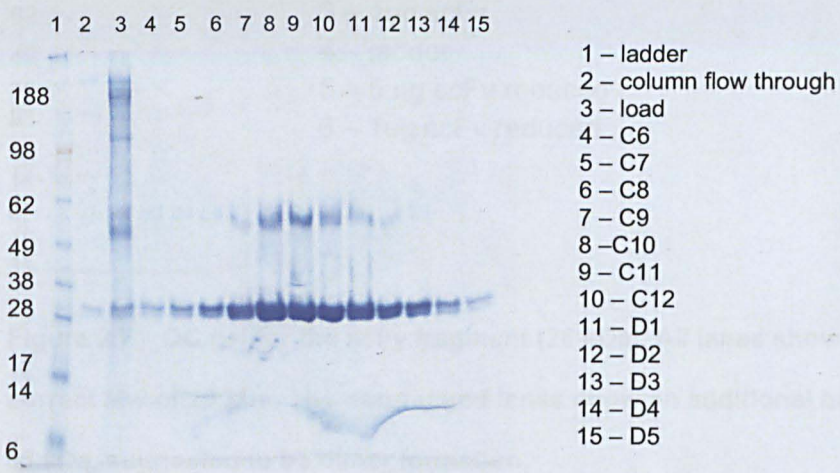
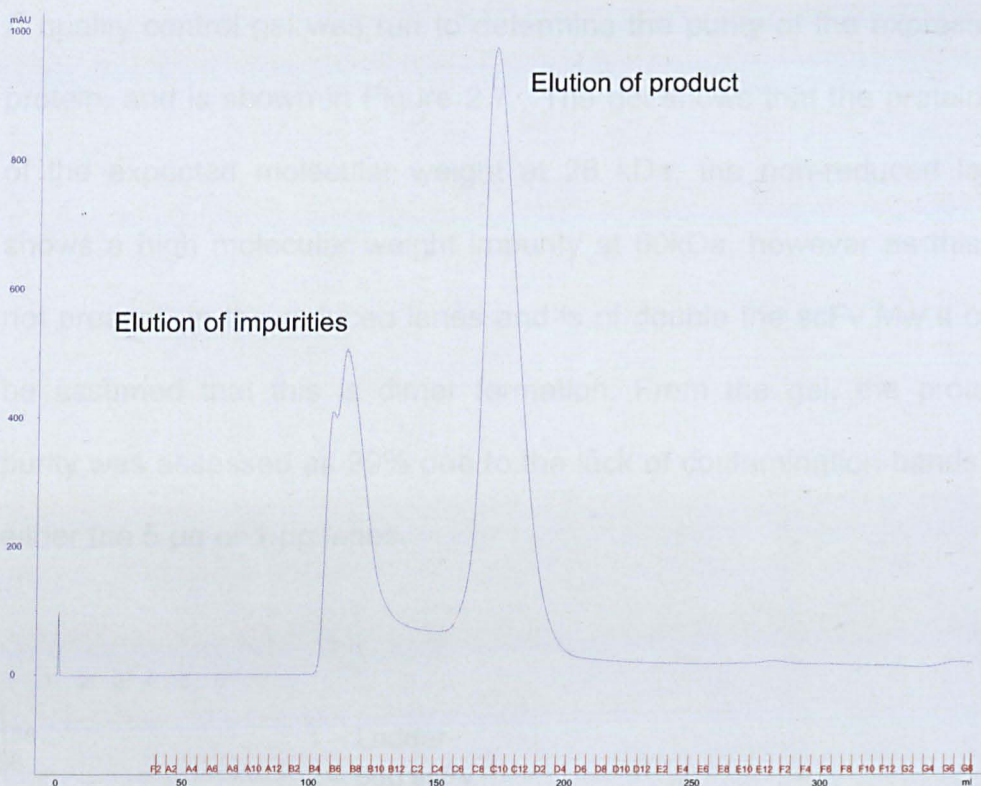


Figure 2.6 - Size exclusion purification elution trace for the scFv fragment (28 kDa), showing the elution of product from fractions C6-D5 as well as the corresponding SDS-PAGE gel of the protein containing fractions, column flow through and the original nickel affinity purified protein loaded.

A quality control gel was run to determine the purity of the expressed protein, and is shown in Figure 2.7. The gel shows that the protein is of the expected molecular weight at 28 kDa, the non-reduced lane shows a high molecular weight impurity at 60kDa, however as this is not present in the reduced lanes and is of double the scFv Mw it can be assumed that this is dimer formation. From the gel, the protein purity was assessed as 99% due to the lack of contamination bands in either the 5 µg or 1 µg lanes.

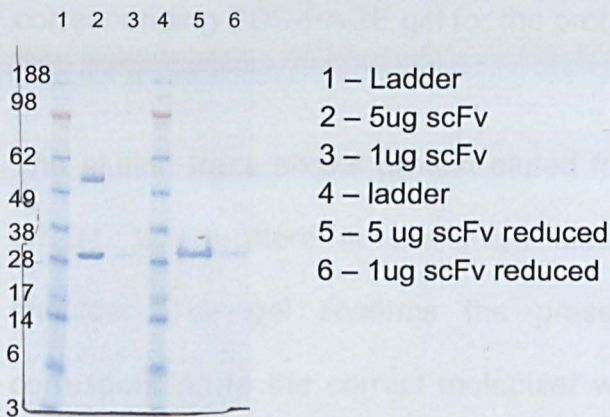


Figure 2.7 - QC gel for the scFv fragment (28 kDa). All lanes show a band at the correct Mw of 28 kDa. The non-reduced lanes show an additional band at approx 55 kDa, suggested to be dimer formation.

The endotoxin levels were assessed as described in section 2.2.6, and determined to be 0.731 Eu/mg. The maximum permitted endotoxin level in a product designed to be used *in vivo* is 50 Eu/mg therefore this very low level of endotoxin means that the scFv fragment is safe to use in the *in vivo* images studies.

In conclusion the purity, endotoxin levels and yield of the scFv fragment are all sufficient for the imaging studies.

2.3.1.3 Expression and purification of FN3 protein

The FN3 protein was expressed with a 10-His tag in BL21(DE3)star *E.coli* and purified by nickel affinity and size exclusion chromatography as detailed in the materials and methods sections. The elution trace from the nickel affinity column is shown in figure 2.8 with the corresponding SDS-PAGE gel for the protein containing fractions.

The elution trace shows protein eluted from the column in fragments C7-D4, where there is one main elution peak with a significant shoulder. The gel confirms the presence of an 11 kDa band corresponding to the correct molecular weight for the FN3 protein in addition to bands at 2 and 3 times the correct molecular weight. It was assumed that these represented dimer and trimer formation. As the protein was not sufficiently pure a further gel filtration purification, preceded by incubation with TCEP to remove dimer and trimer formation, was run. The elution trace and gel for this run are shown in figure 2.9.

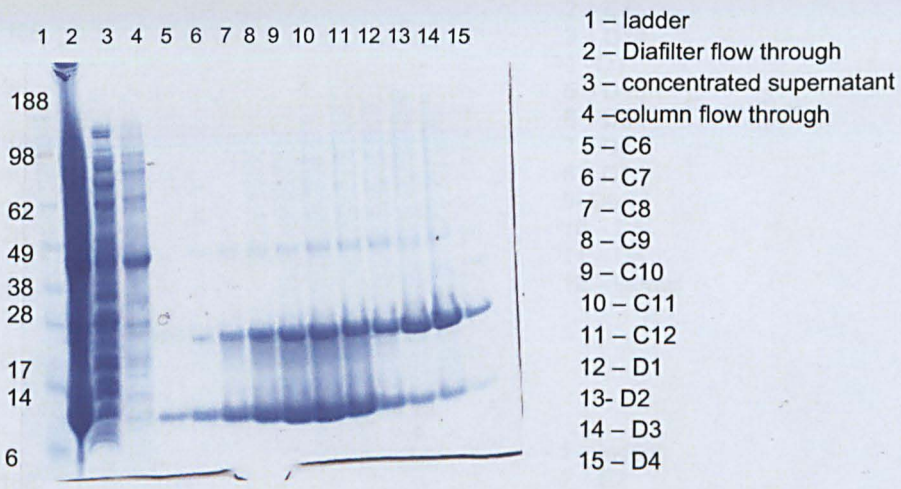
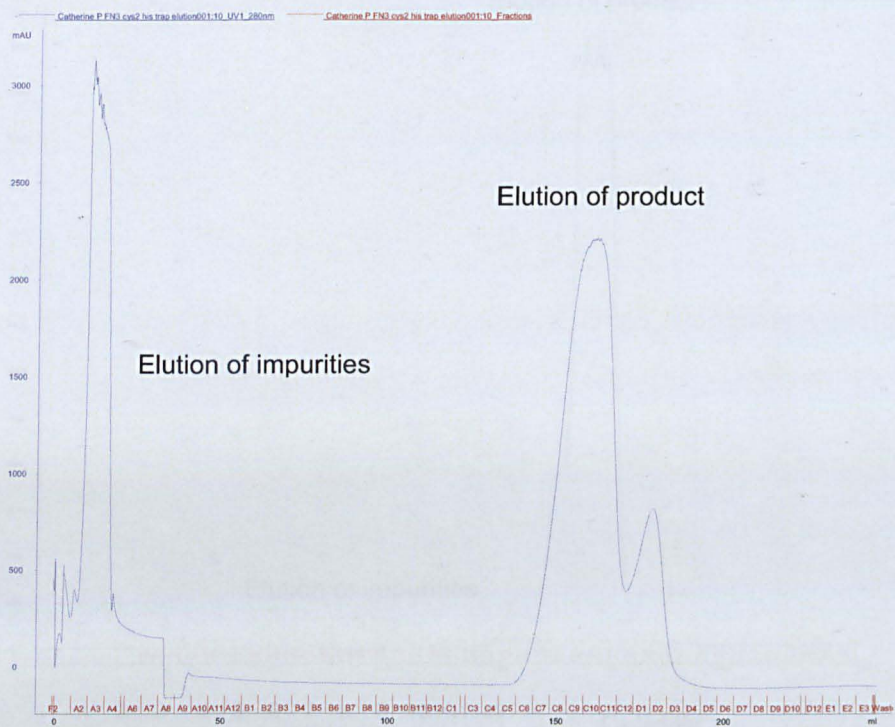


Figure 2.8 - Nickel affinity purification elution trace for the FN3 protein (11 kDa), showing elution of product from Fractions C6-D4 as well as the corresponding SDS-PAGE gel of the protein containing fractions, concentrated cell culture supernatant and column and diafilter flowthroughs.

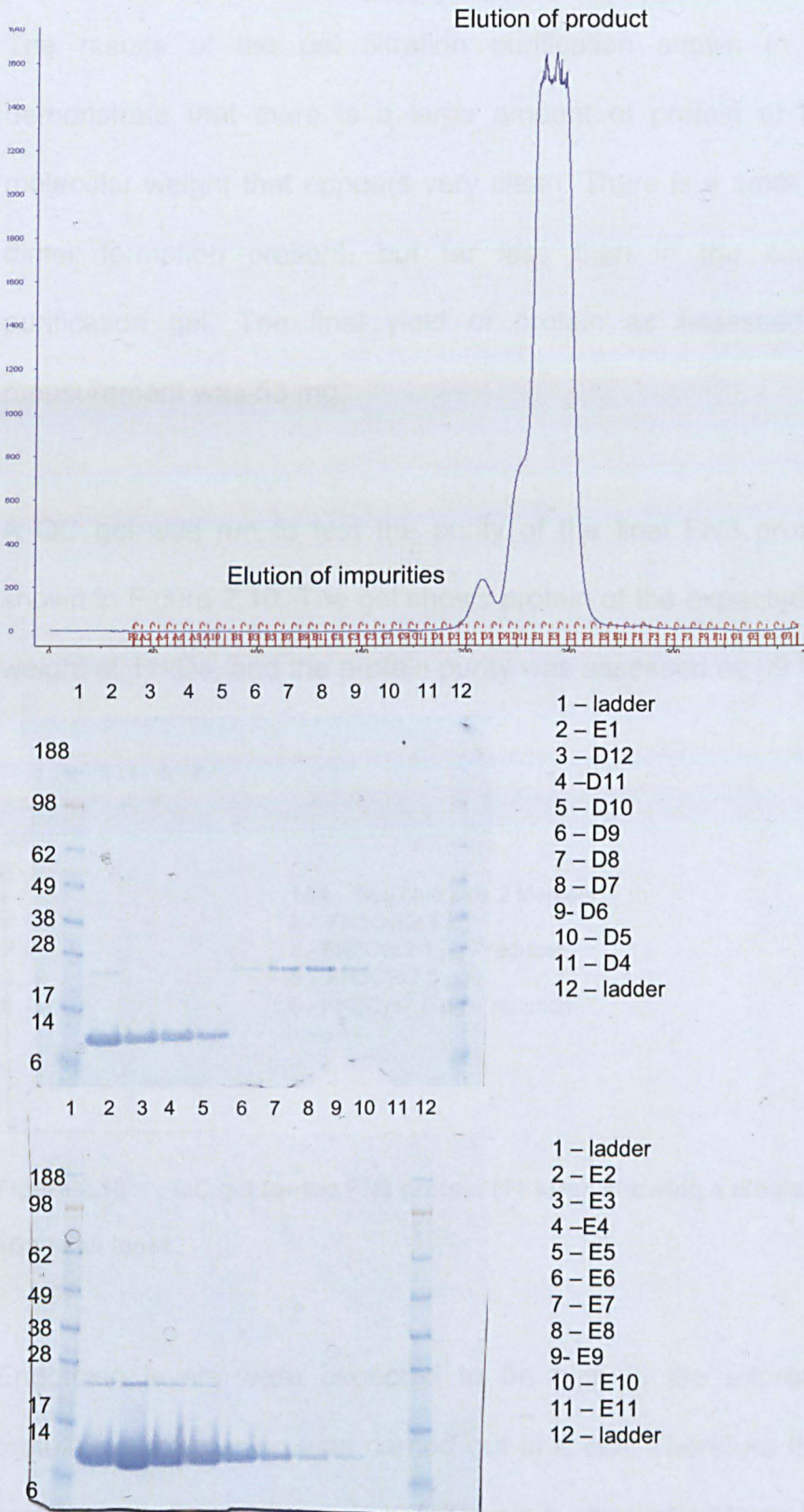


Figure 2.9 - Size exclusion purification elution trace for the FN3 protein (11 kDa), showing the elution of the product from fractions D12-E9 as well as the corresponding SDS-PAGE gel of the protein containing fractions.

The results of the gel filtration purification shown in figure 2.9 demonstrate that there is a large amount of protein at the correct molecular weight that appears very clean. There is a small amount of dimer formation present, but far less than in the nickel affinity purification gel. The final yield of protein as assessed by A280 measurement was 53 mg.

A QC gel was run to test the purity of the final FN3 protein and is shown in Figure 2.10. The gel shows protein of the expected molecular weight at 11kDa, and the protein purity was assessed as 99 %.

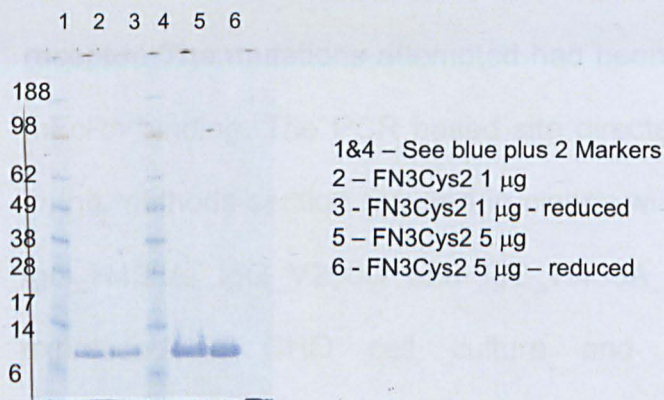


Figure 2.10 - QC gel for the FN3 protein (11 kDa), showing a single band at 11 kDa in all lanes.

Endotoxin levels were expected to be high in the expressed FN3 protein, as expression was carried out in *E.coli*. Therefore the purified protein was passed through a polymixin-b agarose column to remove endotoxin. Following this the endotoxin levels in the sample were assessed as described in section 2.2.6, and determined to be 0.20 Eu/mg. The maximum permitted endotoxin level in a product designed

to be used *in vivo* is 50 Eu/mg therefore this very low level of endotoxin means that the FN3 protein is safe to use in the *in vivo* images studies.

In conclusion the purity, endotoxin levels and yield of the FN3 protein are all sufficient for the imaging studies.

2.3.2 Production and testing of mutant IgG with differing binding affinities to the mFcRn receptor.

Site directed mutagenesis was used to induce point mutations into the heavy chain DNA of the whole IgG to alter binding to the mFcRn receptor. The mutations attempted had been previously shown to alter mFcRn binding. The PCR based site directed mutagenesis described in the methods section resulted in clones with the following mutations, IgG_H435A, IgG_V250Q and IgG_H435A_I253A, which were then expressed in CHO cell culture and purified by Protein A chromatography, as described in the methods section.

2.3.2.1 Expression and purification of the H435A mutant

The supernatant from the CHO cell cultures was concentrated and loaded onto Protein A affinity columns as described in the methods section. The elution trace and corresponding gel for the protein A affinity purification can be seen in Figure 2.11, which shows a large amount of antibody present in the elutions from fractions A4-A7, which

is very clean. However, there is also some antibody remaining in the flow through from the protein A column, which indicates incomplete loading of the antibody onto the column.

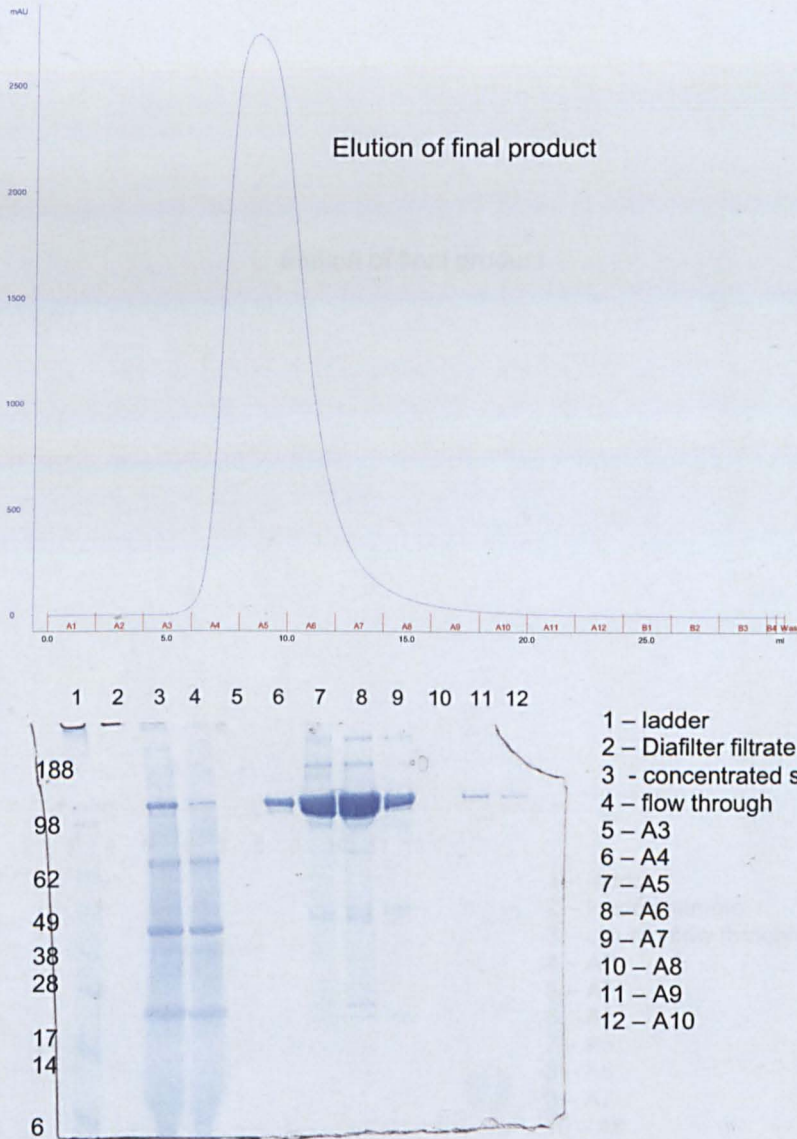


Figure 2.11 - Protein A purification elution trace for the H435A mutant (150 kDa), showing elution of product from Fractions A3-A10 as well as the corresponding SDS-PAGE gel of the protein containing fractions, concentrated cell culture supernatant and diafilter and column flow through.

The antibody containing fractions from this initial protein A purification were pooled and stored at 4 °C whilst the column flow through was re-loaded onto the protein A column and a second protein A purification completed. The elution trace and corresponding gel are shown in figure 2.12.

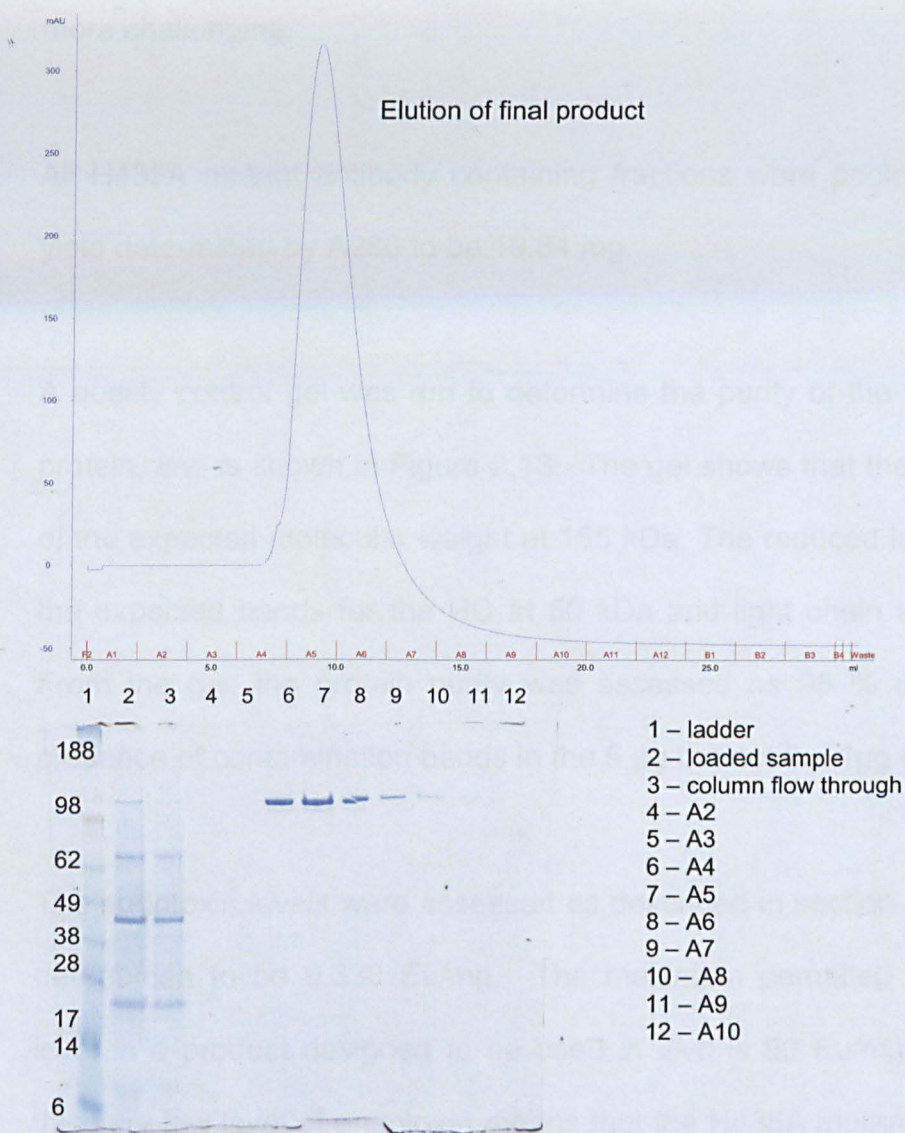


Figure 2.12 - Repeat protein A affinity purification elution trace for the H435A mutant (150 kDa), showing elution of product from Fractions A2-A10 as well as the corresponding SDS-PAGE gel of the protein containing fractions, the flow through from the 1st pass and column flow through.

As seen in Figure 2.12 there is less antibody present in the 2nd pass, however some additional antibody has been recovered from the flow through, improving the total yield of antibody. It should be noted that the interaction between protein A and IgG involves the Fc region of the IgG. It is possible that the H435A mutation introduced into the antibody is reducing the binding affinity with protein A and making purification more challenging.

All H435A mutant antibody containing fractions were pooled and the yield determined by A280 to be 19.84 mg.

A quality control gel was run to determine the purity of the expressed protein, and is shown in Figure 2.13. The gel shows that the protein is of the expected molecular weight at 155 kDa. The reduced lanes show the expected bands for the HC at 50 kDa and light chain at 20 kDa. From the gel, the protein purity was assessed as 95 % due to the presence of contamination bands in the 5 µg but not the 1 µg lanes.

The endotoxin levels were assessed as described in section 2.2.6, and determined to be 0.330 Eu/mg. The maximum permitted endotoxin level in a product designed to be used *in vivo* is 50 Eu/mg therefore this very low level of endotoxin means that the H435A mutant antibody produced is safe to use in the *in vivo* images studies.

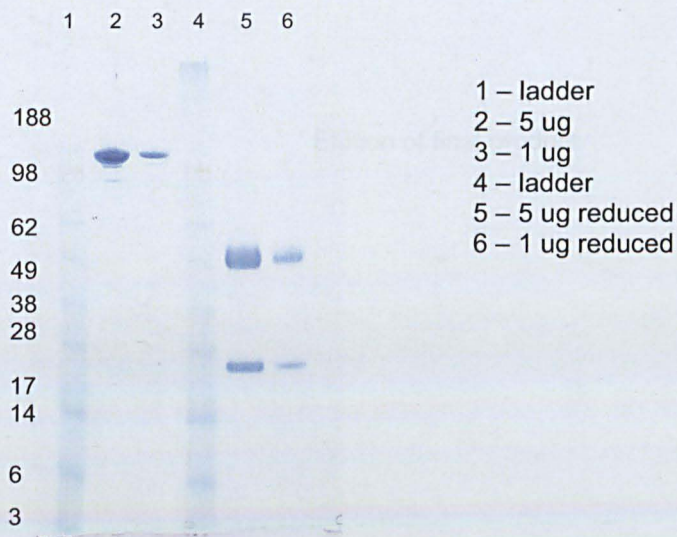


Figure 2.13 - QC gel for the IgG_H435A mutant (150 kDa). Non reduced lanes show a band at the correct Mw of 150 kDa. Reduced lanes show two bands, one at approx 50 kDa corresponding to the heavy chains and one at approx 20 kDa corresponding to the light chains.

The purity, endotoxin levels and yield of the IgG_H435A mutant are all sufficient for the imaging studies.

2.3.2.2 Expression and purification of the IgG V250Q mutant

The supernatant from the CHO cell cultures was concentrated and loaded onto protein A affinity columns as for the H435A mutant and as described in the methods section. The elution trace and corresponding gel for the purification can be seen in Figure 2.14.

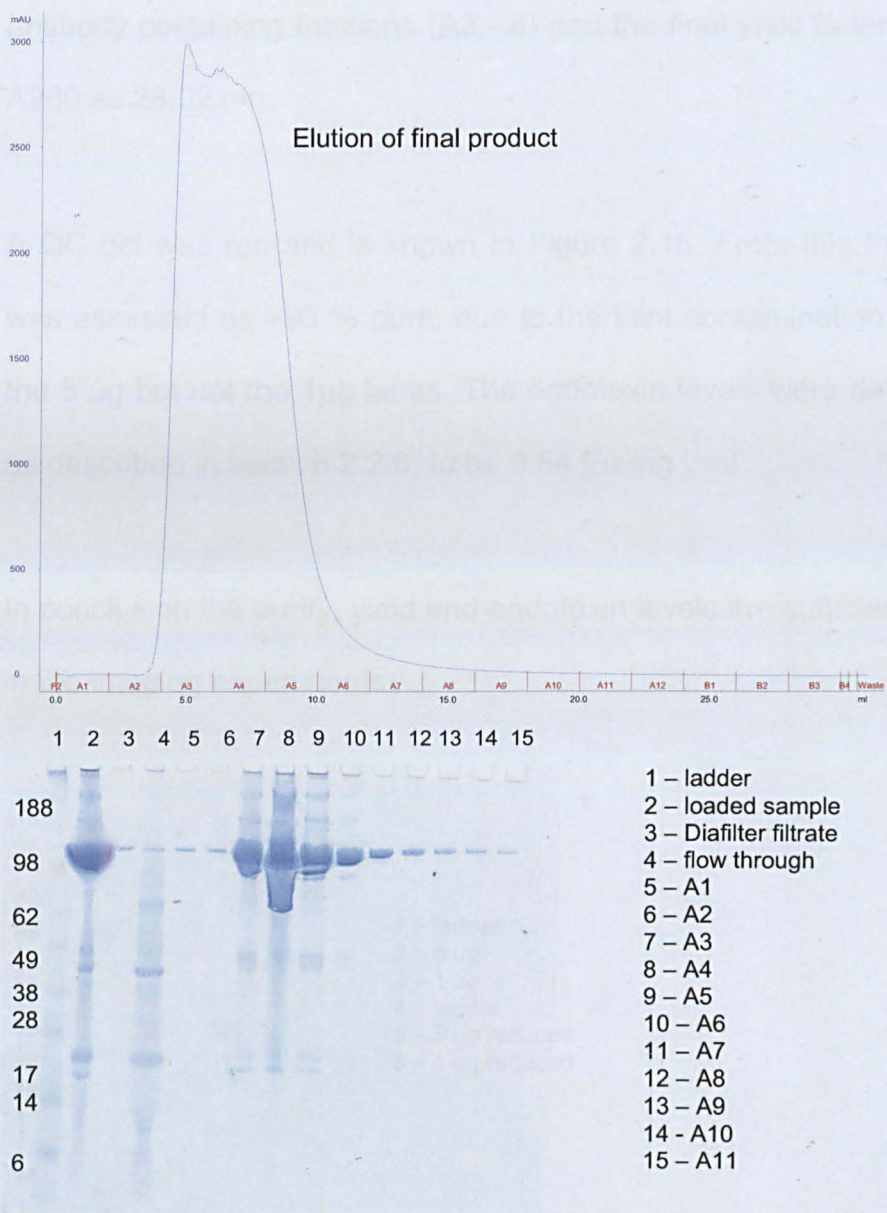


Figure 2.14 - Protein A purification elution trace for the V250Q mutant (150 kDa), showing elution of product from Fractions A1-A11 as well as the corresponding SDS-PAGE gel of the protein containing fractions, and column load and flow through.

The gel in Figure 2.14 shows a very large amount of antibody present in the elution from the column, which is reasonably pure. The largest

antibody containing fractions (A3,- 8) and the final yield determined by A280 as 28.02 mg.

A QC gel was run and is shown in Figure 2.15. From this the protein was assessed as >95 % pure, due to the faint contamination bands in the 5 μ g but not the 1 μ g lanes. The endotoxin levels were determined, as described in section 2.2.6, to be 0.54 Eu/mg.

In conclusion the purity, yield and endotoxin levels are sufficient for use in the imaging experiments.

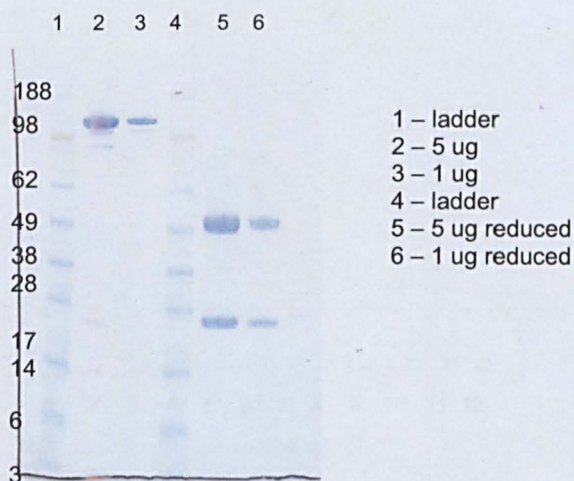


Figure 2.15 - QC gel for the IgG_V250Q mutant (150 kDa). Reduced lanes show two bands, one at approx 50 kDa corresponding to the heavy chains and one at approx 20 kDa corresponding to the light chains.

2.3.2.3 Expression and purification of the H435A I253A double mutant

The supernatant from the CHO cell culture was concentrated and loaded onto a protein A column as described previously. The elution trace and corresponding gel can be seen in Figure 2.16.

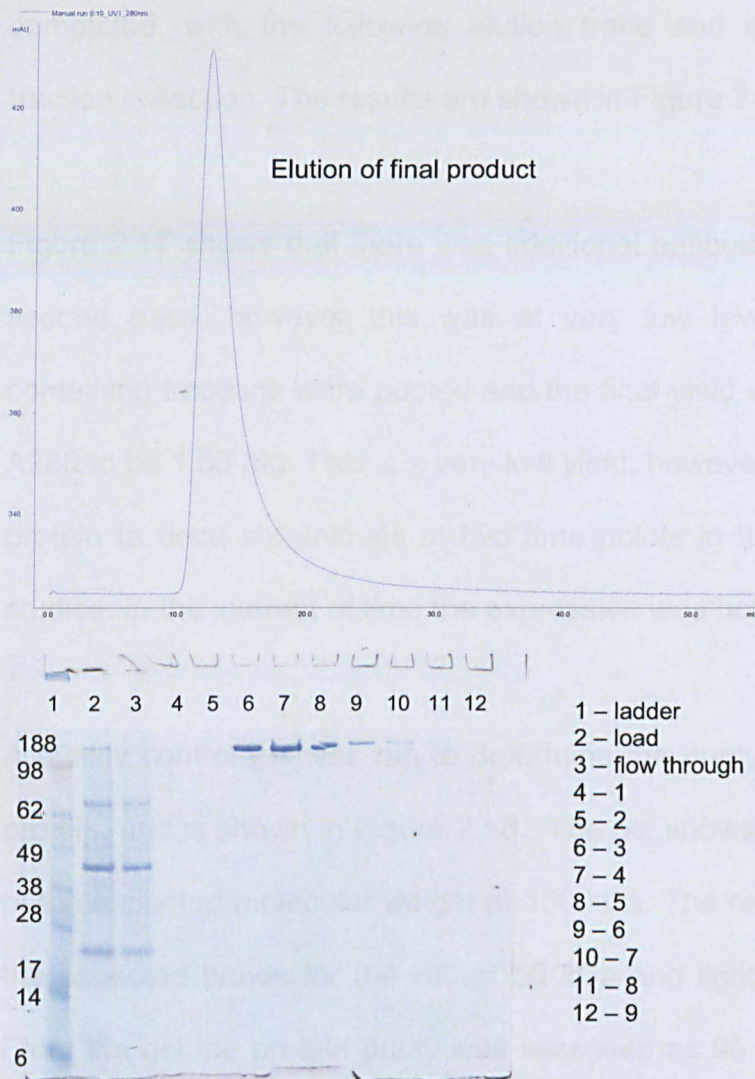


Figure 2.16 - Protein A purification elution trace for the H435A_I243A mutant (150 kDa), showing elution of product from Fractions 1-9 as well as the corresponding SDS-PAGE gel of the protein containing fractions, and column load and flow through

The gel shows that there is antibody present in the elutions, which is very clean, however there is also antibody remaining in the flowthrough, indicating incomplete loading onto the column. This is the same result as seen with the H435A mutant and could be attributed to the mutations disrupting the IgG-protein A interaction.

A 2nd pass of the flowthrough, through the protein A column was completed, with the following elution trace and again with manual fraction collection. The results are shown in Figure 2.17.

Figure 2.17 shows that there was additional antibody purified from the second pass, however this was at very low levels. All antibody containing fractions were pooled and the final yield was determined by A280 to be 1.53 mg. This is a very low yield, however there is sufficient protein to dose six animals at two time points in the *in vivo* imaging studies. In the interest of time the expression was not repeated.

A quality control gel was run to determine the purity of the expressed protein, and is shown in Figure 2.18. The gel shows that the protein is of the expected molecular weight at 150 kDa. The reduced lanes show the expected bands for the HC at 50 kDa and light chain at 20 kDa. From the gel the protein purity was assessed as 95 % due to the lack presence of contamination bands in either 1 µg lanes.

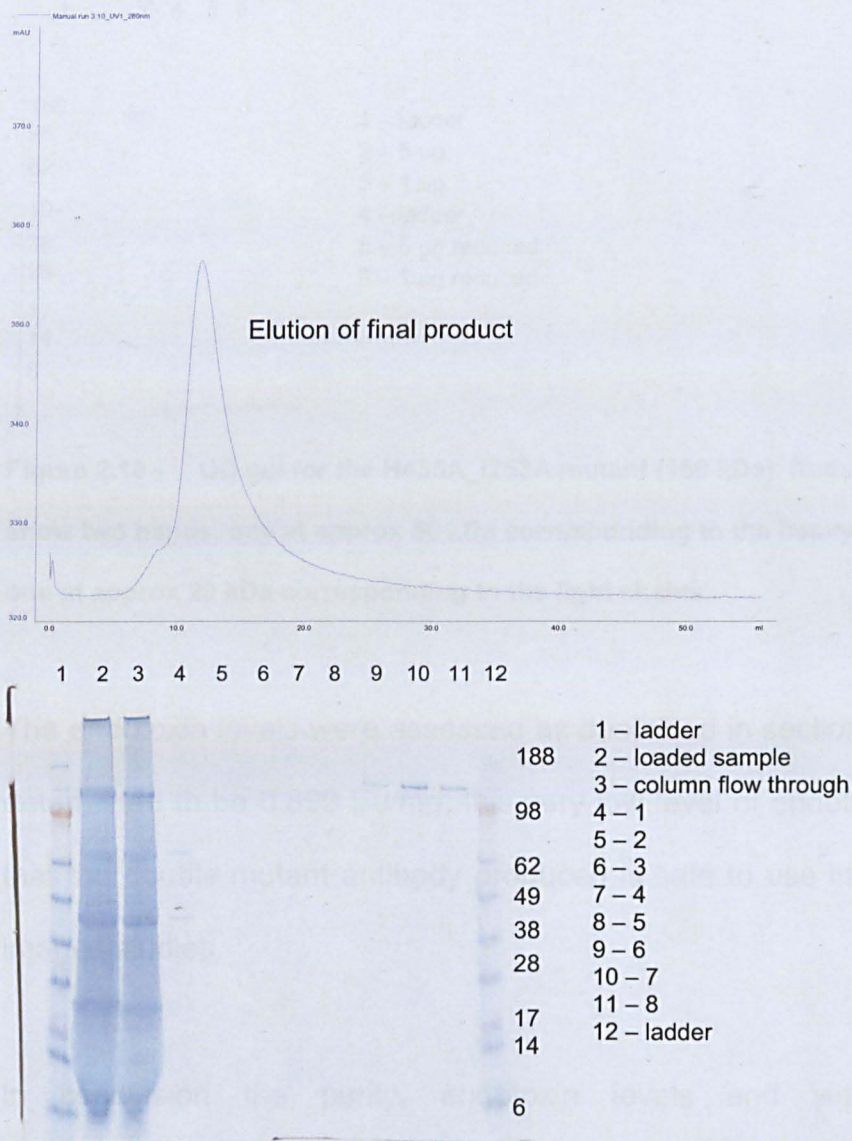


Figure 2.17 - Repeat protein A purification elution trace for the H435A_I253A mutant (150 kDa), showing elution of product from Fractions 1-8 as well as the corresponding SDS-PAGE gel of the protein containing fractions, the flow through from the 1st pass and column flow through

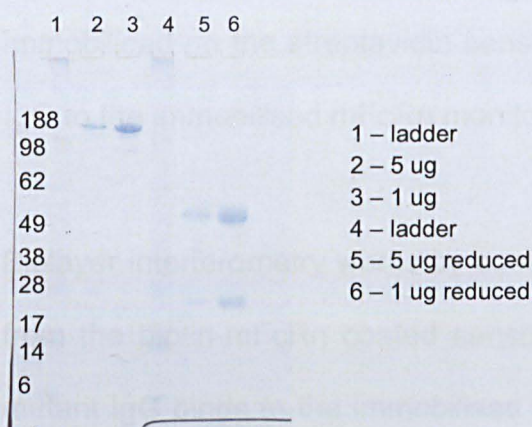


Figure 2.18 - QC gel for the H435A_I253A mutant (150 kDa). Reduced lanes show two bands, one at approx 50 kDa corresponding to the heavy chains and one at approx 20 kDa corresponding to the light chains.

The endotoxin levels were assessed as described in section 2.2.6, and determined to be 0.899 Eu/mg, this very low level of endotoxin means that the double mutant antibody produced is safe to use in the *in vivo* images studies.

In conclusion the purity, endotoxin levels and yield of the IgG_H435A_I253A fragment are all sufficient for the imaging studies.

2.3.3 Assessment of the levels of mFcRn binding of the whole IgG mutants

The octet red system from Biorad was used to determine kinetics of binding between biotinylated mFcRn and the whole IgG mutants. The system measures the kinetics of association and dissociation between two proteins, where one biotinylated protein is immobilised on streptavidin coated biosensors. In this case, biotinylated mFcRn is

immobilised on the streptavidin sensors and the binding of the mutant IgG to the immobilised mFcRn monitored with biolayer interferometry.

Biolayer interferometry works by comparing the profile of reflected light from the biotin-mFcRn coated sensor to a reference material. As the mutant IgG binds to the immobilised mFcRn, the optical density above the sensor changes, altering the pattern of the reflected light. Changes in the reflected pattern of light are proportional to the amount of IgG bound to mFcRn and association/dissociate plots can be generated of the interaction between the antibody and receptor. From these the relative binding and dissociation constants of the IgG-mFcRn interaction can be plotted for each mutant.

Figure 2.19 shows an original association and subsequent dissociation plot for WT IgG over the full range of IgG concentrations. In the graph the wavelength of the reflected light (in nm) is plotted over time. Each green line represents the response of an individual sensor, with each concentration of IgG was tested in duplicate.

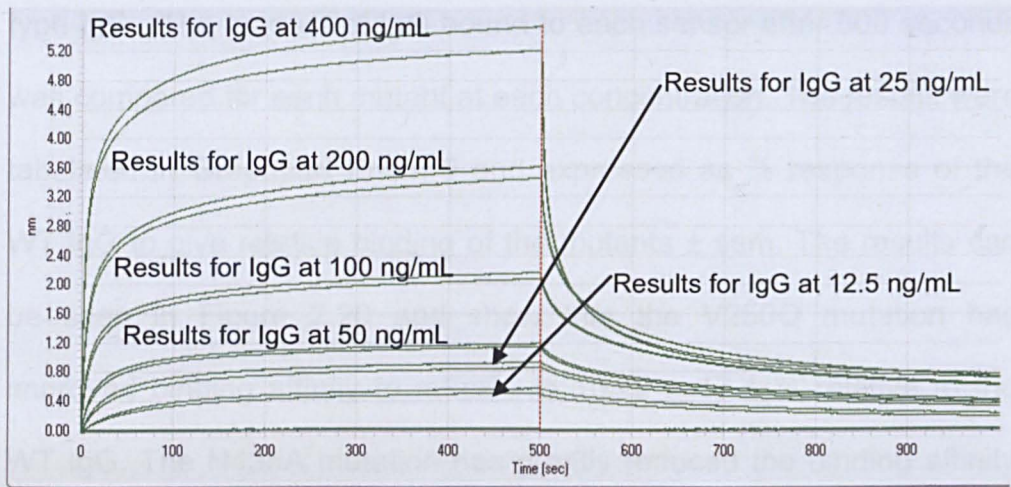


Figure 2.19 - Graph showing association/dissociation of WT IgG to Octet streptavidin sensors coated with mFcRn over the full range of IgG concentrations at pH 7.4. Each green line represents the response recorded for an individual sensor. The red line represents removal of the sensor from IgG containing solution and immersion in fresh buffer.

Figure 2.19 clearly shows an initial phase of binding of WT IgG to FcRn, as evidenced by an increase in the response, which reaches a plateau. Additionally, the response is higher for sensors immersed in higher concentration IgG solutions, indicating that more IgG is binding to the immobilised mFcRn.

After 500 seconds the sensor is removed from the IgG solution and transferred to buffer (shown with a red line on the graph in figure 2.19). At this point in the graph the IgG can be seen to dissociate from the immobilised mFcRn, as evidenced by a decrease in response.

The aim of this experiment was to determine to what extent the H435A, V250Q and H435A_I253A mutants bind mouse FcRn compared to wild

type IgG. The amount of IgG bound to each sensor after 500 seconds was compared for each mutant at each concentration. The results were tabulated in Graphpad Prism 5 and expressed as % response of the WT IgG to give relative binding of the mutants \pm sem. The results can be seen in Figure 2.20 and show that the V250Q mutation has improved binding affinity to mFcRn to 163.2 ± 17.4 % relative to the WT IgG. The H435A mutation has greatly reduced the binding affinity to mFcRn to 11.5 ± 5.2 % and the double mutation has completely ablated binding to the mFcRn receptor.

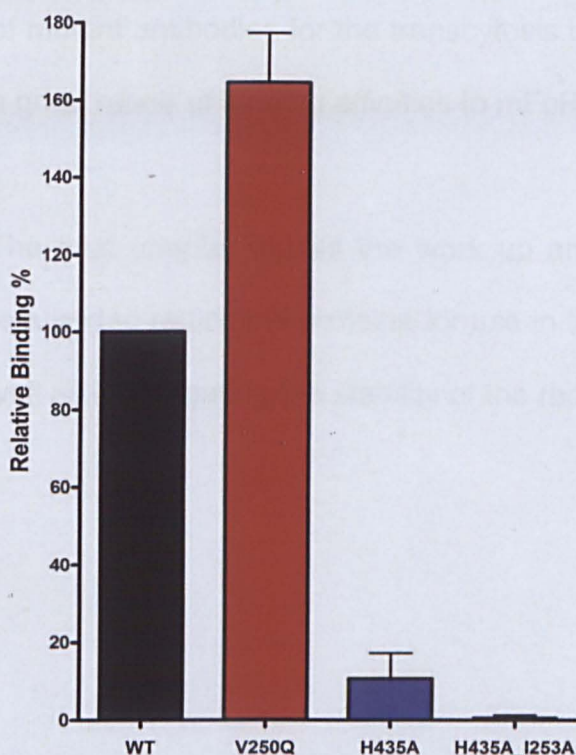


Figure 2.20 - Pooled results from Octet analysis of binding affinity for WT IgG and mutants to mFcRn, at pH 6 and 7.4. Data shows the relative binding affinities to mFcRn as a percentage of the WT binding. Error bars represent \pm sem (n=12 per bar)

It can be concluded from these results that a panel of IgG with differing binding affinities to mFcRn have been produced for use in the *in vivo* imaging experiments.

2.4 Conclusion

In summary, the work detailed in this chapter has resulted in the successful expression of the reagents required for the *in vivo* imaging experiments. The yield, purity and endotoxin levels of each of the proteins expressed are sufficient for *in vivo* use. Additionally, the panel of mutant antibodies for the transcytosis by mFcRn experiments exhibit a good range of binding affinities to mFcRn *in vitro*.

The next chapter details the work up and validation of the chemistry required to radiolabel proteins for use in the *in vivo* imaging studies, as well as investigating the stability of the radiolabelled proteins *in vivo*.

CHAPTER 3: Set up and Validation of *in vivo* Imaging Experiments

3. Overview

This chapter details the work undertaken to set up and validate the imaging technique used to study antibody transport out of the lung *in vivo*.

The overall aim of the work described in this chapter was to determine whether labelling an antibody with technetium reproducibly produced a construct which was stable over the period required in the imaging experiments. Additionally, control experiments to assess the effect of the presence of the technetium label on antibody transport/binding were completed.

3.1 Introduction

Before work could begin on imaging the redistribution of an intra-tracheally instilled antibody *in vivo* it was necessary to thoroughly validate a suitable labelling method to introduce a radiolabel into the antibody of interest. The SPECT imaging technique used, as described in section 1.9.1, produces a map of the distribution of radioactivity within the animal. The antibody of interest does not possess any radioactive atoms and as such it is necessary to introduce a radiolabel

to allow detection of the antibody during imaging. Common radiolabels are gamma emitting isotopes of technetium (^{99m}Tc), iodine (^{123}I) or gallium (^{67}Ga). The isotope ^{99m}Tc was chosen for this work as it was readily available and research by (Mather & Ellison, 1990) determined a simple and reproducible two step process to add technetium labels to antibodies. The original method proposed utilises β -mercaptoethanol to reduce the disulphide bridges at the hinge region in the antibody, then the reduced antibody is reacted with technetium to give the final labelled antibody. β -mercaptoethanol has an unpleasant odour and today is commonly replaced with the alternative reducing agent Tris(2-carboxyethyl)phosphine (TCEP). As TCEP will be used to reduce the antibody in this work, it is necessary to carefully re-validate the chemistry used to generate the labelled antibody to ensure that this alteration to the original method is suitable.

Once generated, the technetium labelled antibody is only suitable for use in the imaging experiments if the label remains associated with the antibody over the course of the experiment. As such it is necessary to determine the *in vivo* stability of the construct over time. Another important factor is that the technetium label must not greatly affect the conformation of the antibody, and alter either its binding to target antigen or its transport out of the lung. It was therefore necessary to validate the technetium labelled antibody to ensure its suitability for the imaging experiments.

3.2 Materials and Methods

3.2.1 Materials

Antibodies and antibody fragments were produced as detailed in Chapter 2. Technetium was supplied as sodium pertechnetate (NaTcO_4) in saline solution by the radiopharmacy departments at either the Queens Medical Centre, Nottingham or The Christie Hospital, Manchester.

3.2.2 Methods

3.2.2.1 Reduction of antibody and fragments

5 mg antibody (or fragment) was reduced by reaction with 20 μL 0.1 M TCEP, for 30 min at room temperature. The reduced antibody/fragment was purified by gel filtration through a PD-10 desalting column (GE Healthcare), eluting with 3.5 mL cold, deoxygenated DPBS and the success of the reduction determined by colorimetric assay with Ellman's reagent.

3.2.2.2 Ellman's Assay

The assay determined the concentration of free thiol groups on the reduced antibody. Ellman's reagent was prepared as a 1 mM solution

in 100 mM phosphate buffer at pH 8.0. Samples were tested in duplicate, with 10 μ L sample diluted with 90 μ L Ellman's reagent. The standard for the colourimetric assay was 1 mM cystine hydrochloride in 100 mM phosphate buffer at pH 8.0 and standards points were measured between 1000 μ M and 1 μ M. The SoftMax Pro 4.6 software package calculated the mean concentration of thiol groups for an unknown sample, based upon the slope of the standard curve. This was used to determine the number of reduced thiols per antibody using the following formula:

$$\text{Reduced thiols per molecule} = \frac{(\text{measured thiol conc. M} \times \text{molecular weight})}{\text{protein concentration mg/mL}}$$

The reduced antibody was then stored in 0.5 mg aliquots under nitrogen at -80 °C until required and defrosted just prior to reaction with technetium.

3.2.2.3 Production of the final conjugate

An MDP vial, (GE healthcare) containing sodium medronate and tin chloride, was reconstituted with 5 mL 0.9 % saline and 50 μ L MDP/saline was added to 0.5 mg reduced antibody/fragment. Sodium pertechnetate solution (approx. 400 MBq) was added to the antibody/MDP solution and allowed to react for 10 min at room temperature. During this reaction the sodium pertechnetate was

reacted with the strong reducing agent tin (II) chloride in the presence of medronic acid, to give a medronate-technetium chelate with technetium in the 4+ oxidation state. The technetium chelate was further reacted with the reduced antibody, with the technetium chelating with the free thiol groups in the antibody hinge region producing the final labelled antibody.

The radiochemical purity of the tagged antibody, a measure of the success of the tagging reaction, showing what percentage of antibody has been successfully tagged, was assessed using Thin Layer Chromatography (TLC).

3.2.2.4 Thin layer chromatography

1 μL of tagged antibody, diluted to give an activity of 30-100 kBq / μL , was spotted onto TLC plates and the TLC run with a 0.9 % saline mobile phase until the solvent front reached the line at the top of the plate, after approximately 20 min. The TLC plate was cut in half and the activity of each half recorded with a well counter, radiochemical purity was then calculated as:

$$\text{Radiochemical Purity (RCP) \%} = 100 \times \left[\frac{\text{Activity at } R_f0}{\text{Activity at } R_f1 + \text{Activity at } R_f0} \right]$$

The RCP should be greater than 90 % in all cases and any batch with an RCP of <80 % was discarded.

TLC separates free and bound technetium based upon differences in solubility in saline solution. Free technetium is highly soluble in saline, whereas technetium bound antibody is highly insoluble. Free technetium has an Rf value of 1, whereas radiolabelled antibody has an Rf of 0. There are no other labelled components in the reaction mixture and as such the plate contains technetium at either Rf 0 or 1 with no substances having an Rf between 0 and 1.

A small sample of the reaction solution was spotted onto a cellulose coated TLC plate, and the plate stood vertically in the saline mobile phase. Any ^{99m}Tc not associated with the antibody moves up the TLC plate with the solvent front, whereas any ^{99m}Tc remaining associated with the antibody remains in the spot at the bottom of the plate, as shown in Figure 3.1.

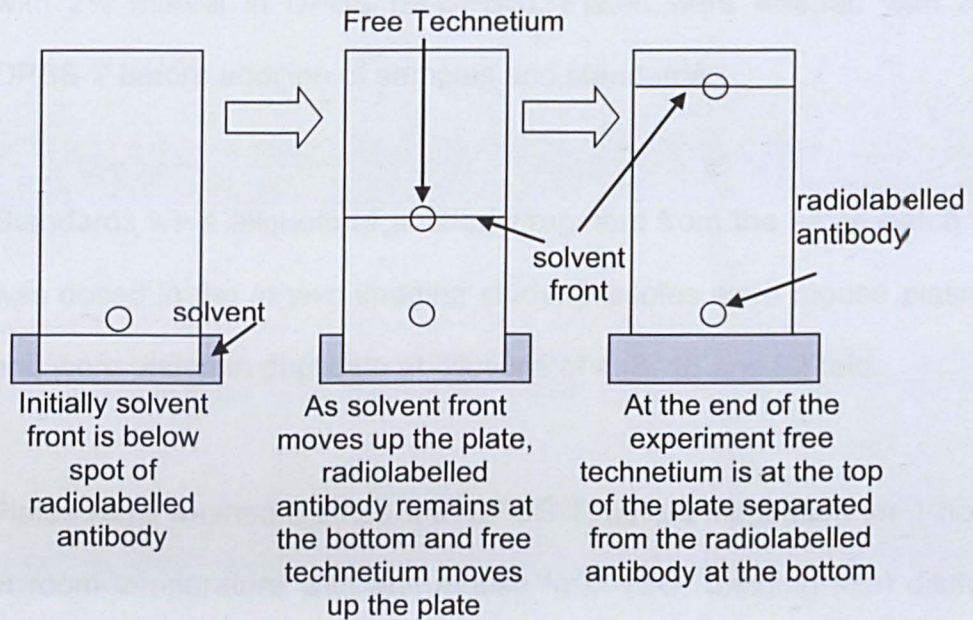


Figure 3.1 - Diagram showing principles of thin layer chromatography (TLC)

3.2.2.5 Measurement of sample activity in the well counter

A well counter was calibrated to ^{99m}Tc . Before testing the sample the background reading was recorded, then the samples placed directly inside the counter for approximately 10 seconds until a stable activity reading was recorded. The counter records the total activity of the sample in MBq.

3.2.2.6 ELISA – to detect mlgG1

Nunc maxisorb 96 well plates were coated with antigen diluted to 4 $\mu\text{g}/\text{mL}$ in DPBS overnight at 4-8 $^{\circ}\text{C}$. Plates were washed 3 times with 250 μl DPBS + 0.05% Tween 20 (DPBS-T), before blocking for 1 hour

with 2% marvel in DPBS (M-DPBS). Plates were washed with 3 x DPBS-T before addition of samples and standards.

Standards were aliquots of antibody/fragment from the same batch as was dosed in the *in vivo* imaging study. Samples were mouse plasma and were tested in duplicate at dilutions of 4, 8, 16 and 32-fold.

Plates were washed 3 times with DPBS-T, before incubation for 1 hour at room temperature with anti mouse IgG1-HRP (binding site) diluted 1:6000 with M-DPBS. Plates were washed 5 x with DPBS-T, before addition of 50 μ L tetramethylbenzidine (liquid substrate for ELISA, Sigma-Aldrich UK), after 30 min at room temperature the reaction was stopped with addition of 50 μ L 1M sulphuric acid and plates were read at 450 nm.

Data was plotted in Microsoft Excel; the standard curve fit was a log/log plot with linear regression from 200 ng/ml to 0.2 ng/ml and the linear regression fit must have r^2 value of >0.95. Samples were calibrated from the standard curve and values multiplied by the dilution factor, sample CV should be \leq 15%.

3.2.2.7 Imaging on the planar gamma camera

All *in vivo* experiments were performed in compliance with licences issued under the UK Animals (Scientific Procedures) Act 1986 following local ethical review.

Two female BALB/c mice (mean weight 19.9 ± 0.15 g) were terminally anaesthetised with 0.1 mL/kg ketamine/medetomidine mixture at a dose rate of 75 mg/kg ketamine and 1 mg/kg medetomidine. One animal was intratracheally instilled with 50 μ L labelled antibody at 0.5 mg/mL in 0.9 % saline at approx 200 MBq/mL. The second animal was intratracheally instilled with 50 μ L sodium pertechnetate solution at approx 200 MBq/ml. The animals were placed supine on the planar gamma camera and imaged for 60 min, before being euthanised with an overdose of sodium pentobarbitone.

Images were analysed in GammaVision+ (AMETEK, Inc.) with regions of interest (ROI) manually determined to cover the lungs, stomach, thyroid and bladder. The total activity within each ROI was determined over 1 minute segments of the total scan, with the first data point covering the time between 0 and 1 minute and the final data point covering the time between 59 and 60 minutes. Activities in each ROI were then plotted over the course of the experiment in an activity vs. time plot.

3.2.2.8 Comparison of pulmonary transport of labelled vs. unlabelled antibody after intratracheal instillation.

All *in vivo* experiments were performed in compliance with licences issued under the UK Animals (Scientific Procedures) Act 1986 following local ethical review.

12 Female BALB/c mice (Charles River, UK, mean weight 21.7 ± 0.26 g) were anaesthetised in an induction chamber with isoflurane. Anaesthetised animals were suspended by the front incisors on a tilted board and intratracheally dosed by insertion of a dosing needle through the larynx with 50 μ L antibody at 0.5 mg/mL in PBS.

Animals were allowed to recover from anaesthesia and returned to their home cages. Three animals were euthanized with an overdose of sodium pentobarbitone at each of 4 time points, 0, 1, 2 and 4 hours post dose. Blood was taken from the descending vena cava, spun down in a bench top centrifuge and the plasma stored at -80 °C prior to analysis by ELISA.

3.3 Results and Discussion

3.3.1 Validation of labelling chemistry with Ellman's reagent and TLC

The chemistry to introduce a technetium label to the antibodies and fragments is a modified version of the protocol from (Mather & Ellison, 1990). In brief the protein is reduced to release free thiol groups, which on reaction with technetium produce the radiolabelled antibody. The model antibody which was to be initially tested in the imaging experiments was labelled with ^{99m}Tc in a trial run of the conjugation chemistry, as described in the methods section. The reaction is a two step process, initially producing the reduced antibody and then further reacting this reduced species with technetium to yield the final labelled antibody.

The first step of the chemistry is a reduction with TCEP, the success of which was determined using Ellman's assay. The assay is colourmetric with higher concentrations of free thiols producing a more intense yellow colour. Figure 3.2 shows the results obtained from Ellman's assay carried out on the reduced antibody, immediately following reaction with TCEP and after one month storage at -80°C , compared to the unreduced starting material.

	Conc. thiol groups (μM)	Standard deviation	Free thiol groups per molecule
Unreduced IgG	7.5	3.316	0.62 ± 0.27
Reduced IgG	65.1	9.395	5.39 ± 0.78
Reduced IgG - after 1 month at -80°C	58.9	8.126	4.87 ± 0.67

Figure 3.2 - Data for IgG at 1.79 mg/mL, Mw of 148125. Table showing the values obtained from Ellman's assay of both reduced and unreduced antibody in triplicate, as well as a re-test of the same batch of reduced IgG after 1 month storage at -80°C .

The number of free thiol groups per molecule of the unreduced antibody is 0.6, the reduced antibody contains 5.4 free thiol groups per molecule immediately after reduction and 4.87 free thiol groups after one month storage at -80°C . The increase in detectable free thiol groups after reduction indicates that the reaction has been successful. In addition, after storage under nitrogen at -80°C for 1 month no re-oxidation of the free thiols occurred with a re-test of the number of free thiols present on the same batch of reduced IgG being the same within experimental error.

The theoretical maximum number of free thiol groups available per molecule of reduced antibody is the number of thiols which can be produced from the reduction of the interchain disulphide bridges, plus the number of free cystine residues on the antibody. Each disulphide bridge reduction produces two free thiol groups.

The unreduced antibody shows 0.6 detectable thiols per molecule, therefore we can use 0.6 as the number of detectable cystine residues per molecule. The maximum number of thiols which can be released from the reduction of disulphide bridges is 8, 2 from each of the 4 interchain disulphide bridges on a mouse IgG1. However, (Blauenstein, et al., 1995) showed that reduction with TCEP under the conditions used here, results in selective reduction of the disulphide bridges at the hinge region. The disulphide bridges connecting the heavy and light chains are not reduced, minimising any potential conformational changes in the antigen binding domain and therefore any affect on antibody activity. This gives an expected number of free thiols for this antibody as 4 from the reduction of the 2 hinge region disulphide bridges, plus 0.6 free cystine residue. This is exactly in line with the observed results of 4-5 free thiols per molecule.

The second stage of the labelling chemistry is the reaction of the reduced antibody with technetium in the presence of low affinity binding site blocking agents and a reducing agent. The percentage of ^{99m}Tc associated with the antibody was determined by comparison of the amount of activity at the bottom and top of the plate, as described in section 3.2.2.4.

TLC was run on samples of the radiolabelled antibody after 0.5, 5 and 24 hrs storage at room temperature in order to provide a preliminary assessment of the stability of the labelled antibody. Figure 3.3 shows

the results of the TLC experiments designed to determine the success of the final reaction to incorporate the technetium label into the reduced antibody, as analysed in the well counter.

	Activity at R_f1 (kBq/s)	Activity at R_f0 (kBq/s)	Radiochemical Purity (%)
After 0.5 hrs	0	12	100
After 5 hrs	0	25	100
After 24 hrs	0	28	100

Figure 3.3 - Activities of bottom and top halves of TLC plates as determined by the well counter. Calculated RCP (%) are 100 % at all time points.

As seen in Figure 3.3, analysis of the TLC plates using the well counter produced 100% calculated RCP for the labelled antibody tested at 0.5, 5 and 24 hrs post reaction. This indicates that the labelled antibody is stable in solution for up to 24 hrs. Further validation experiments were then run to determine the stability of the labelled antibody *in vivo*.

3.3.2 Experiments to validate the stability of the labelled antibody *in vivo*

Several experiments were conducted to verify the *in vivo* stability of the labelled antibody. Initially the pulmonary clearance of intratracheally instilled labelled antibody was compared to that of intratracheally instilled free technetium with imaging on the planar gamma camera.

The planar gamma camera produces a 2D image of radioactivity within the animal. There is no resolution in the z direction and so the image is not able to separate, for example, activity recorded in the lungs from activity in the tissue directly above and below the lungs.

Figure 3.4 shows the distribution of free technetium within the same mouse over 46 minutes in graphical form, together with images taken at 1, 23 and 46 minutes post dose. The images provide the anatomical perspective required to determine the location of the activity signals within the animal. Regions of interest are drawn around areas representing specific organs and the changing level of activity recorded in these organs over the course of the scan, is represented in the accompanying graph. It is important to note that over the course of the experiment, the ^{99m}Tc is decaying. In order to account for this the figures were decay corrected, meaning that each figure was corrected back to show how much technetium would have been present in the sample at $t=0$.

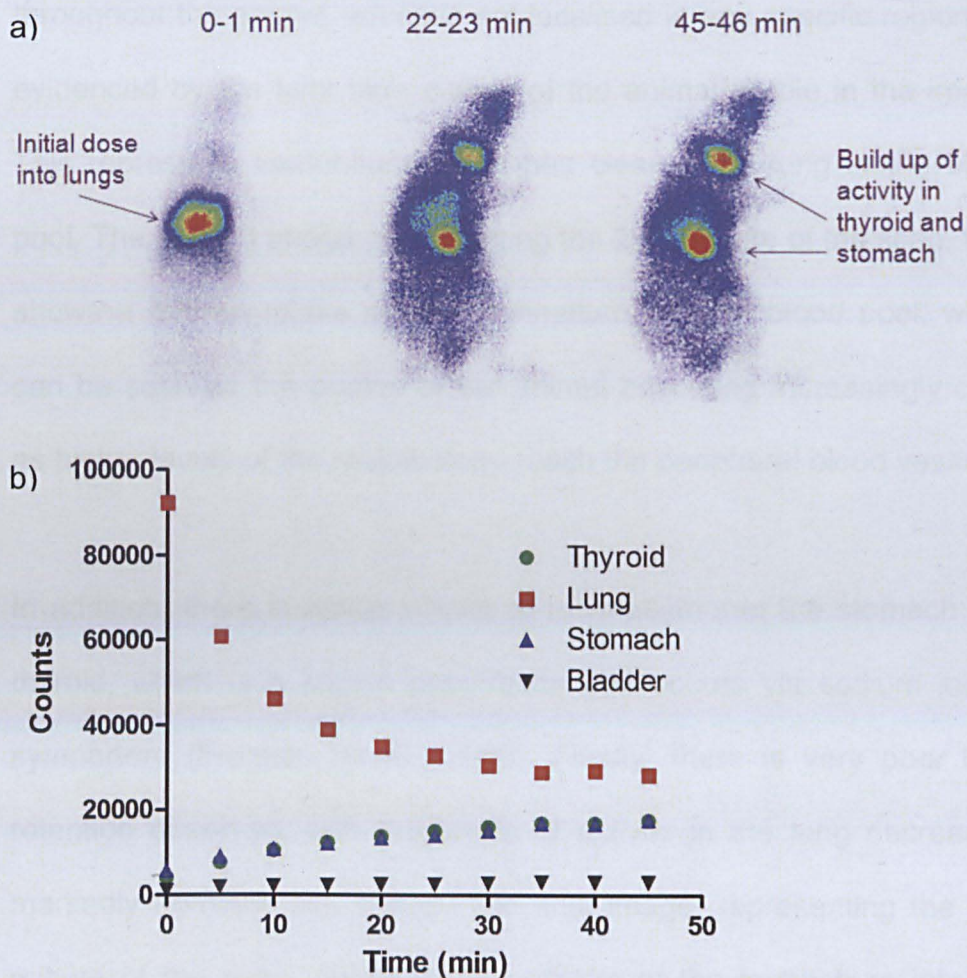


Figure 3.4 - A series of gamma camera images showing a) the redistribution of free ^{99m}Tc within one mouse over 46 minutes, with b) a graph quantifying the activity observed in different organs over 46 minutes. Activity is initially highest in the lung, dropping rapidly to a plateau at approx background levels after 30 mins. Activity in the thyroid and stomach is initially very low increasing over the course of the scan. Activity in the bladder remains roughly constant at low levels throughout the scan.

It can be seen in Figure 3.4 that in the image representing the first minute post dose, high levels of activity are present within in the lungs. This is expected from the intratracheal dosing method used, which delivers 100 % of the dose into the lungs. There is a low level of activity

throughout the animal, which is not localised in any specific region, as evidenced by the faint blue outline of the animal visible in the image. This represents technetium which has cleared the lung in the blood pool. The second image, representing the 22nd minute of the scan, then shows a further uptake of free technetium into the blood pool, which can be seen as the outline of the animal becoming increasingly clear as higher levels of the radioisotope reach the peripheral blood vessels.

In addition, there is active uptake of technetium into the stomach and thyroid, which is a known occurrence and occurs via sodium iodide symporters (Franken, et al., 2010). Finally, there is very poor lung retention observed, with the levels of activity in the lung decreasing markedly from the first image. The final image, representing the 45th minute of the scan, shows further uptake of the technetium into the stomach and thyroid, with levels of activity in the lung decreasing to become no higher than other highly perfused areas of the animal. This indicates that there is total pulmonary clearance of free technetium from the lungs between 23 and 46 minutes post dose.

The graph in Figure 3.4 quantifies the trends observed in the images. Activity in the lungs drops by 70 % over 40 minutes, whereas activity in the stomach and thyroid increases by 420 and 300 % respectively. Activity in the bladder remains roughly constant over the course of the scan. The activity in the lungs reaches a plateau at 30 minutes post dose, which represents total clearance of the instilled technetium. The

observed decrease of 70 % underestimates the total level of clearance as the lungs are highly perfused and the 2D nature of the image records the total activity of the blood present in the entire upper thorax of the animal. Taking into account this overestimation of total activity in a given organ when there are high levels of activity present in the blood pool, the data still provides a re-distribution profile of free technetium *in vivo* over 46 minutes.

The experiment described for free technetium was repeated for the technetium labelled antibody in order to compare the redistribution profile of the two species after intratracheal instillation. The graph in Figure 3.5 shows the total activity in specific organs over the course of the scan.

The level of activity recorded in the lungs is high over the course of the scan, dropping by only 9 % over 46 minutes, as compared to a 70 % drop in activity recorded for the free technetium. Additionally, activity levels in the stomach and thyroid/larynx do not increase over the course of the experiment, in contrast to the increases observed for free technetium. As observed previously for free technetium no increase in activity is recorded in the bladder over the course of the scan.

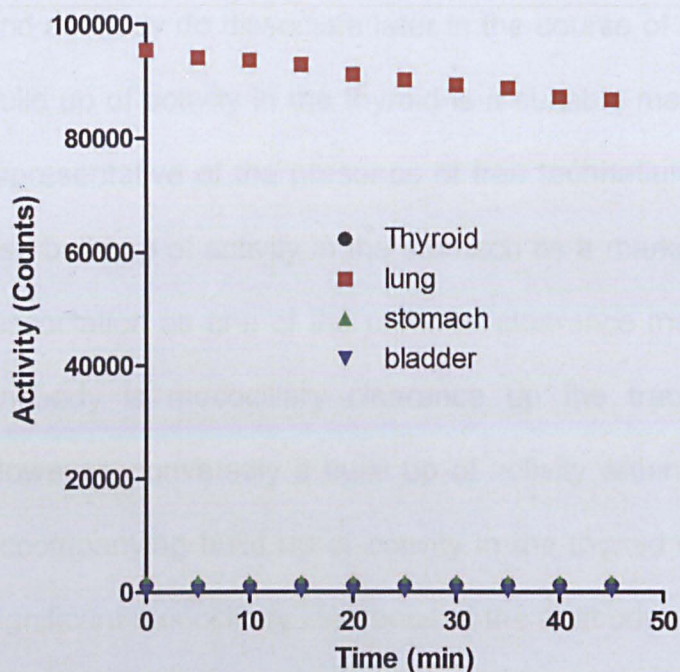


Figure 3.5 - Graph showing the quantification of levels of activity within the lung, bladder, stomach and thyroid over the course of a 46 min scan. High levels of initial activity persist within the lung over the course of the scan. Very low levels of activity are recorded in the thyroid, stomach and bladder, which do not increase over 46 minutes.

The redistribution pattern of the labelled antibody is therefore very different to that of free technetium, with far longer pulmonary retention and no build up of activity within the stomach or thyroid. This is important as a method to determine whether the technetium remains bound to the antibody *in vivo* and can be applied in two ways. Firstly as free technetium is cleared from the lungs within 30 minutes, if images of the distribution of labelled antibodies shows radiation remaining in the lungs for longer than 30 minutes it can be concluded that labelled antibody is stable, as it would be impossible to generate such images if the ^{99m}Tc tag had dissociated from the antibody. Secondly if the label

and antibody do dissociate later in the course of the experiment then a build up of activity in the thyroid is a suitable marker for this, as this is representative of the presence of free technetium. It is not possible to use build up of activity in the stomach as a marker of labelled antibody dissociation as one of the potential clearance methods for the instilled antibody is mucociliary clearance up the trachea and swallowing. However, conversely a build up of activity within the stomach, without accompanying build up of activity in the thyroid would be indicative of significant mucociliary clearance of the antibody.

Overall these data provide initial evidence that the labelled antibody is stable *in vivo*, however the experiments only cover the first 46 minutes post dose. Further experiments were then run to determine labelled antibody stability *in vivo* out to 24 hrs post dose.

3.3.3 Comparison of detection of construct in same plasma samples by ELISA or radioactivity measurements.

The labelled antibody consists of two independently detectable parts, the antibody itself is detectable by ELISA and the label is detectable by measurement of total radioactivity within the sample. If the labelled antibody is stable over 24 hrs then determination of the concentration of labelled antibody in the same samples by both ELISA and total activity measurement should be equal.

An experiment was run to test this, with the concentration of labelled antibody determined in the same plasma samples, taken at 0, 2, 4 and 24 hours post intratracheal instillation. The detection methods used were immediate quantification of the activity in the sample using the well counter to report an activity in Bq/ml or by ELISA to give antibody concentration in ng/ml.

Figure 3.6 shows the results of these experiments normalised to the signal reported at time 0. This normalisation is necessary to be able to compare the results of the separate detection methods on the same graph. The results show relative increases from baseline ($t = 0$) at 1, 2, 4 and 24 hrs post dose for each detection method. It is clear from the graph that within experimental error, concentrations determined by either detection method are equal. This is also demonstrated by the fact that comparison of the results for ELISA and radioactivity measurements using Student's unpaired t-test did not reach statistical significance ($p > 0.05$) at any time point.

The results of this experiment strongly indicate that the labelled antibody is stable *in vivo* over 24 hrs. However the presence of the label could still affect both the conformation and so binding ability of the antibody and/or transport of the antibody out of the lung.

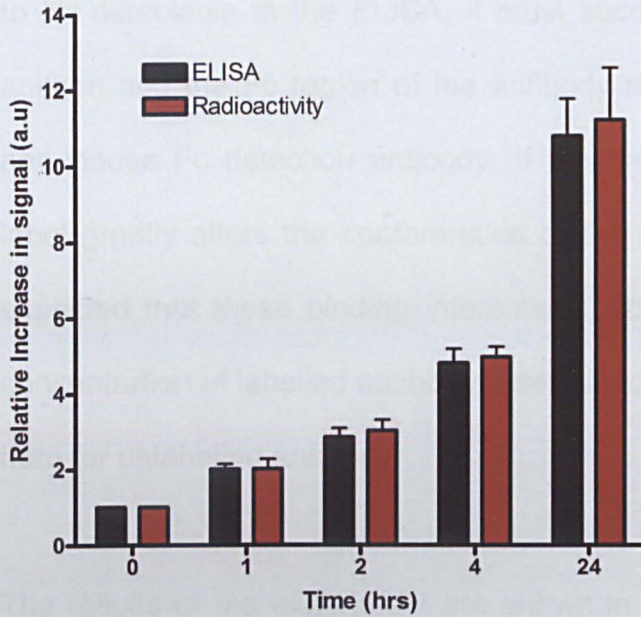


Figure 3.6 - Comparison of detection of ^{99m}Tc -IgG by ELISA (detecting antibody) or by total activity of the sample as determined in the well counter (detecting the label). Expressed as % relative increase from t=0 with error bars of \pm sem (n=6). The graph indicates that the level of radiolabelled antibody reported by either detection method is highly similar.

3.3.4 Detection of known concentrations of IgG and ^{99m}Tc labelled IgG by ELISA to determine whether presence of label affects conformation

If the presence of the technetium label affects the conformation of the antibody it could result in the data generated in the SPECT imaging experiments not being representative of true pulmonary antibody clearance.

An ELISA experiment was run comparing detection of known concentrations of whole IgG and labelled whole IgG. For the antibody

to be detectable in the ELISA, it must successfully bind to its target antigen and the Fc region of the antibody must successfully bind the anti-mouse Fc detection antibody. If the presence of the technetium label greatly alters the conformation of the antibody then it would be expected that these binding interactions would be disturbed and the concentration of labelled antibody determined by ELISA would be lower than for unlabelled antibody.

The results of the experiment are shown in Figure 3.7 and show that within experimental error, the ELISA protocol returns accurate concentrations for both the labelled and unlabelled IgG between 50 and 800 ng/ml. Comparison of the results for labelled and unlabelled antibody using Student's unpaired t-test did not reach statistical significance ($p > 0.05$) at any timepoint. This result indicates that the presence of the technetium label does not greatly affect the conformation of the antibody.

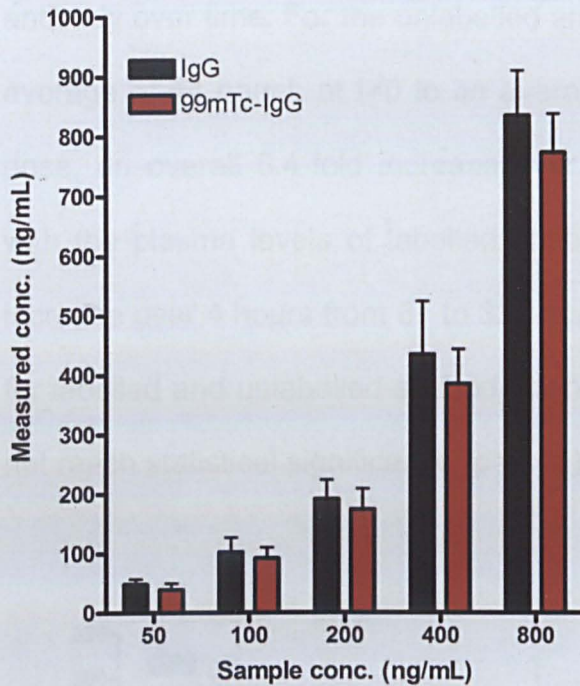


Figure 3.7 - Results of experiment comparing analysis of known concentrations of labelled and unlabelled antibody determined by ELISA. Graph shows that the ELISA reports correct concentrations of both labelled and unlabelled antibody, within experimental error. Error bars are \pm sem (n=6).

3.3.5 Experiments to confirm whether the presence of the technetium label affects antibody transport out of the lung

In order for imaging to be a suitable method to determine the re-distribution of an intratracheally instilled antibody, the presence of the tracer cannot interfere with antibody transport. A study was undertaken to confirm whether the presence of the technetium label would affect transport out of the lung. This compared levels of labelled and unlabelled antibody detected in the plasma of animals taken 0, 1, 2 and 4 hours post dose. The data is shown in Figure 3.8 and shows an increase in plasma concentrations of both labelled and unlabelled

antibody over time. For the unlabelled antibody, the increase is from an average of 44 ng/mL at t=0 to an average of 236 ng/mL 4 hours post dose, an overall 5.4-fold increase over 4 hours. This correlates well with the plasma levels of labelled antibody, which showed a 5.2-fold increase over 4 hours from 61 to 321 ng/mL. Comparison of the results for labelled and unlabelled antibody using Student's unpaired t-test did not reach statistical significance ($p>0.05$) at any timepoint.

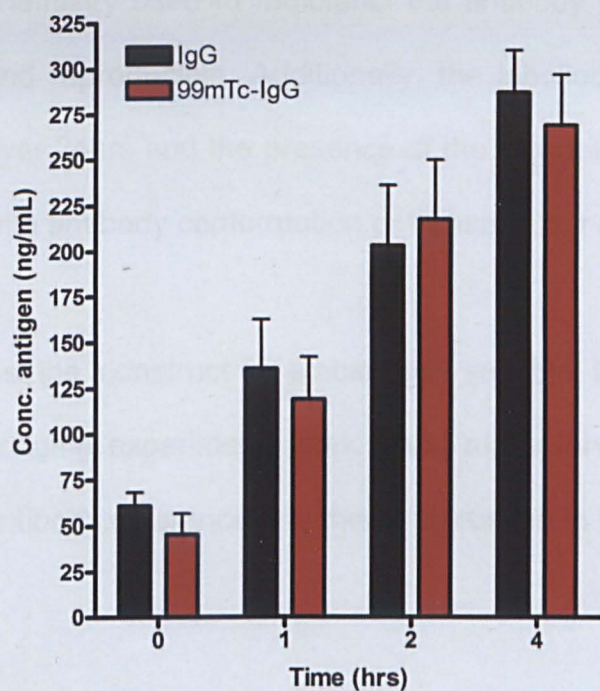


Figure 3.8 - Graph showing that the concentration of labelled and unlabelled antibody detected by ELISA in plasma samples taken up to 4 hours post dose are highly similar. Error bars are \pm sem (n=6).

The results described in Figure 3.8 indicate that the presence of the technetium label is not affecting transport of the antibody out of the lung. This means that technetium is a suitable tracer to use in the

imaging experiments and that quantification of the re-distribution of an instilled technetium labelled antibody after intratracheal instillation will provide an accurate description of the *in vivo* pulmonary clearance of antibodies.

3.4 Conclusions

In summary the work detailed in this chapter indicates that the chemistry used to radiolabel the antibody with technetium is effective and reproducible. Additionally, the labelled antibody is stable *in vivo* over 24hrs and the presence of the technetium label does not interfere with antibody conformation or transport out of the lung.

As the construct is stable and suitable for use as a tracer in the imaging experiment, work could move forward in imaging pulmonary antibody clearance and this is discussed in the next chapter.

CHAPTER 4: Imaging Pulmonary Antibody Clearance

4. Overview

This chapter details the results obtained from the imaging experiments designed to determine the rate and mechanism of antibody transport out of the lung.

To determine the relative contributions of passive and active transport to the rate of antibody clearance, the clearance rates for whole IgG, antibody fragments and mutant IgG with different binding affinities for mFcRn are presented. The expression of mFcRn in the mouse lung is also investigated using immunohistochemical staining of paraffin embedded lung sections, in order to determine the extent of receptor availability for active transcytosis of intratracheally instilled IgG.

4.1 Introduction

This chapter details the results of the experiments designed to determine the rate and mechanism of pulmonary antibody clearance. Determination of the rate of clearance was achieved by imaging the distribution of an intratracheally instilled radiolabelled antibody, *in vivo*, over time using a combination of SPECT and CT imaging. In addition, the clearance of antibody fragments and the FN3 protein were

determined in the same manner to provide information regarding the extent of passive diffusion controlled processes on antibody clearance.

As passive diffusion is inversely proportional to molecular weight it is expected that if passive diffusion is important in pulmonary antibody clearance then the increase in clearance rate of the IgG, Fab, scFv and FN3 plotted against molecular weight will be linear. The contribution of active transcytosis by mFcRn (see section 1.5 for more detail) to antibody clearance will be investigated using the mutant IgG produced in Chapter 2, with different binding affinities to mFcRn. If transcytosis by mFcRn is important in pulmonary antibody clearance then the clearance profiles of the IgG mutants would be expected to be significantly different, with the reduced and null binding mutants cleared more slowly than wild type IgG and with the improved binder perhaps being transported out of the lung faster than wild type.

4.1.1 SPECT/CT imaging

The imaging technique used to study the redistribution of the intratracheally instilled antibody, fragments and mutants in this work is a combination of CT and SPECT imaging. In brief, the combination of CT and SPECT imaging allows for the 3 dimensional localisation of radioactivity *in vivo*. The two images (CT and SPECT) are taken in the same animal in the exact same position, so that the images can be fused. The CT image is in essence a 3D X-ray of the animal and

provides anatomical information, which is overlaid with the 3D radioactivity map provided by the SPECT image. This results in an easily interpretable qualitative picture of the 3D distribution of the radiolabelled antibody within the animal, which can be quantified in terms of levels of radioactivity within a given region of interest.

It is anticipated that the SPECT/CT images will provide the redistribution patterns for the radiolabelled proteins studied, both qualitatively in terms of which organs the proteins build up in over time and quantitatively in terms of the percentage of the originally instilled dose that remains in the lungs over the course of the experiment. Ultimately pulmonary retention profiles of the intratracheally instilled proteins will be generated over 24hrs.

4.2 Materials and Methods

4.2.1 Materials

Technetium labelled WT IgG, Fab, scFv, FN3, IgG_H435A, IgG_V250Q and IgG_H435A_I253A were prepared as described in Chapter 3.

4.2.2 Methods

4.2.2.1 Statement of ethics for *in vivo* studies

All *in vivo* experiments were performed in compliance with licences issued under the UK Animals (Scientific Procedures) Act 1986 following local ethical review.

4.2.2.2 SPECT/CT imaging protocol

Female BALB/c mice, aged 8–12 weeks (n=6 per group), were purchased from Charles River UK Ltd (Margate, Kent, UK). The animals were housed in specific pathogen-free conditions in plastic cages with absorbent bedding material and maintained on a 12 hour daylight cycle. Food and water were provided *ad libitum*. The animals were acclimatised for a minimum of 7 days before commencement of studies.

Animals were anaesthetized with 2.5% isoflurane in oxygen, suspended by the front incisors on a nose cone delivering 1.5% isoflurane in oxygen to maintain anaesthesia. Animals were intratracheally dosed with radiolabelled-antibody/fragment at 3 mg/kg and 20 MBq/mouse, by insertion of a dosing needle through the larynx and into the top of the trachea. Animals were allowed to recover and returned to their home cage.

At timepoints of 0, 2, 4, 8, 18 and 24 hours post dose, animals were terminally anaesthetized with ketamine (at 25 mg/kg) and medetomidine (at 1 mg/kg) delivered at a dose of 0.1 mL/kg via the intraperitoneal route. All imaging was performed on spontaneously breathing animals on a nanoSPECT/CT small animal imager (Bioscan Inc, Washington, DC, USA). CT acquisition was made at 45 kVp over 360 continuous projections and the length of each CT scan was ~3 min. Respiratory gating was not employed in the study. Calibration of images for Hounsfield Unit (HU) scaling was performed using a water-filled phantom once per day of imaging. SPECT acquisition was then performed using 24 projections each 20 s long.

Following the completion of the SPECT scan, animals were sacrificed with an overdose of pentobarbitone sodium. The entire animal was placed in the well counter and total activity recorded. Blood was taken from the descending vena cava into pre-weighed EDTA anti-coagulant tubes, the sample was weighed and the total activity present assessed with the well counter. Blood samples were spun for 10 min at 5000 g and the plasma separated into fresh microfuge tubes. The lungs were also excised and total lung activity determined using the well counter.

4.2.2.3 Image processing and fusion

CT and SPECT images were processed with Amira 4.1 software (Visage Imaging, Andover, MA, USA). Both SPECT and CT images

were smoothed using a low pass 3D Gaussian filter. The skeleton was segmented in the CT image using an automatic threshold of 700 HU, this was manually inspected and altered to include all bone areas and excluded any non-bone areas. SPECT images were enlarged to the same dimensions as the corresponding CT image. Regions of interest were generated to include all activity above 50 units (arbitrary intensity units) either a) within the ribcage or b) outside of the ribcage. Activity within the rib cage was labelled as total lung activity. Finally, the skeleton from the CT image and 2 regions of interested from the SPECT image were viewed as, three dimensional isosurfaces.

4.2.2.4 Histopathological measurement of mFcRn expression in healthy BALB/c mouse lung

Two female BALB/c mice, aged 8 weeks (Harlan, UK), were euthanized with an overdose of sodium pentobarbitone. At necropsy, the trachea was cannulated and the lungs instilled with 10% neutral buffered formalin at a constant pressure of 25 cm H₂O. Once the lungs were fully distended, the trachea was tied off and the lungs removed from the thoracic cavity and post-fixed in 10 % neutral buffered formalin for 48 hours. Individual lobes were then trimmed and embedded in paraffin.

Sections were cut at a thickness of 3 µm, floated onto glass slides, dried overnight at 37 °C and baked for 30 minutes at 60 °C. Sections

were dewaxed and rehydrated on a Leiko Autostainer XL and heat mediated antigen retrieval was performed by boiling the rehydrated sections in Low pH Antigen Unmasking Solution (Vector, H-3300) in a pressure cooker for 2 minutes. The pressure cooker was cooled and sections washed for 10 minutes in running tap water. Sections were then peroxidase blocked by immersion in 3 % hydrogen peroxide in methanol for 10 min. Sections were washed for 10 minutes in cold running tap water before loading onto a Dako Autostainer.

Sections were blocked for 20 min in 2.5 % casein in DPBS, rinsed with DPBS-T, incubated for 60 minutes with goat anti-mFcRn primary antibody at 1 µg/mL (R&D systems AF6673) or in DPBS-T for diluent controls. Sections were rinsed with DPBS-T, incubated with anti-goat ImmPress-HRP reagent (Vector, MP-7401) for 30 minutes, rinsed again with DPBS-T and incubated with DAB+ substrate/chromagen (Dako, K3468) for 5 mins. Sections were rinsed with MilliQ water and counterstained with Gills II Haematoxylin (Pioneer Research Chemicals, Colchester, Essex, UK) and Eosin Y (Acros Organics, Fisher Scientific, Loughborough, Leicestershire, UK) according to standard protocols. Slides were imaged on an Aperio digital slide scanner.

4.3 Results and Discussion

4.3.1 Pulmonary clearance of a whole IgG

Images of the redistribution of intratracheally instilled wild type IgG were generated at 0, 2, 4, 6, 18 or 24 hrs post dose. The CT scan from each animal was processed to generate a 3D representation of the skeleton, which was then overlaid with the radiation activity map from the SPECT image. The resulting fused image shows the distribution of the radiolabelled antibody throughout the body over time. Representative images for whole IgG redistribution at 0, 2, 4 and 24 hrs post intratracheal instillation are shown in Figure 4.1. The images show qualitatively how the antibody redistributes.

It can be seen from Figure 4.1 that high levels of radioactivity are present in the lungs up to 24 hrs post dose, with levels of lung activity appearing to decrease over the course of the experiment. Initially there is evidence of radiation within the trachea and larynx, it is expected that this has deposited during dosing as the dosing needle is put through the larynx and into the top of the trachea. The activity in the larynx/trachea is not detectable from 2 hours post dose, indicating that it is rapidly cleared, however it is not clear whether this activity is cleared by mucociliary clearance and swallowed or whether the antibody crosses the tracheal epithelium either by passive or active transport.

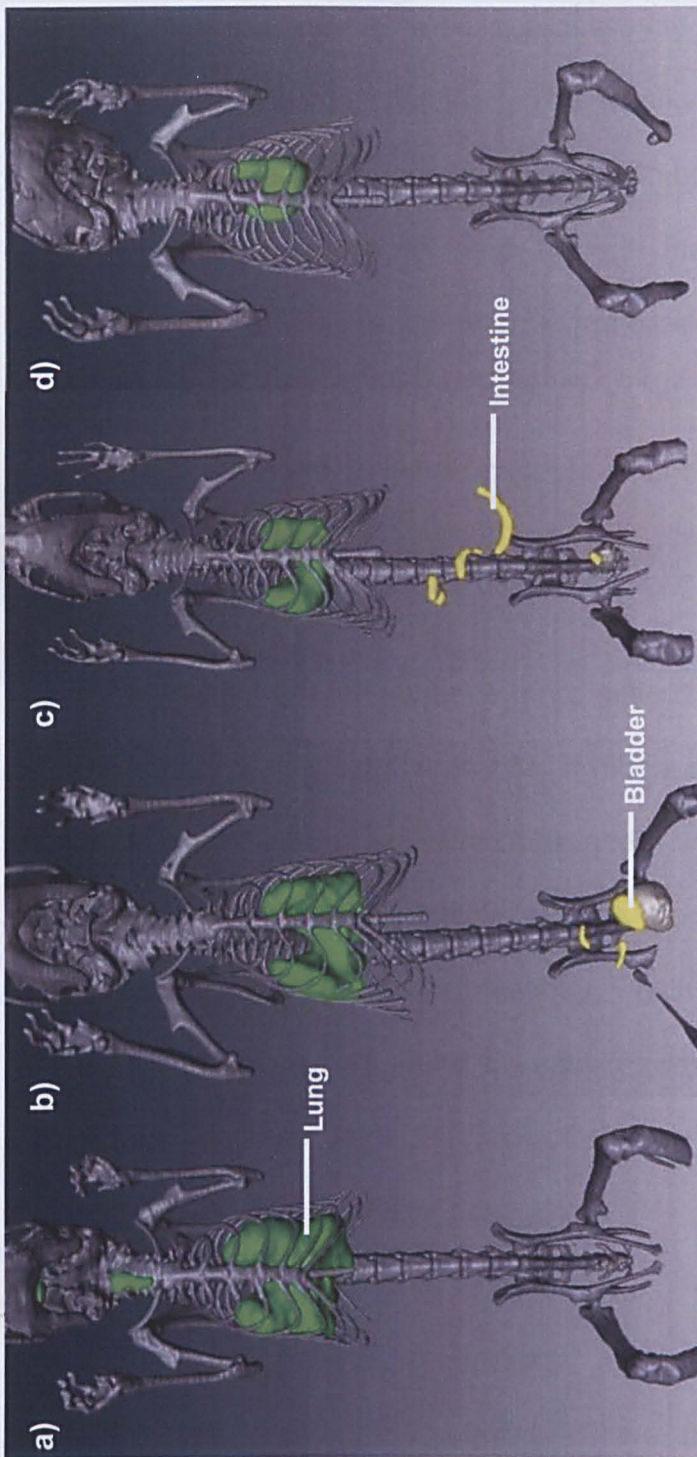


Figure 4.1 - Representative SPECT/CT images showing pulmonary retention of IgG at a) 0, b) 2, c) 4 and d) 24 hrs. Areas of lung activity are shaded green and areas of activity outside the lung shaded yellow. The images show decreasing levels of activity in the lung over 24 hrs, with activity visible within the bladder and intestines at some timepoints.

The later images also show a buildup of activity within the bladder and what appears to be the intestines. The activity in the bladder is not indicative of free technetium and is unlikely to be labelled antibody, as a 150 kDa protein would not pass through the healthy kidney. It is thought that this activity represents tagged breakdown products of the labelled antibody, where the radiolabel is attached to a sufficiently small protein fragment, which is capable of undergoing renal filtration (i.e. less than 25 kDa).

The activity within the intestines is more difficult to interpret, but could be indicative of mucociliary clearance. If mucociliary clearance was an important mechanism in antibody clearance it would be expected that later images would show activity moving from the trachea to the oesophagus stomach and then intestines, which is not observed in the images. No evidence was found for activity within the stomach in any animal from any time point, this lack of stomach activity is suggestive that mucociliary clearance is not occurring.

Investigation of murine mucociliary clearance by scintigraphy suggested that clearance occurred in two phases, with tracheo-bronchially deposited particles cleared over 24 hrs and alveolar deposited particles cleared over several months (Foster et al., 2001). However, the particles studied by Foster were insoluble in water and the antibody solution instilled here is likely to rapidly diffuse through the mucus layer. From this we have concluded that liquid based

formulations of antibodies are unlikely to undergo significant mucociliary clearance.

Importantly, there is no build up of activity observed within the stomach or thyroid, which is where free technetium would accumulate, This confirms that the radiolabelled antibody is stable *in vivo* over 24 hrs.

The images in Figure 4.1 represent qualitatively the antibody redistribution after intratracheal instillation. However, by determining the activity present in the lung at each time point and relating this to the dose initially given to the animal it is possible to record the percentage of the instilled dose that remains in the lungs over the course of the experiment. This is represented graphically in Figure 4.2 and provides insight into the pulmonary retention rate of intratracheally instilled antibody.

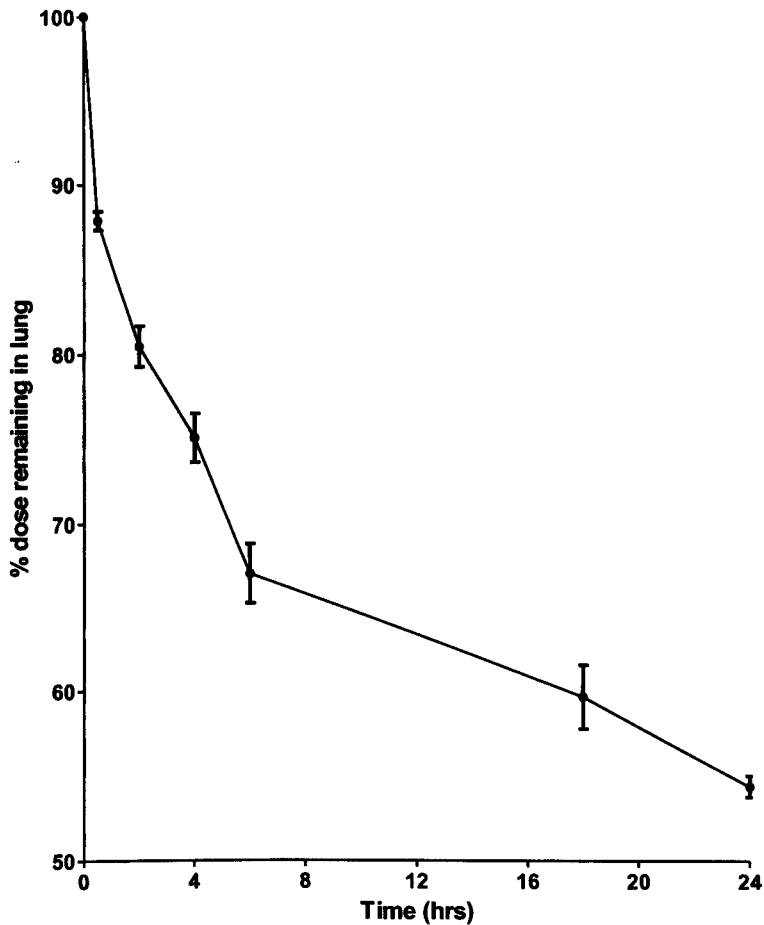


Figure 4.2 - Graph showing the pulmonary retention of intratracheally instilled antibody over 24 hrs. Error bars are \pm sem (n=6).

Figure 4.2 shows the pulmonary retention of whole IgG over 24 hrs post intratracheal instillation. Initially there is a phase of comparatively rapid clearance up to 6 hours post dose, which is followed by a slower clearance phase up to 24 hours post dose. Non-linear regression, performed in GraphPad Prism 5, indicated that a biphasic exponential decay curve best described the data, the parameters for which can be seen in figure 4.3.

Parameter	Best fit value
Y0	100 % (fixed)
Plateau	55.37 ± 1.47 %
%Fast	22.10 ± 7.13 %
Kfast	6.24 ± 1.31 h ⁻¹
Kslow	0.16 ± 0.033 h ⁻¹
Half life (slow)	4.35 h
Half life (fast)	0.11 h
F Test p value	0.575

Figure 4.3 - Table showing the best fit values for non-linear regression analysis (biphasic exponential decay model) for pulmonary clearance of WT whole mlgG.

The data in figure 4.3 show that the pulmonary clearance of intratracheally instilled whole mlgG1 can be described by a two phase exponential decay model. The F test is a measure of whether the model is adequate to describe the data and compares the scatter between replicates at each timepoint to the distance between the point and the curve. A small p value indicates poor fit of the data to the model as the distance from the curve for each point is much greater than the distance between individual replicates. In this case the p value is above 0.05, which indicates adequate fit of the data to a biphasic exponential decay model.

The data in figure 4.3 show that the pulmonary clearance of antibody can be described by an initial fast phase of clearance with a half life of

4.35 h, followed by a second slower phase of clearance with a half life of 0.11 h. Clearance reaches a plateau with 56 % of the originally instilled dose retained in the lungs after 24 hrs. Additional points post 24 hrs would further help to define the plateau and further refine the model; however this is not possible using the SPECT/CT method employed as the natural decay of the technetium tracer makes time points post 24 hrs impossible to measure.

4.3.2 Pulmonary clearance of antibody fragments and the FN3 protein

The clearance rates of inhaled antibody fragments from the lungs were then determined in order to investigate the importance of passive diffusion to the rate of antibody clearance. Images showing the redistribution of the instilled Fab and scFv fragments at 0,2,4 and 24 hours post dose are shown in Figure 4.4.

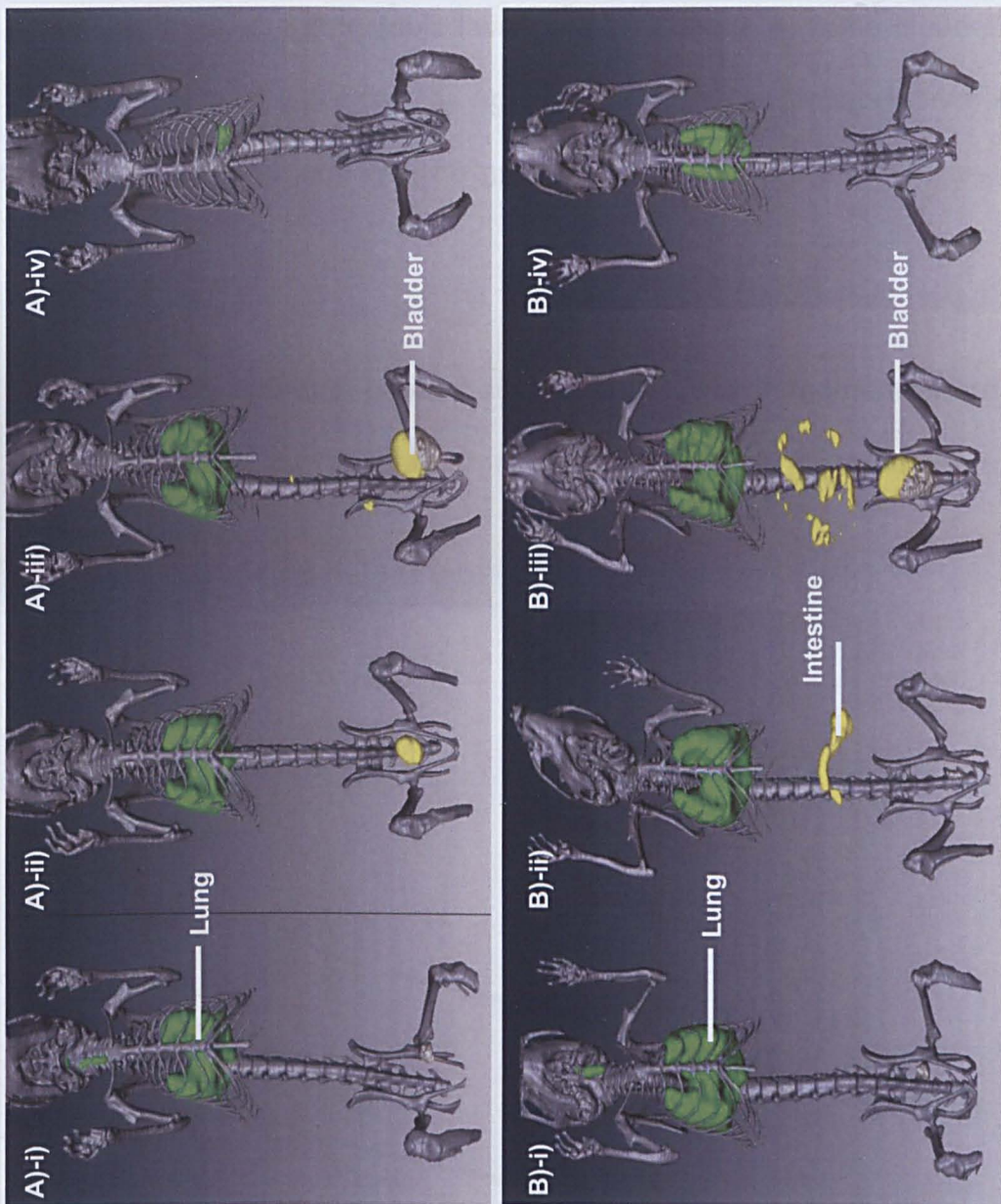


Figure 4.4 - Representative SPECT/CT images showing pulmonary retention of A) Fab and B) scFv at i) 0, ii) 2, iii) 4 and iv) 24 hrs. Areas of lung activity are shaded green and areas of activity outside the lung shaded yellow . The images show decreasing levels of activity in the lung over 24 hrs, with activity visible within the bladder and intestines at some timepoints.

The time courses for the antibody fragments in figure 4.4 show similar redistribution profiles to the original whole IgG. There is rapidly cleared tracheal deposition, decreasing lung activity over the course of the

experiment, but with detectable levels out to 24 hrs and some bladder and intestinal build-up of activity. Again there is no convincing evidence of mucociliary clearance with no gastric activity ever observed in any animal.

The pulmonary retention profiles of the Fab and scFv fragments were determined as a percentage of the initially instilled dose and are expressed in Figure 4.5.

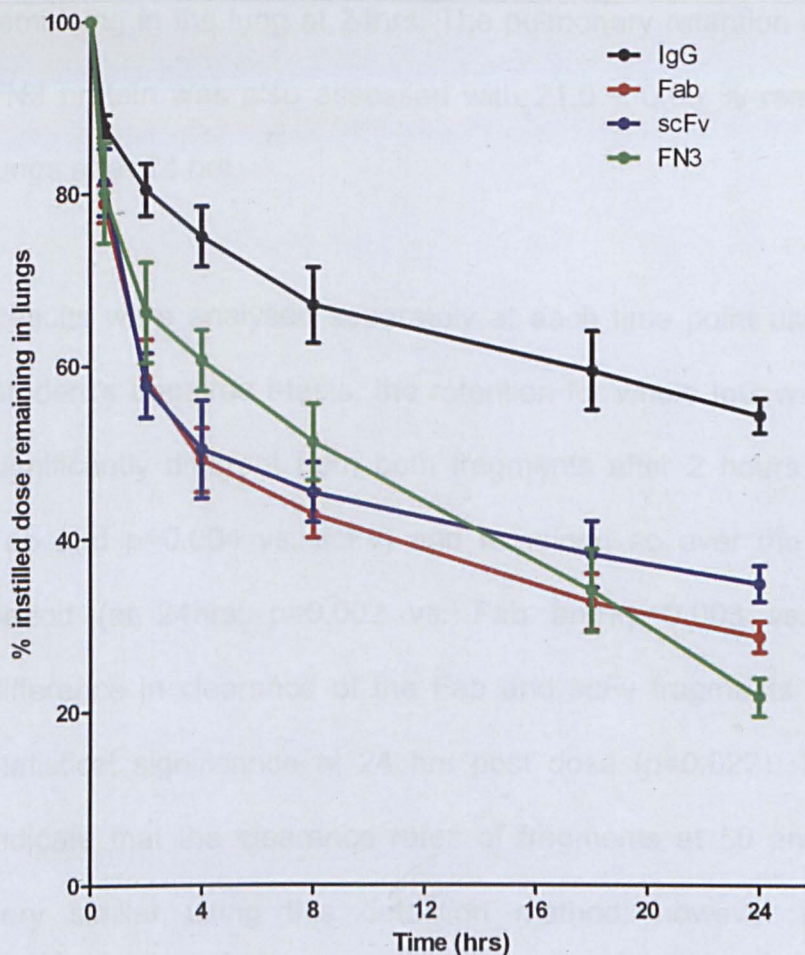


Figure 4.5 - Graph showing the pulmonary retention profiles of intratracheally instilled antibody, fragments and the FN3 protein over 24 hrs. Error bars are \pm sem (n=6 per point).

Figure 4.5 shows that the pulmonary retention of whole IgG is significantly greater over 24 hrs than for either the Fab or scFv fragments. The fragments are initially cleared more rapidly than the whole IgG and, although the shapes of the curves are similar, the plateau reached for fragment retention is far lower than that for whole IgG. Specifically, it was determined that 54.4 ± 0.63 % of the total instilled dose of a whole monoclonal antibody remains in the lung over 24 hrs, with Fab and scFv fragments cleared significantly quicker with 28.7 ± 0.73 % and 34.9 ± 0.85 % respectively of the total instilled dose remaining in the lung at 24hrs. The pulmonary retention of the 11 kDa FN3 protein was also assessed with 21.0 ± 0.65 % remaining in the lungs after 24 hrs.

Results were analysed separately at each time point using two tailed Student's unpaired t-tests; the retention for whole IgG was statistically significantly different from both fragments after 2 hours ($p=0.008$ vs. Fab and $p=0.004$ vs. scFv) and remained so over the whole 24 hr period (at 24hrs: $p=0.002$ vs. Fab and $p=0.003$ vs. scFv). The difference in clearance of the Fab and scFv fragments only reached statistical significance at 24 hrs post dose ($p=0.022$). These results indicate that the clearance rates of fragments at 50 and 28kDa are very similar using this detection method; however they can be distinguished from whole IgG.

The 11kDa FN3 protein, the fibronectin III domain, which mimics an antibody fold, was used as a surrogate smaller antibody fragment than the scFv. The protein is not capable of binding antigen and its sequence is not related to the other proteins used in this work, inclusion of the data for this protein was simply to determine the pulmonary retention of a species smaller than an scFv.

A lower pulmonary retention level at 24 hrs is expected for smaller fragments, in comparison to the larger fragments. However, the shape of the curve in Figure 4.5 for FN3 is indicative of a different clearance profile than the other proteins. The images in Figure 4.6a) show the redistribution of instilled labelled FN3 protein at 0,2,4 and 24 hrs post dose. Figure 4.6b) shows a rotated view of the 2 hr image, with two slices through the SPECT image at this time point, one showing activity within the kidney and the other activity within the lungs.

The images in Figure 4.6 show the different redistribution pattern for the FN3 protein in comparison to the other proteins tested. There is significant renal filtration of labelled FN3, as evidenced by the very high levels of activity observed in the kidney from 2-4 hrs post dose. The images in Figure 4.6b) confirm renal filtration of the FN3 fragment, with the renal cortex highlighted in the SPECT image. In addition the SPECT images of the lung shows good coverage of the periphery, with the instilled antibody covering the majority of the lung not just central regions.

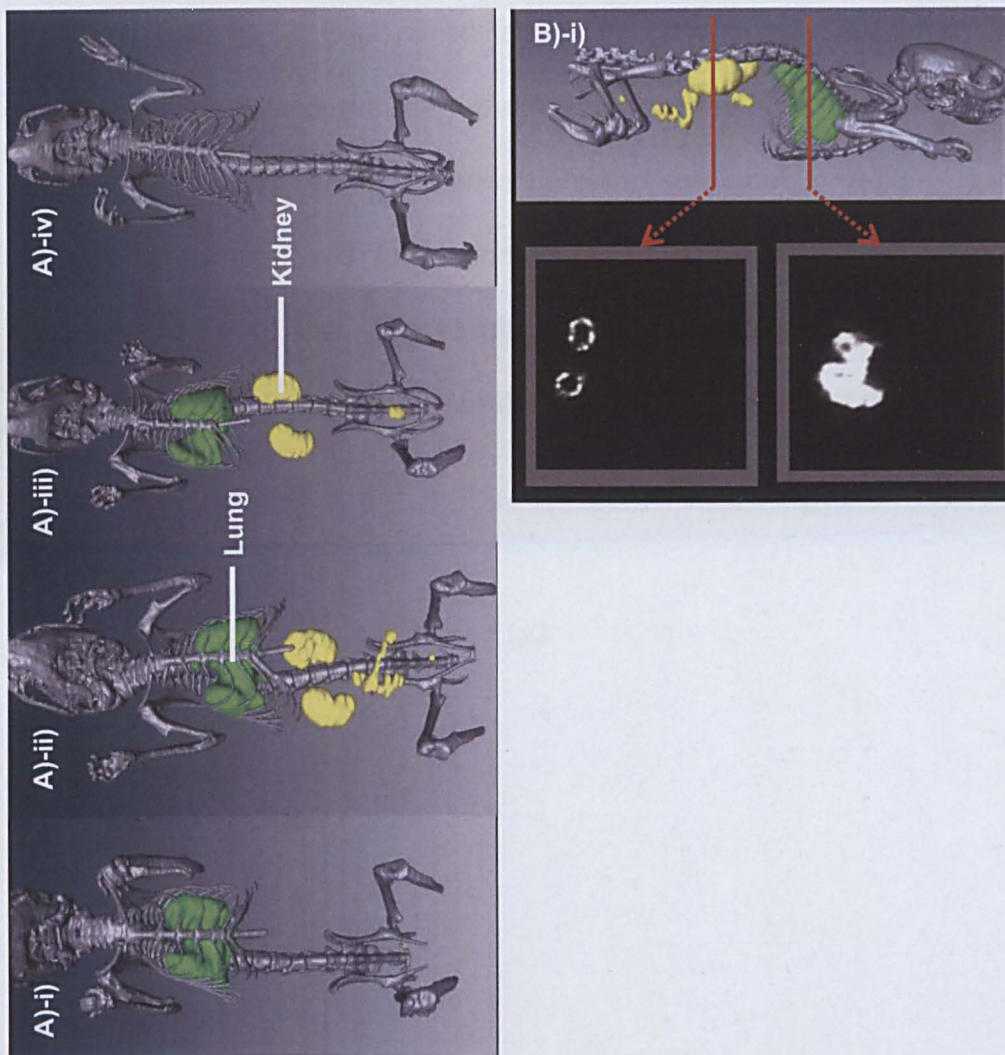


Figure 4.6 - Representative SPECT/CT images showing:

A) pulmonary retention of FN3 protein at i) 0, ii) 2, iii) 4 and iv) 24 hrs. Areas of lung activity are shaded green and areas of activity outside the lung shaded yellow. The images show decreasing levels of activity in the lung over 24 hrs, with activity visible within the bladder and intestines at some timepoints. In addition, there is activity visible in the kidneys between 2 and 4 hours post dose

B) Rotated FN3 2 hr image with views from original SPECT scan showing activity in kidney and lungs. Black represents low activity and white represents high activity.

The pulmonary retention levels of each protein were plotted against molecular weight. If passive diffusive processes are important in determining the rate of antibody clearance from the lungs then a linear relationship would be expected between molecular weight and pulmonary retention, with larger molecules being more easily retained, according to Fick's law. The results of the comparison of pulmonary retention at 24hrs for each fragment are shown in Figure 4.7.

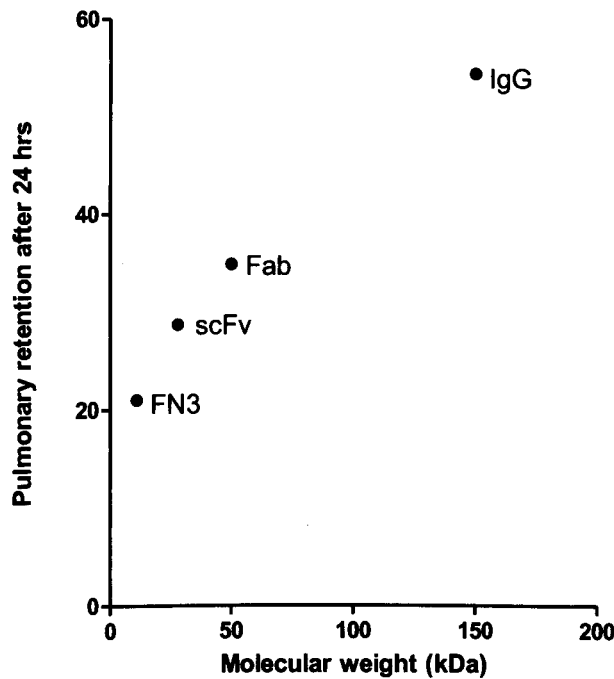


Figure 4.7 - Graph showing pulmonary retention of IgG, Fab, scFv and FN3 protein 24 hrs post i.t instillation as a function of molecular weight.

The results generally show the expected trend, with the larger proteins retained to greater extents than the smaller proteins, however the trend is not completely linear in appearance, appearing to plateau at larger molecular weights, with IgG cleared slightly quicker than a linear

relationship would suggest. Although there are only 4 data points the graph provides some indication that diffusion controlled processes are important in pulmonary antibody clearance and further implies that there could be a small, but significant role for active transport of IgG out of the lung.

4.3.3 Pulmonary retention of mutant mIgG with differing binding affinities to mFcRn

The pulmonary retention of the mutant versions of the whole IgG with differing binding affinities to mFcRn was determined. The results showing the percentage of the instilled dose remaining in the lungs over 24 hrs for each mutant is shown in Figure 4.8.

Figure 4.8 shows that the pulmonary retention of each of the IgGs tested is very similar. Again there is initially comparatively rapid clearance which begins to plateau around 18-24hrs post dose. Two tailed, unpaired Student's t-tests were used to compare % pulmonary retention between each mutant separately at each time point, with no statistically significant differences reported below the $p=0.05$ level. This indicates that the clearance of each of the mutants, as determined here, is equal. This provides strong evidence that active transport by mFcRn is not important in pulmonary antibody clearance.

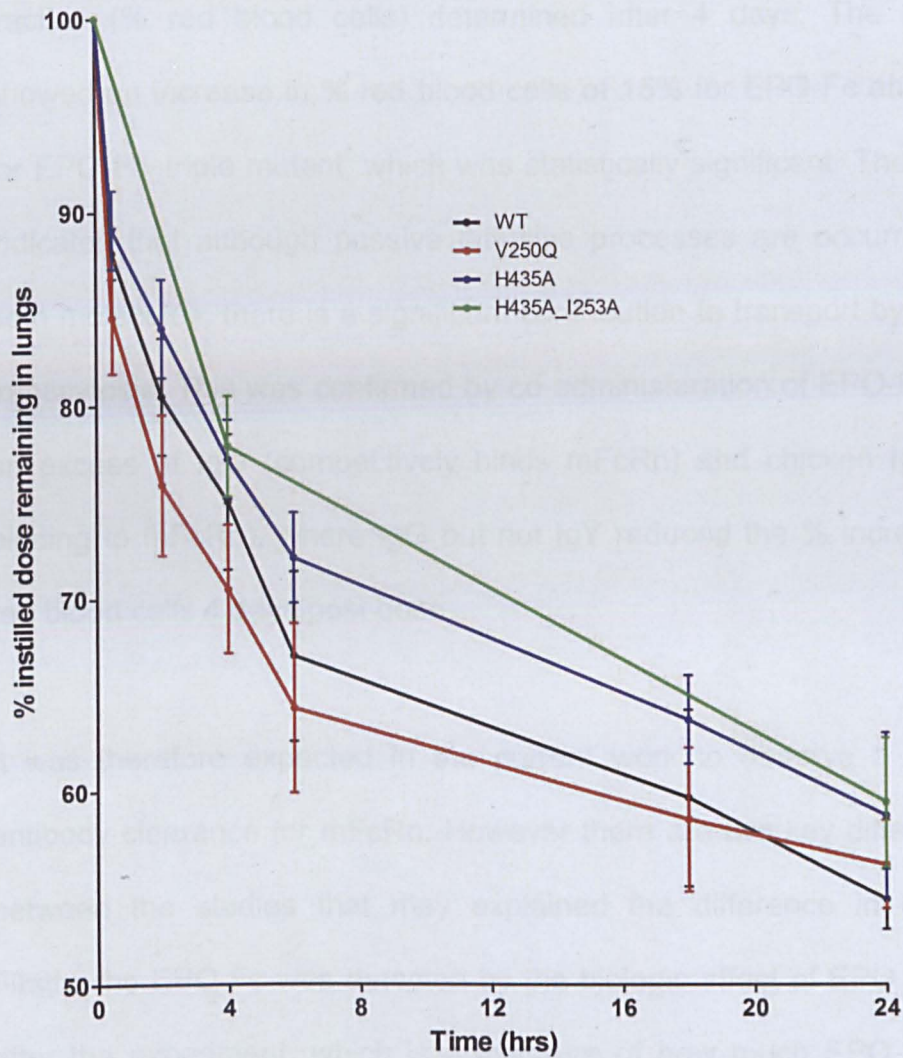


Figure 4.8 - Graph showing the pulmonary retention of intratracheally instilled antibody and FcRn binding mutants over 24 hrs. Error bars are \pm sem (n=6 per point).

The result showing the mFcRn transport is not important in pulmonary antibody clearance is unexpected. Previous work by (Spiekermann, et al., 2002) clearly demonstrated active pulmonary transport of erythropoietin (EPO) conjugated to an IgG Fc region. In the study EPO-Fc and EPO-Fc with binding to mFcRn ablated (Triple mutant including the H435A, I243 and an additional H310A mutation) were delivered intranasally to female BALB/c mice and the reticulocyte

fraction (% red blood cells) determined after 4 days. The results showed an increase in % red blood cells of 15% for EPO-Fc and 10% for EPO-Fc_triple mutant, which was statistically significant. The result indicates that although passive diffusive processes are occurring for both molecules, there is a significant contribution to transport by active transcytosis. This was confirmed by co-administration of EPO-Fc with an excess of IgG (competitively binds mFcRn) and chicken IgY (no binding to mFcRn), where IgG but not IgY reduced the % increase in red blood cells 4 days post dose.

It was therefore expected in the current work to observe a role in antibody clearance for mFcRn. However there are two key differences between the studies that may explain the difference in results. Firstly, the EPO-Fc was detected by the biologic effect of EPO 4 days after the experiment, which is a measure of how much EPO-Fc has crossed the lung over 4 days and starts from an automatic 0 % value. In the study reported here, the pulmonary retention is calculated up to 24 hrs post dose. The pulmonary retention starts from 100 % and drops over the course of the experiment. An increase from a zero baseline is more easily observed than a decrease from a 100 % baseline, so this may result in the EPO study being more sensitive to small changes in the amount of EPO-Fc transferred.

Secondly, the 4 day experimental length in the case of EPO allows more time for the antibody clearance to plateau and perhaps for the

clearance profiles of the WT and mutant version to diverge. In summary, the current research demonstrates that transcytosis of mFcRn is not important in antibody clearance from the lung over the first 24 hrs post dose. However, the research cannot rule out a contribution from active transcytosis which only becomes apparent at later time points, when passive diffusion is less dominant.

4.3.4 Immunohistochemical analysis of the expression of mFcRn in the normal mouse lung

In order to further examine the result showing no involvement of mFcRn transcytosis in antibody clearance from the lung, immunohistochemical analysis of female BALB/c mouse lung tissue was carried out to test for the presence of mFcRn. The evidence for mFcRn expression in the lung in the literature is conflicting; several studies have found no evidence for mFcRn expression (Kuo & Avensen, 2011) (Akilesh, et al., 2007), however two studies have shown expression of mFcRn at low levels, one in the epithelium (Spiekermann, et al., 2002) and one throughout the entire lung (Sakagami, et al., 2006).

The histological analysis was performed as detailed in section 4.2.2.3 and resulting images from the IHC are shown in Figure 4.9.

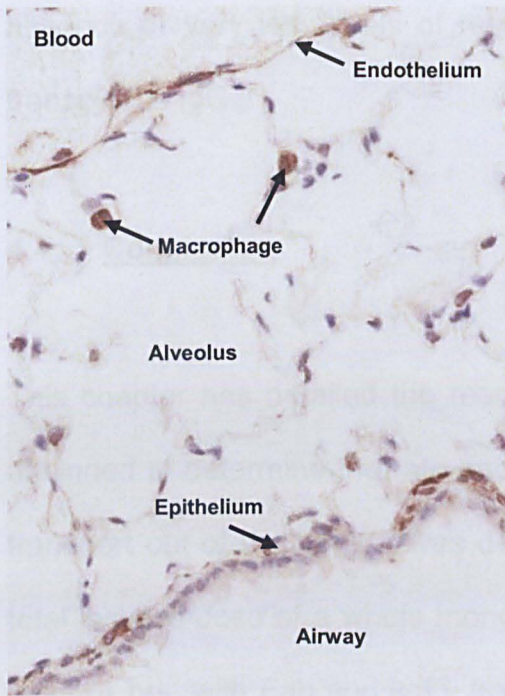


Figure 4.9 - Image of mouse lung stained with anti-mFcRn antibody at x20 magnification. Brown areas represent mFcRn expression, visible in the epithelium, endothelium and on alveolar macrophages.

In Figure 4.9 the brown colour represented mFcRn expression. The image covers a section of the lung containing alveoli, large airways and smaller blood vessels. mFcRn is known to be expressed at the endothelium and to be very strongly expressed on alveolar macrophages, it should be noted that FcRn expressed on macrophages would not contribute to transcytosis. Expression on alveolar macrophages was strong and there was some evidence for endothelial staining in blood vessels, however there was no evidence for epithelial staining for mFcRn in either the airways or alveoli. This result helps to explain the result observed with the mutant IgG, as there is no evidence for mFcRn expression in the lung and so the capacity of the mFcRn transcytosis pathway is expected to be low, due to the

absence or very low levels of receptor in the appropriate location to transcytose IgG.

4.4 Conclusion

This chapter has detailed the results obtained in the imaging studies designed to determine the rate and transport mechanisms for antibody transport out of the lung. It was determined that 54.4 ± 0.63 % of the total instilled dose of a whole monoclonal antibody remains in the lung over 24 hrs, with Fab and scFv fragments cleared significantly quicker with 28.7 ± 0.73 % and 34.9 ± 0.85 % respectively of the total instilled dose remaining in the lung at 24hrs. The pulmonary retention of the 11 kDa FN3 protein was also assessed with 21.0 ± 0.65 % remaining in the lungs after 24 hrs.

The results showed that passive diffusion controlled pathways are important in pulmonary antibody clearance and that, at least over the first 24 hrs, the contribution to clearance by transcytosis by mFcRn is not significant. This result was further clarified by the lack of evidence for mFcRn on the air facing surfaces of the lung as determined by IHC. Work now moved forward to investigate antibody clearance from the lung in a model of lung disease, which is detailed in the next chapter.

CHAPTER 5: Further Characterisation of and Investigation of Pulmonary Antibody Clearance in a Murine House Dust Mite Model of Asthma

5. Overview

This chapter details the work undertaken to further characterise the murine house dust mite (HDM) model of asthma and to determine whether pulmonary antibody clearance is altered in the diseased lung. Lung density changes following HDM exposure are assessed by CT imaging and related to cellular infiltration and pathology results. In addition the transport of IgG out of the HDM exposed lung is investigated, with the aim of determining how the rate of antibody clearance changes in the diseased lung. Finally the expression of the mFcRn receptor is determined in the HDM exposed lung in order to evaluate whether there will be any expected change in the contribution of active transcytosis to the pulmonary clearance of an intratracheally instilled antibody following HDM exposure.

5.1 Introduction

In practical terms, inhaled antibodies are unlikely to be delivered to the healthy lung in patients. The more promising targets for pulmonary delivery of biologics are within the lung and as such delivery is expected to be in the diseased lung. One possible disease which may

benefit from inhaled biological treatments is asthma and there is some ongoing research in this area. An inhaled synthetic analogue of vasoactive intestinal peptide has been shown to successfully induce bronchodilation in patients with stable asthma (Linden, et al., 2003). In addition inhaled interleukin (IL) -4 receptor has been shown to stabilise asthma in patients upon the withdrawal of inhaled glucocorticosteroids (Borish, et al., 1999). An anti-IL 13 antibody given intratracheally in mice has been shown to dose dependently attenuate the airway hyperresponsiveness caused by subsequent inhalation of IL-13 (Blanchard, et al., 2005). It was therefore decided to evaluate antibody clearance from the lung in an *in vivo* model of asthma, as a relevant diseased lung of interest.

There are a number of *in vivo* models of asthma. The chronic murine house dust mite model of asthma has been shown to lead to severe and persistent airway inflammation, extensive airway eosinophilia, remodelling and a Th2-biased immune response, with increased airway resistance and bronchoconstrictor response to methacholine in house dust mite exposed animals. The inflammatory response can be reduced by treatment with corticosteroids and phosphodiesterase 4 inhibitors, as is the case in human asthma (Nials & Uddin, 2008).

In this work, further characterisation of the murine house dust mite (HDM) model will be undertaken to determine whether the changes in lung pathology can be monitored non-invasively with CT imaging.

Previous work has shown that CT imaging can be successfully employed to determine the density changes observed in the ovalbumin exposed lung, with an increase in density corresponding to an increase in pulmonary oedema and cellular infiltrate in the lungs.

5.1.1 Affect of the diseased lung on antibody transport

As the HDM exposed lung has been shown to be severely inflamed it is anticipated that the disruption to the epithelial surface will lead to greater epithelial permeability and an increase in the rate of antibody transport out of the lung by passive diffusion between the epithelial cells. There is currently no information available regarding the expression of mFcRn in the HDM exposed murine lung. This work will determine whether there is any up or down regulation of the mFcRn expression after HDM expose and will use the result to determine whether there is any change in the relative contribution to the pulmonary clearance of an inhaled antibody is expected.

5.2 Materials and methods

5.2.1.1 Statement of ethics for *in vivo* studies

All *in vivo* experiments were performed in compliance with licences issued under the UK Animals (Scientific Procedures) Act 1986 following local ethical review.

5.2.2 HDM dosing protocol used in CT imaging experiments

Female BALB/c mice, aged 8–12 weeks (n=6 per group), were purchased from Charles River UK Ltd (Margate, Kent, UK). The animals were housed in specific pathogen-free conditions in plastic cages with absorbent bedding material and maintained on a 12 hour daylight cycle. Food and water were provided *ad libitum*. The animals were acclimatised for a minimum of 7 days before commencement of studies.

Mice were exposed to house dust mite, HDM, according to an established chronic allergen exposure protocol. Under sterile conditions, extract of whole body purified and lyophilised *Dermatophagoides pteronyssinus* house dust mites (Greer Laboratories, NC, USA) was re-suspended in sterile 0.9 % saline (Kabi Fresenius, UK) at a solution concentration of 500 µg/mL total protein. The extract solution contained Der p1 at 12.64 µg/mL and bacterial endotoxin at 13 EU/ml. HDM aliquots were maintained until use at +4 °C, with a single aliquot used each day and any remaining solution discarded once the aliquot had been opened.

All mice receiving HDM were exposed to the allergen through a single daily 50 µL intranasal dose given under light isoflurane anaesthesia, on 5 days each week, for up to 7 weeks. Control animals received a sham exposure of 50 µL sterile saline over the same time period using the

same method of administration. Over the final 2 weeks of HDM exposure, one group of animals was orally dosed with budesonide (Sigma-Aldrich, Poole, UK) at an initial dose of 3 mg/kg budesonide per day. Following significant weight loss, the dose was dropped to 1mg/kg after one day, for 2 weeks. All other animals (both HDM and saline control) received oral dose of saline.

5.2.3 CT Imaging

CT images were obtained once weekly from the week prior to exposure and 48 hours following the last HDM exposure in weeks 1, 2, 3, 4, 5, 6 and 7. Animals were anaesthetized with 2.5 % isoflurane in oxygen. All imaging was performed on spontaneously breathing animals on a nanoSPECT/CT small animal imager (Bioscan Inc, Washington, DC, USA). CT acquisition was made at 45 kVp over 360 continuous projections and the length of each CT scan was ~3 min. Respiratory gating was not employed in the study. Calibration of images for Hounsfield Unit (HU) scaling was performed using a water-filled phantom once per day of imaging.

CT images were processed with Amira 4.1 software (Visage Imaging, Andover, MA, USA). Air filled lung volumes were selected using a computer-assisted volume selection from -1000 to -250 HU, which was visually inspected and altered as necessary to ensure inclusion of all lung areas and exclusion of any non-lung areas.

Three dimensional images were low pass filtered (Gaussian) and density histograms were produced with 150 bins describing a range from -1000 to 0 HU (7 HU/bin). Air filled lung volumes were determined by calculating the air volume in each bin based on the mean HU value, then summing the amount of air in each bin over the entire lung volume.

Comparisons of lung density between treatment groups in each week were calculated using PROC MIXED in SAS v9.2, based on the modal lung density of each group. The model generated determined a 2 way analysis of variance, reflecting repeated measurements on the same animals each week, with pairwise contrasts of interest used to test the difference between treatment groups in each of the weeks. Results were deemed significant at the $p=0.05$ level.

5.2.4 Assessment of antibody transport out of HDM exposed lung

HDM sensitised and saline control mice, produced as described in section 5.2.2, were intratracheally dosed with whole IgG. Mice were anaesthetised with ketamine (80 mg/kg) and xylazine (8 mg/kg) given intraperitoneally (volume 5 mL/kg). Mice were suspended on a dedicated PennCentury mouse dosing platform on a surgical table. The neck area was swabbed with 70 % ethanol and a small incision made with fine scissors above the trachea. Intratracheal administration of 50

μ L whole IgG solution at 1.5 mg/ml was given into the trachea through the muscle layer using a 1mL syringe multi-stepper and a P30 needle. The skin incision was closed with VetBond cyanoacrylate adhesive and the mouse suspended for one minute on the dosing platform before being transferred to a warming cabinet until recovery (animals righted and ambulatory) or taken for necropsy. For post operative analgesia mice were given buprenorphine at 0.1 mg/kg.

At time points 0, 2, 4, 6, 18 and 24hrs post dose animals were sacrificed with an overdose of pentobarbitone sodium. The lungs were lavaged with 3 x 0.3 mL cold DPBS. Total and differential cell counts were determined using a Sysmex automated haemocytometer and total mlgG1 content analysed by ELISA, as described in section 5.4.2.

The large left lobe of the lungs was tied off and inflated with 1mL 10% neutral buffered formalin, post fixed in 10 % NBF for 48 hours, before being embedded in paraffin. The paraffin embedded lung sections were analysed for mFcRn expression by IHC as described in section 4.2.2.3.

5.2.5 mlgG1 ELISA

Total mlgG1 in BAL and lung homogenate was determined by ELISA using a total mlgG1 ELISA kit (eBioscience, UK). Nunc maxisorb 96 well plates were coated with 100 μ L/well anti-mouseIgG1 capture antibody diluted 1:250 in DPBS, sealed and incubated overnight at 4

°C. The plate was washed 2 x with 400 µL DPBS-T then blocked with 250 µl/well 10% BSA in DPBS-T for 2 hours at room temperature. The plate was washed 2 x with 400 µl/well DPBS-T and samples added at dilutions of 1:5, 1:50 and 1:500. Standard was mIgG1 at 200 – 6.25 ng/mL. Plates were then incubated with 50 µL/well anti-mouse IgG-HRP detection antibody at 1:250 dilution in DPBS-T at room temperature for 3 hours. Plates were washed 4 x with 400 µL/well DPBS-T and incubated with 100 µL/well TMB for 15 minutes, when 100 µL/well 1M sulphuric acid was added to each well. The plate was read at 450 nm.

Results for HDM animals had background levels of increased mIgG1 in the HDM exposed mouse BALF (68.46 ± 21.39 µg/ml) deducted from the ELISA result.

5.2.6 Immunohistochemistry

Lungs from HDM exposed and saline control animals were analysed for mFcRn expression as described in section 4.2.2.3. Additional sections were prepared as described in section 4.2.2.3 and stained with Gills II Haematoxylin (Pioneer Research Chemicals, Colchester, Essex, UK) and Eosin Y (Acros Organics, Fisher Scientific, Loughborough, Leicestershire, UK) according to standard protocols, to analyse disease progression.

5.3 Results

5.3.1 Model development/characterisation

5.3.1.1 Lung inflammatory cell influx

Mice were exposed to HDM over the course of 7 weeks, the results of cell levels detectable in BALF showed that repeated intranasal delivery of house dust mite extract resulted in a robust and significant inflammatory response in the lungs, shown in Figure 5.1. When compared to saline control animals, HDM exposed animals showed a 9-fold increase in total inflammatory cell numbers from $0.13 \pm 0.02 \times 10^6$ cells/mL to $1.17 \pm 0.21 \times 10^6$ cells/ml. After 2 weeks budesonide treated total cell counts compared the HDM group reduced approximately 3-fold to $0.43 \pm 0.12 \times 10^6$ cells/mL.

Numbers of eosinophils were significantly increased in HDM treated animals with $0.8 \pm 0.05 \times 10^4$ cells/ml detected in saline control animals compared to $0.65 \pm 0.09 \times 10^6$ cells/ml in HDM treated animals. Budesonide treatment significantly reduced levels of eosinophils observed in HDM exposed animals to $0.16 \pm 0.04 \times 10^5$ cells/ml.

Total BAL lymphocytes numbers increased from $0.89 \pm 0.16 \times 10^4$ cells/ml in saline control animals to $0.22 \pm 0.04 \times 10^6$ cells/ml in HDM exposed animals. Budesonide treatment significantly reduced

lymphocyte numbers in HDM treated animals to $0.42 \pm 0.07 \times 10^5$ cells/ml.

Additionally, neutrophil numbers in saline treated animals increased from $0.2 \pm 0.02 \times 10^5$ cells/ml to $0.22 \pm 0.04 \times 10^6$ cells/ml in the HDM exposed group. Budesonide treatment had no effect on neutrophil numbers. Numbers of monocytes remained relatively unchanged with HDM exposure and were unaffected by budesonide treatment.

These results are represented graphically in Figure 5.1, which shows that the increased total cell, eosinophil, lymphocyte and neutrophil levels in HDM exposed animals reach statistical significance at the $p > 0.005$ level when compared to saline controls. Additionally, the changes in eosinophil numbers after HDM exposure reach statistical significance at the $p > 0.005$ level when compared to HDM exposed animals which did not undergo budesonide treatment. Similar comparisons between HDM exposed and HDM exposed budesonide treated animals show reductions in total lymphocyte numbers reaching significance at the $p > 0.01$ level.

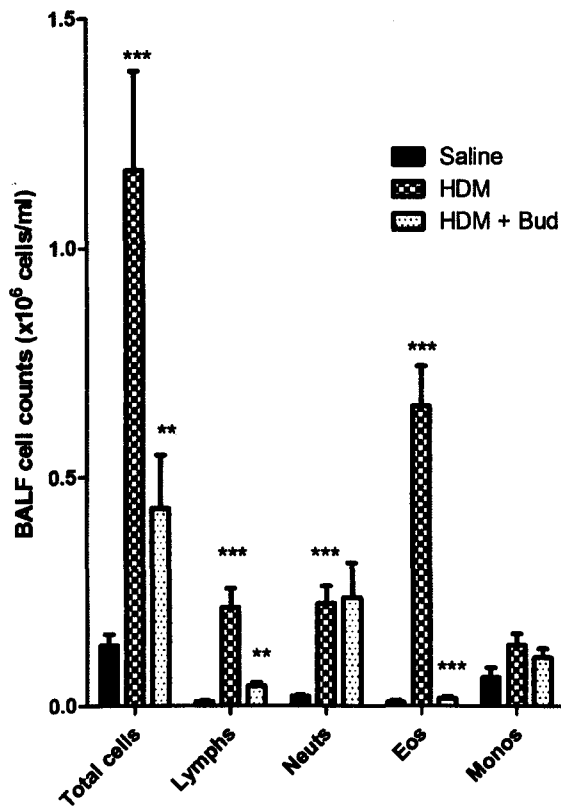


Figure 5.1 - Graph showing cell numbers in BALF from saline control, HDM exposed and HDM exposed budesonide treated mice after 7 weeks HDM exposure and 2 week budesonide treatment. HDM exposure results in statistically significant increases in total cell numbers, Eos, Neuts and Lymphs. Numbers of Monos do not change. Budesonide treatment results in a statistically significant decrease in numbers of total cells, Eos and Lymphs. Analysis is with one tailed Student's unpaired t-test, * is $p < 0.05$, ** is $p < 0.01$ and * is $p < 0.005$. Error bars are \pm sem ($n=6$ per group).**

5.3.1.2 CT Imaging results

Animals were imaged once per week during HDM exposure. Representative CT slices for a saline control and a HDM exposed animal in weeks, 1, 5 and 7 are shown in figure 5.2, together with a

representative image of a HDM exposed budesonide treated animal in week 7.

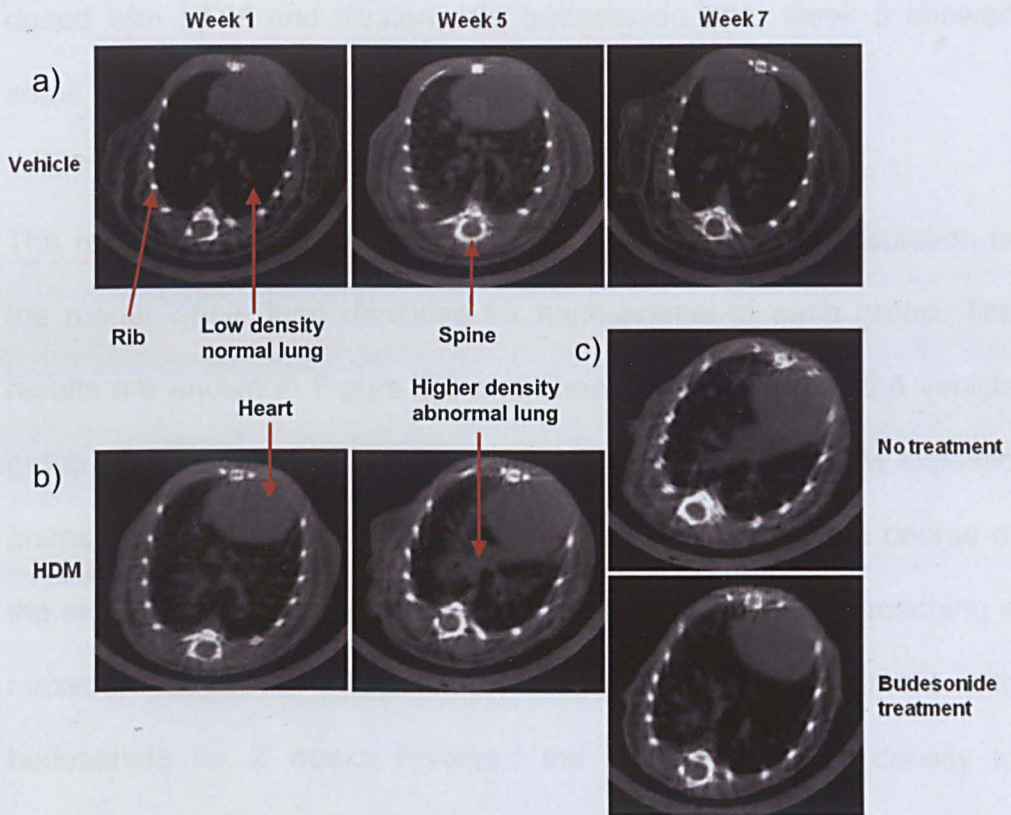


Figure 5.2 - Representative CT slices through mouse lungs exposed to a) saline or b) HDM over 7 weeks including c) an image comparing lungs of HDM exposed animals with or without budesonide treatment. Images show black as low density and white areas as higher density. Vehicle images showed no density changes over 7 weeks. HDM images showed a large area of increased density in week 5, which persists into week 7 if left untreated. Treatment with budesonide, results in a reduction in high density areas in week 7.

The images in figure 5.2 show no changes in density within the lungs in an animal dosed with vehicle for 7 weeks, this is indicative of no development of lung pathology in this animal. However, representative slices of an animal dosed with HDM for 7 weeks show significant changes in lung structure, with increased high density areas clearly

visible after 5 weeks that persisted into week 7. Inflammation was generally observed to be peri-bronchial in nature. In contrast, animals dosed with HDM and treated with budesonide after week 5 showed some reversal of the HDM-induced pathology.

The results observed in the images were quantified by calculation of the modal whole lung densities for each animal in each group. The results are shown in Figure 5.3 and show lung density for the vehicle group remaining constant over the 7 weeks. However, HDM exposed animals showed a marked increase in lung density over the course of the study, which became statistically significant at 2 weeks reaching a maximum at week 5 before reaching a plateau. Treatment with budesonide for 2 weeks reversed the increase in lung density to baseline levels with statistically significant differences in HDM exposed and HDM exposed budesonide treated groups in weeks 6 and 7 at $p > 0.01$ and $p > 0.005$ respectively.

The CT data indicate that the lung density changes which occurred following HDM exposure are peri-bronchial in nature and are likely to be oedema or cellular inflammation. This conclusion is supported by the results seen in the BAL cell counts, which confirmed significant cellular infiltration in the airways and eosinophilic inflammation. The reversal of both the increase in density seen in the CT scans and increase in cell counts observed in BALF by steroid treatment again

point to increased cellular infiltration, although this does not rule out the presence of oedema.

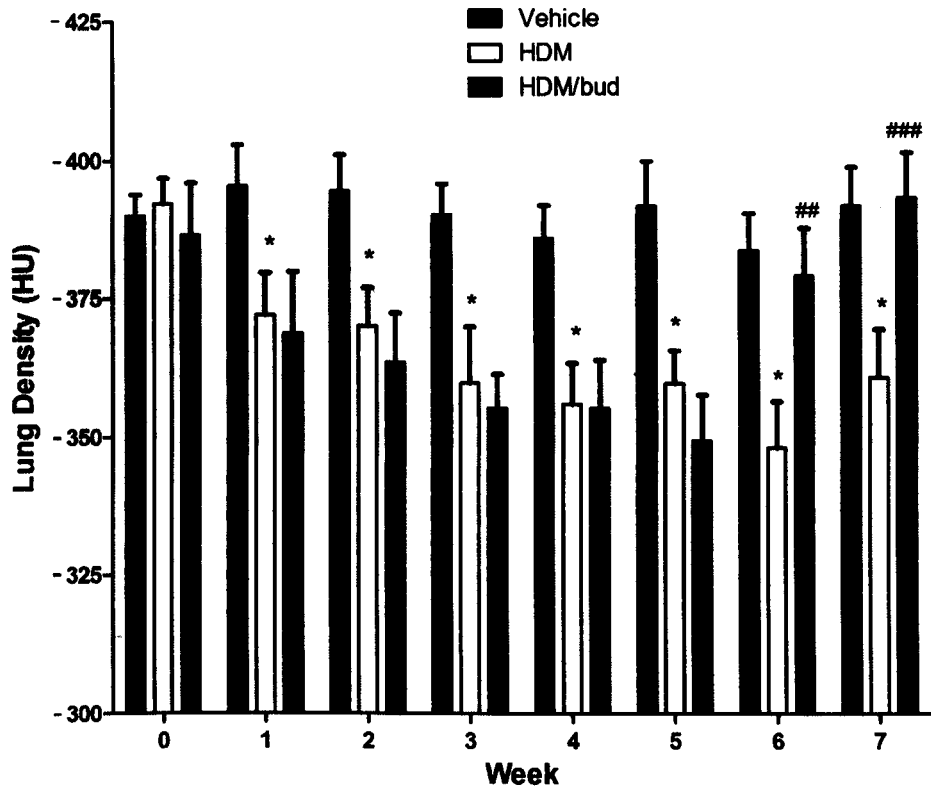


Figure 5.3 - Graph showing modal lung densities determined by CT imaging over 7 weeks for saline, HDM and HDM + budesonide exposed animals. HDM exposure results in increased lung density after 1 week, which persists over 7 weeks if no treatment is given. Treatment with budesonide reverts lung density to baseline levels . * statistically significant changes in density between HDM and vehicle groups $p < 0.05$, # statistically significant change in lung density between HDM and HDM + budesonide groups, at ## = $p < 0.01$ and ### = $p < 0.005$. Error bars are \pm sem (n=6 per group).

5.3.2 Histology

5.3.2.1 Disease progression and mFcRn expression

Representative images from the histological analysis of the saline control and HDM exposed lung can be seen in Figure 5.4. Images include areas of airway, vessel and alveoli.

Histological examination showed that HDM exposure leads to both alveolitis and pneumonitis in the alveolar bed. There was also a marked perivascular cuffing, particularly of the systemic vessels and marked epithelial reaction, with an epithelial metaplasia typical of a reparative reaction within the mucosa. Giant multi-nuclear macrophages were also observed throughout the alveolar bed in HDM exposed animals, particularly close to the pleura. Additionally, there is very significant eosinophilia in the HDM exposed lung. These results are in line with other reports of the histology observed in HDM model.

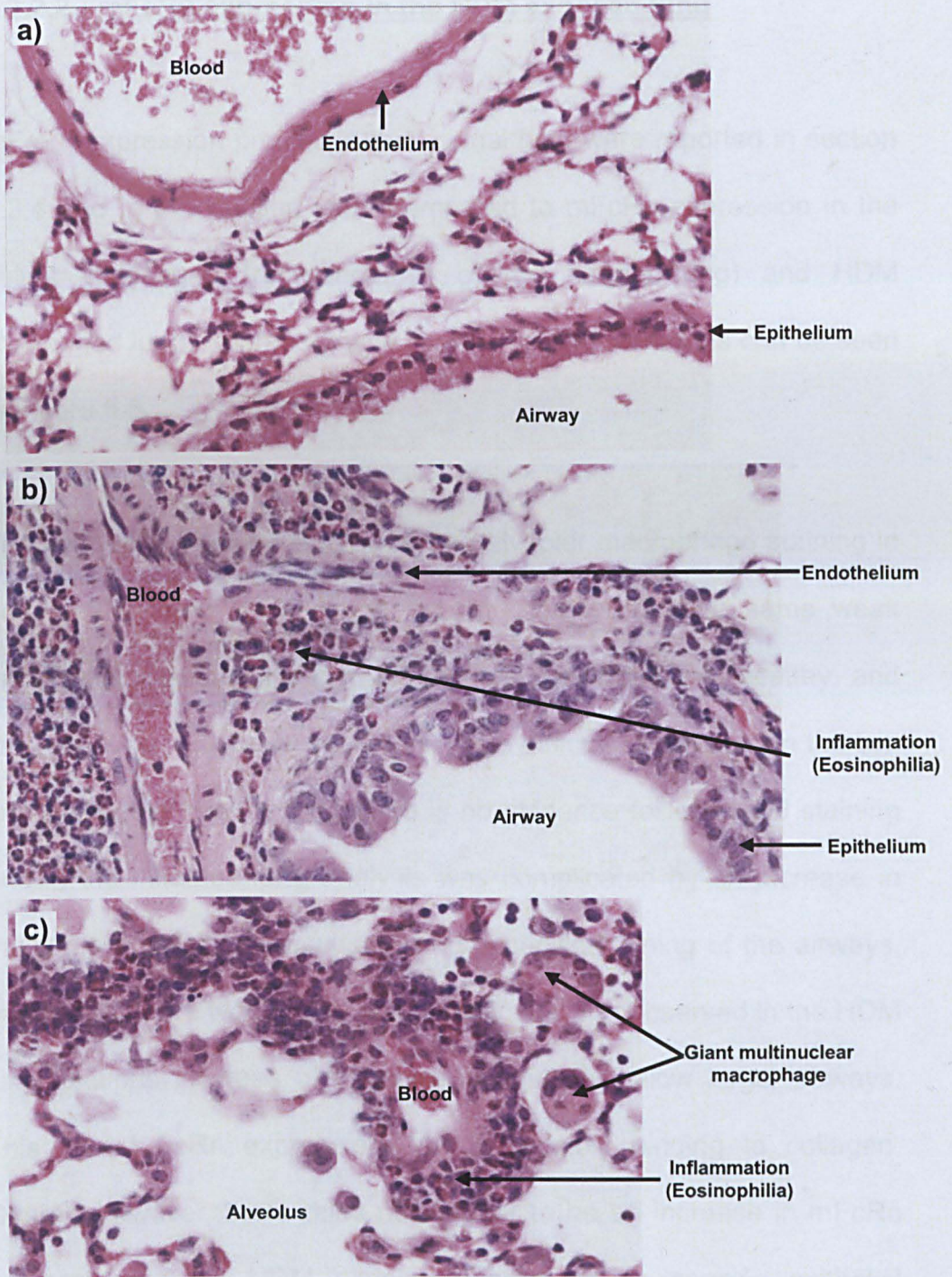


Figure 5.4 - Images showing extent of inflammation in histological samples of a) saline and b) and c) HDM exposed lungs at x20 magnification. Image a) shows healthy lung. Image b) shows massive inflammation localised around airways and vessels. Image c) shows giant multinuclear macrophages in HDM exposed alveoli and inflammation around small vessels.

5.3.2.2 mFcRn expression in the HDM exposed lung

mFcRn expression profiles in the normal lung were reported in section 4.3.4 and in this section were compared to mFcRn expression in the saline challenged (representative of the normal lung) and HDM challenged lung. Representative images from this analysis can be seen in Figure 5.5.

The images in Figure 5.5 show strong alveolar macrophage staining in both healthy and HDM exposed lung. Additionally, the same weak endothelial staining pattern is observed in both the healthy and inflamed lung. Epithelial staining is more difficult to compare in the two images. In the healthy lung there is no evidence for epithelial staining and in the inflamed lung analysis was complicated by an increase in mucus in the airways resulting in non-specific staining of the airways. In addition, there was strong non-specific staining observed in the HDM lung sections in areas of inflammation directly below larger airways. This is not FcRn expression and is possibly binding to collagen. Overall, however, there does not appear to be an increase in mFcRn expression in the HDM exposed lung, with no specific epithelial staining observed.

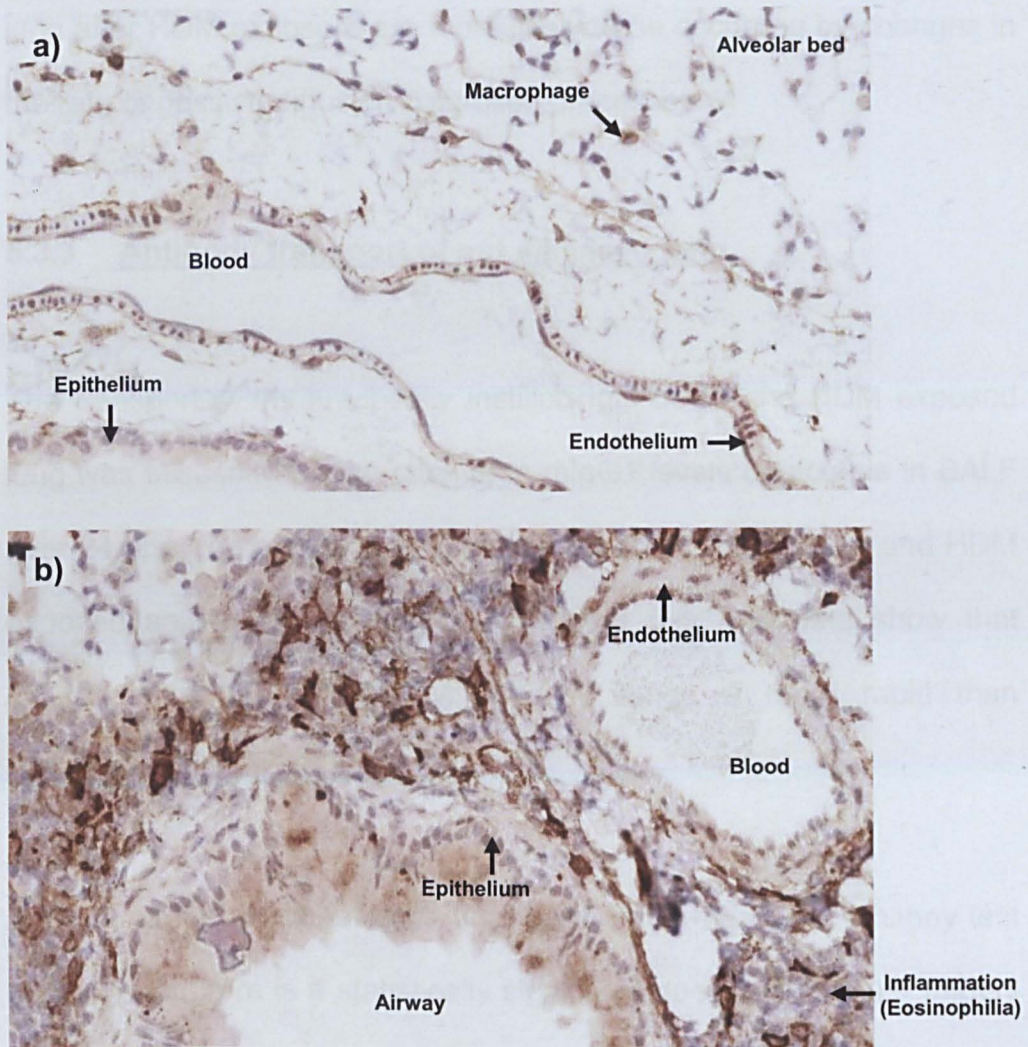


Figure 5.5 - Images showing extent of mFcRn expression in histological samples of a) saline and b) HDM exposed lungs at x20 magnification. Brown colour indicates mFcRn expression or non-specific binding and in healthy lung (a) is visible on macrophages and epithelium. In HDM exposed lung (b) there is significant non-specific binding to mucus in the airways and in inflamed areas directly beneath the airways.

As the level of mFcRn expression in the lung does not change with HDM exposure, transcytosis by mFcRn as a mechanism of antibody clearance from the lung is not expected to increase after HDM exposure. This indicates that any changes in antibody clearance in the

lung after HDM exposure are more likely to be occurring by changes in the rate of passive diffusion controlled processes.

5.3.3 Antibody transport of out diseased lung

The transport of intratracheally instilled IgG out of the HDM exposed lung was assessed by the change in mIgG1 levels detectable in BALF over 24 hrs. The results of BAL mIgG1 levels for both saline and HDM exposed animals are presented in Figure 5.6. The data show that clearance of IgG from HDM exposed lungs is more rapid than clearance from control lungs.

Analysis of the results at each time point using the Mann Whitney test showed that there is a statistically significant decrease in BALF mIgG1 levels after 2 hour, which lasts for 24 hrs. Results indicate that the damage induced by HDM to the mucosal surfaces of the lung leads to more rapid pulmonary clearance of macromolecules. This is the expected result and can be explained by an increase in epithelial permeability occurring due to an increase in passive diffusion controlled processes, probably paracellular diffusion between cells in the disrupted epithelium.

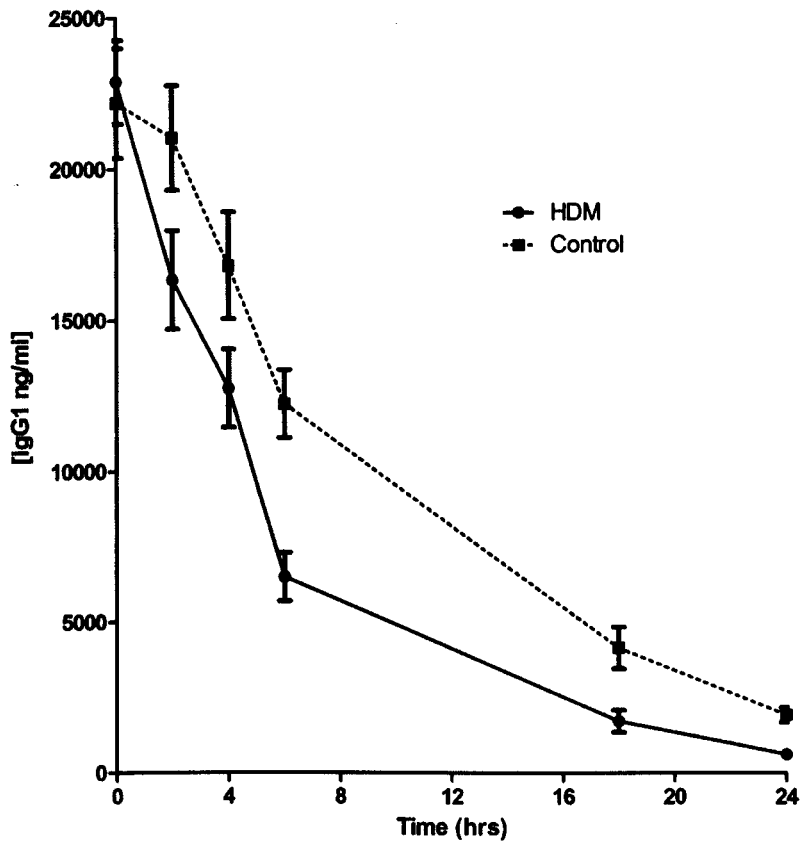


Figure 5.6 - Graph showing levels of antibody recoverable from the BALF over 24hrs post intratracheal instillation in either HDM or saline control animals. Error bars are \pm sem (n=6).

5.4 Conclusion

This penultimate chapter described the changes in X-ray anatomy and density of HDM exposed lungs using CT and related this to the pathology and cell infiltration in the HDM model. In addition the expression of mFcRn was found not to change following HDM exposure. Finally, the transport of antibody out of the HDM exposed lung was found to be more rapid than in the healthy lung, due to an increase in diffusion controlled transport out of the lung.

CHAPTER 6: Summary, Final Conclusions and Suggestions for Future Work

6. Summary and final conclusions

The work presented in this thesis has covered the set-up and validation of a SPECT/CT imaging based method to determine pulmonary antibody retention over 24 hrs. Pulmonary retention profiles were generated for a whole mIgG1, its Fab and scFv fragments, the FN3 protein and a pool of three point mutated IgG with differing binding affinities to the mFcRn receptor.

A SPECT/CT imaging method was successfully developed to investigate pulmonary antibody retention *in vivo*. The chemistry required to introduce the radiotracer to the antibody was proven to be simple and reproducible with no effect on antibody functionality. In addition, the radiolabelled antibody was proven to be stable *in vivo* over 24 hrs, which allowed for successful determination of the pulmonary retention profiles of intratracheally instilled proteins. In addition the SPECT/CT images showed no build up of activity in either the stomach or oesophagus, which strongly indicates that mucociliary clearance is not an important transport mechanism for intratracheally instilled antibody solutions in mice.

Comparison of the pulmonary retention rates for the whole IgG to those for the fragments and FN3 protein allowed determination of whether passive diffusion controlled processes were important in antibody clearance from the lung. This covers two separate diffusion controlled processes, paracellular transport and non-specific transcytosis. It was found that the pulmonary retention of whole antibody was significantly greater than for the smaller proteins. The retention profiles for the Fab and scFv fragments were very similar, but the FN3 protein was cleared more rapidly from the lung and also underwent significant levels of renal filtration. These results demonstrated a molecular weight dependence in pulmonary clearance, suggesting that diffusion controlled process were of greatest importance in determining the rate of antibody transport out of the lung.

Comparison of the pulmonary retention of the WT mIgG1 with three mutants with differing binding affinities to mFcRn was completed to determine whether active transcytosis by mFcRn was an important mechanism for IgG transport out of the lungs. The results showed that the WT IgG and all mutants had very similar pulmonary retention profiles over 24 hrs indicating that, at least over the first 24 hrs, the capacity of the active transcytosis pathway to remove IgG from the lung is not high. Therefore over the first 24 hrs after dosing it appears that passive diffusion controlled pathways are responsible for the clearance of the majority of an intratracheally instilled antibody from the mouse lung.

In order to further explain this result the expression pattern of the mFcRn receptor was investigated immunohistochemically in the lung. There was no direct evidence for mFcRn expression in the pulmonary epithelium, although the results were difficult to interpret.

The murine HDM model of asthma was used to investigate pulmonary antibody retention in the diseased lung. Additionally, the expression of the mFcRn receptor after exposure to HDM was investigated to determine whether active transcytosis would be expected to contribute to antibody clearance in the diseased lung. Finally, lung density changes on continuing exposure to HDM, were non invasively assessed by CT imaging.

It was found that lung density increases progressively with increasing exposure to HDM. The density increase is a useful biomarker for the airway remodelling and inflammatory changes occurring in the lung and may represent an informative non-invasive method to assess disease progression. This could result in the need to use fewer animals in future HDM model studies, as fewer terminal procedures such as histological analysis could be required.

In terms of antibody retention in the diseased lung, it was found that an intratracheally instilled antibody is less easily retained in the diseased lung than the normal lung. This was the expected result as it is known that mucosal barrier function is disrupted in the HDM model,

which was expected to lead to increased paracellular transport of antibody out of the lung. mFcRn expression appeared to be unchanged following HDM exposure, perhaps indicating that the increase in antibody transport out of the diseased lung was occurring through increased paracellular diffusion and not active transport by mFcRn.

The major conclusion that can be drawn from this work is that antibodies are transported slowly from the normal lung at a rate of roughly half the initially deposited dose over 24 hrs and that the mechanism for this transport is diffusion controlled, at least over the first 24 hrs in the mouse. Furthermore the rate of antibody clearance from the diseased murine lung is higher than that in the normal lung and this increase appears to be driven by an increase in the rate of diffusion controlled clearance mechanisms.

The results described above are indicative of retention of sufficient material to feasibly reach and maintain therapeutic levels of an inhaled antibody in the lung. The work also implies that for tailored delivery of biologics to the lung, pulmonary retention is increased in formats with high molecular weights. This impacts the possible formulation of biologics for inhalational delivery in that these results strongly suggest that the major factor influencing the pulmonary retention time for an inhaled protein is molecular weight. Therefore an antibody based therapy designed for inhalational treatment of asthma, cystic fibrosis or lung cancer may perform optimally as a full IgG rather than a fragment.

By comparing the results observed in this work to the literature, in particular regarding FcRn expression patterns in the lung, it is not clear how replicable these experiments would be in the human lung. More specifically, it appears that in the mouse, the active transcytosis pathway of IgG out of the lung by FcRn is not highly involved in antibody clearance; however there is convincing evidence for hFcRn expression in the human lung (Roopenian & Akilesh, 2007), so it is unclear whether this observation would hold true in human lungs.

6.1 Suggestions for future work

The work presented in this thesis provides a basis for the use of SPECT/CT imaging in understanding the pulmonary retention of antibodies *in vivo* over 24 hours. The inability to extend these studies beyond 24 hours, due to the radioactive decay of the technetium radiolabel, is one of the major limitations of this work. Analysis of the results has shown that it may be useful to extend the total time of the experiments beyond the 24 hr point, to obtain a better understanding of the terminal clearance mechanisms. This could be achieved by the use of a longer lived radiotracer than ^{99m}Tc , which has a 6 hour half life, for example ^{123}I with a half life of 13 hours or ^{131}I with an 8 day half life. In addition it would be possible to modify the protocol developed in this thesis to make use of PET/CT imaging and use longer lived PET traces such as ^{89}Zr or ^{68}Ga .

In more general terms there are a number of groups currently working on various aspects of the formulation of antibodies and other biologics for inhalational delivery. Work is ongoing to further elucidate factors influencing and mechanisms underpinning pulmonary drug dissolution, absorption transport and metabolism as well as to determine how to target specific lung regions and/or cell types. The continuation of this work is likely to result in the identification of a wider variety of biologics suitable for inhalational delivery and ultimately allow for the formulation of these molecules into effective inhaled medicines.

REFERENCES

Aaron, S. D. et al., 2013. TNF α antagonists for acute exacerbations of COPD: a randomised double-blind controlled trial, *Thorax*, 68(2), pp. 142-148

Abrahmason, D. R. & Rodewald, R., 1981. The mechanisms of intestinal uptake and transcellular transport of IgG in the neonatal rat. *J Cell Biol*, Volume 91, pp. 270-280.

Akilesh, S., Christianson, G. J., Roopenian, D. C. & Shaw, A. S., 2007. Neonatal FcR expression in bone marrow derived cells functions to protect serum IgG from catabolism. *J Immunol*, Volume 179, pp. 4580-4588.

Alberts, B. et al., 1994. *Molecular biology of the cell*. 3rd ed. New York: Garland Science.

Antosova, Z., Mackova, M., Kral, V. & Macek, T., 2009. Therapeutic application of peptides and proteins: parenteral forever?. *Trends in biotechnology*, 27(11), pp. 628-635.

Bailey, C. J. & Barnett, A. H., 2007. Why is exubera being withdrawn?. *British Medical Journal*, Volume 335, p. 1156.

Barnes, P. J., 2001. Th2 cytokines and asthma: an introduction. *Respiratory research*, Volume 2, pp. 64-65.

Bates, J. H. T., Rincin, M. & Irvin, C. G., 2009. Animal models of asthma. *Am J Physiol Lung Cell Mol Physiol*, Volume 297, pp. 401-410.

Bitonti, A. J. & Dumont, J. A., 2006. Pulmonary administration of therapeutic proteins using an immunoglobulin transport pathway. *Adv Drug Deliv Rev*, Volume 58, pp. 1106-1118.

Blanchard, C., Mishra, A. & Saito-Akei, H., 2005. Inhibition of human interleukin-13 induced respiratory and oesophageal inflammation by anti-human-interleukin-13 antibody (CAT354). *Clin Exp Allergy*, Volume 35, pp. 1096-1103.

Blauenstein, P. et al., 1995. Experience with the iodine-123 and technetium-99m labeled anti-granulocyte antibody Mab47: a comparison of labeling methods. *Eur J Nucl Med*, Volume 22, pp. 690-698.

Blyth, D. I. et al., 1996. Lung inflammation and epithelial changes in a murine model of atopic asthma. *Am J Respir Cell Mol Biol*, 14(5), pp. 425-438.

Borgstron, L., Olsoon, B. & Thorsson, L., 2006. Degree of throat deposition can explain the variability in lung deposition of inhaled drugs. *J Aerosol Med*, 19(4), pp. 473-483.

Borish, L. C. et al., 1999. Interleukin-4-receptor in moderate atopic asthma. A phase I/II randomized, placebo-controlled trial. *Am J Respir Crit Care Med*, 160(6), pp. 1816-1823.

Bousquet, J. J. et al., 2000. Asthma: From Bronchoconstriction to airway inflammation and remodeling. *Am J Respir Crit Care Med*, 161(5), pp. 1720-1745.

Boyce, J. A. & Austen, K. F., 2005. No audible wheezing: nuggets and conundrums from mouse asthma models. *J Exp Med*, 201(12), pp. 1869-1873.

Brambell, F. W. R., 1970. *The transmission of passive immunity from mother to young*. Amsterdam: North Holland Publishing Corp..

Brown, L. R., 2005. Commercial challenges of protein drug delivery. *Expert Opinions in Drug Delivery*, 2(1), pp. 29-42.

Busse, W. W. & Holgate, S. T., 2008. *Asthma and Rhinitis*. 2 ed. London: Blackwell Science.

Byron, P. R. & Patton, J. R., 1994. Drug delivery via the respiratory tract. *J Aerosol Med*, Volume 7, pp. 49-75.

Chames, P., Regenmortel, M. V., Weiss, E. & Baty, D., 2009. Therapeutic antibodies: successes, limitations and hopes for the future. *British Journal of Pharmacology*, Volume 157, pp. 220-233.

Chapman, R. W., 2008. Canine models of asthma and COPD. *Pulm Pharmacol Ther*, 21(5), pp. 731-742.

Charles-River, 2003. *The endosafe-PTS users guide*. version 7 ed. s.l.:Charles River.

Chatziioannou, A. F., 2005. Instrumentation for molecular imaging in preclinical research. *Proc Am Thorac soc*, 2(6), pp. 533-536.

Chen-Quay, S. C., Eiting, K. T., Li, A. W. & Quay, N. L., 2009. Identification of tight junction modulating lipids. *J Pharm Sci*, Volume 98, pp. 606-619.

Cho, J. Y. et al., 2004. Inhibition of airway remodeling in IL-5 deficient mice. *J Clin Invest*, 113(4), pp. 551-560.

Chrystal, R. D., West, J. B., Weiberland, E. R. & Barnes, P. J., 1997. *The lung: Scientific Foundations*. Philadelphia: Lippincott-Rowan.

Clarke, J., Cota, E., Fowler, S. B. & Hamill, S. J., 1999. Folding studies of immunoglobulin-like B-sandwich proteins suggest that they share a common folding pathway. *Structure*, 7(9), pp. 1145-1153.

Coffman, R. L. & Hessel, E. M., 2005. Nonhuman primate models of asthma. *J. Exp. Med*, 201(12), pp. 1875-1879.

Constantino, H. R. et al., 1998b. Effect of mannitol crystallisation on the stability and aerosol performance of a spray-dried pharmaceutical protein, recombinant humanized anti-IgE monoclonal antibody. *J Pharm Sci*, 87(11), pp. 1406-1411.

Constantino, H. R. et al., 1998. Effect of excipients on the stability and structure of lyophilized recombinant human growth hormone. *J Pharm Sci*, 87(11), pp. 1412-1420.

Crapo, J. D. et al., 1983. Morphometric characteristics of cells in the alveolar region of mammalian lungs. *Am Rev Respir Dis*, 128(2), pp. S42-46.

Cuand, Y. & Saltzmann, W. M., 2009. Stealth particles give mucus the slip. *Adv Drug Deliv Rev*, Volume 8, pp. 11-13.

Dall'Acqua, W. F. et al., 2002. Increasing the affinity of a human IgG1 for the neonatal Fc receptor: Biological consequences. *J Immunol*, Volume 169, pp. 5171-5180.

Datta-Mannan, A. et al., 2007. Monoclonal antibody clearance. *J Biol Chem*, 282(3), pp. 1709-1717.

Delbeke, D. & Isreal, O., 2009. *Hybrid PET/CT and SPECT/CT imaging*. New York: Springer.

Deng, R. et al., 2010. Pharmacokinetics of humanised monoclonal anti-tumour necrosis factor alpha antibody and its neonatal Fc receptor

variants in mice and cynomolgus monkeys. *Drug Metabolism and Disposition*, 38(4), pp. 600-605.

DePuey, E. G., Garcia, E. V. & Berman, D. S., 2000. *Cardiac SPECT imaging*. Philadelphia: Lippincott Williams and Wilkins.

Effros, R. M. & Mason, G. R., 1983. Measurements of pulmonary epithelial permeability in vivo. *Am Rev Respir Dis*, Volume 127, pp. S59-S66.

Ehrhardt, C., Laue, M. & Kim, K. J., 2008. Chapter 11: In vitro models of the alveolar epithelial barrier. In: K. J. Kim & C. Ehrhardt, eds. *Drug absorption studies: in situ, in vitro and in silico models*. New York: Springer, pp. 258-282.

Eisenstein, M., 2011. Something new under the skin. *Nature Biotechnology*, 29(2), pp. 107-109.

Fall, C. P., Maryland, E. S., Wagner, J. M. & Tyson, J. J., 2005. *Computational Cell Biology*. New York: Springer.

Fanta, C. H., 2009. Drug Therapy: Asthma. *NEJM*, Volume 360, pp. 1002-1014.

Fish, J. E. & Peters, S. P., 1999. Airway remodeling and persistent airways obstruction in asthma. *J Allergy Clin. Immunol*, Volume 104, pp. 509-516.

Foster, P. S. et al., 1996. Interleukin 5 deficiency abolishes eosinophilia, airways hyperreactivity and lung damage in a mouse asthma model. *J Exp Med*, 183(1), pp. 195-201.

Foster, W. M., Walters, D. M., Longphre, M., Macri, K. and Miller, L. M., 2001. *J. Applied Physiol.*, 90(3), pp. 1111-1118.

Franc, B. L., Acton, P. D., Mari, C. & Hasegawa, B. H., 2008. Small animal SPECT and SPECT/CT: Important tools for preclinical investigation. *J Nucl Med*, 49(10), pp. 1651-1663.

Franken, P. R. et al., 2010. Distribution and dynamics of ^{99m}Tc pertechnetate uptake in the thyroid and other organs assessed by single photon emission computed tomography in living mice. *Thyroid*, 20(5), pp. 519-526.

Fuchs, B. & Braun, A., 2008. Improved mouse models of allergy and allergic asthma - chances beyond ovalbumin. *Curr Drug Targets*, 9(6), pp. 495-502.

Furuse, M. et al., 1993. Occludin: a novel integral membrane protein localizing at tight junctions. *J cell Biol*, Volume 123, pp. 1777-1788.

GE-Healthcare, 2005. *Handbook: Ni Sepharose High performance*. s.l.:GE Healthcare.

Ghetie, V. et al., 1996. Abnormally short serum half lives of IgG in $\beta 2$ -microglobulin deficient mice. *Eur J Immunol*, Volume 26, pp. 690-696.

Ghishan, F. K., Merchant, J. L. & Said, H. M., 2006. *Physiology of the gastrointestinal tract*. 4, illustrated ed. London: Elsevier.

Gueders, M. M. et al., 2009. Mouse models of asthma: a comparison between C57BL/6 and BALB/c strains regarding bronchial responsiveness, inflammation and cytokine production. *Inflamm Res*, Volume 58, pp. 845-854.

Gumbleton, M., 2001. Caveolae as potential macromolecule trafficking compartments within the alveolar epithelium. *Adv Drug Deliv Rev*, Volume 49, pp. 281-300.

Gumbleton, M. et al., 2003. Targeting caveolae for vesicular drug transport. *J Cont Rel*, Volume 87, pp. 139-151.

Henderson, W. R. et al., 2002. A role for cysteinyl leukotrienes in airway remodeling in a mouse asthma model. *Am J Respir Crit Care Med*, 165(1), pp. 108-116.

Herbert, C. et al., 2008. Suppression of cytokine expression by roflumilast and dexamethasone in a model of chronic asthma. *Clin Exp Allergy*, 38(5), pp. 847-856.

Isaacs, K., Rosati, J. A. & Martonen, T. B., 2004. Mechanisms of particle deposition. In: *Aerosols Handbook: measurement, dosimetry and health effects*. Boca Raton: CRC Press, pp. 85-115.

Itoh, H., Nishino, M. & Hatabu, H., 2004. Architecture of the lung: morphology and function. *J Thorac Imaging*, Volume 19, pp. 221-227.

J D Andya, Y. F. M. et al., 1999. The effect of formulation excipients on protein stability and aerosol performance of spray-dried powders of a recombinant humanized anti-IgE monoclonal antibody. *Pharm Res*, 16(3), pp. 350-358.

Jobse, B. N. et al., 2009. Evaluation of allergic pulmonary inflammation by computed tomography in a rat model in vivo. *Eur Respir J*, Volume 33, pp. 1437-1447.

Johnson, J. R. et al., 2004. Continuous exposure to house dust mite elicits chronic airway inflammation and structural remodelling. *Am J Respir Crit Care Med*, Volume 169, pp. 378-385.

Jones, B. G., Dickinson, P. A., Gumbleton, M. & Kellaway, I. W., 2002. The inhibition of phagocytosis of respirable microspheres by alveolar and peritoneal macrophages. *Int J Pharm*, Volume 236, pp. 65-79.

Kabat, E. A. et al., 1991. Identifying amino acid residues that influence plasma clearance of murine IgG1 fragments by site directed mutagenesis. *Eur J Immunol*, Volume 24, p. 542.

Kastner, M., 2000. *Protein Liquid Chromatography*. Vol 61 ed. Amsterdam: Elsevier.

Khanvilkar, K., Donovan, M. D. & Flanagan, D. R., 2001. Drug transfer through mucus. *Adv Drug Deliv Rev*, Volume 48, pp. 173-193.

Kim, H. et al., 2008. Mapping of the neonatal Fc receptor in the rodent eye. *Invest J Ophthalmol Vis Sci*, Volume 49, pp. 2025-2029.

Kim, S. J. et al., 2009. Effects of tranilast and pentoxifylline in a mouse model of chronic asthma using house dust mite antigen. *J Asthma*, 46(9), pp. 884-894.

Kips, J. C. et al., 2003. Effect of SCH55700, a humanised anti-human interleukin-5 antibody, in severe persistent asthma: a pilot study. *Am J Respir Crit Care Med*, 167(12), pp. 1655-1659.

Knoll, G. F., 2010. *Radiation detection and measurement*. 4th ed. Hoboken, NJ, USA: John Wiley and Sons.

Kobayashi, S., Kondo, S. & Juni, K., 1995. Permeability of peptides and proteins in human cultures alveolar A549 monolayers. *Pharm Res*, Volume 12, pp. 1115-1119.

Kumar, R. K., Herbert, C. & Foster, P. S., 2008. The classical ovalbumin challenge model of asthma in mice. *Curr Drug Targets*, 9(6), pp. 485-494.

Kumar, R. K., Herbert, C. & Kasper, M., 2004. Reversibility of airway inflammation and remodeling following cessation of antigenic challenge in a model of chronic asthma. *Clin Exp Allergy*, 34(11), pp. 1796-1802.

- Kuo, T. T. & Avensen, V. G., 2011. Neonatal Fc receptor and IgG based therapeutics. *mAbs*, 3(5), pp. 422-430.
- Kutscher, H. L. et al., 2010. Enhanced passive pulmonary targeting and retention of PEGylated rigid microparticles in rats. *Int J Pharm*, 402(1), pp. 64-71.
- L Heslet, C. B. & Nepper-Christensen, S., 2012. Inhaled granulocyte macrophage colony stimulating factor for cystic fibrosis. *J Inflamm Res*, 5(1), pp. 19-27.
- Leach, J. L. et al., 1996. Isolation from human placenta of the IgG transporter FcRn and localization to the syncytiotrophoblast: implications for maternal-fetal antibody transport. *J Immunol*, Volume 157, pp. 3317-3322.
- Lenaerts, V. & Gurny, R., 1990. *Bioadhesive drug delivery systems*. Boca Ralton, USA: CRC Press.
- Linden, A. et al., 2003. Bronchodilation by an inhaled VPAC2 receptor agonist in patients with stable asthma. *Thorax*, Volume 58, pp. 217-221.
- Lloyd, C. M., 2007. Building better mouse models of asthma. *Curr Allergy Asthma Rep.*, 7(3), pp. 231-236.
- Madara, J. L., 1998. Regulation of the movement of solutes across tight junctions. *Annu Rev Physiol*, Volume 60, pp. 143-159.
- Maillet, A. et al., 2008. Aerodynamic, Immunological and pharmacological properties of the anticancer antibody cetuximab following nebulisation. *Pharm Res.*, 25(6), pp. 1318-1326.

Maillet, A. et al., 2011. The airways, a novel route for delivering monoclonal antibodies to treat lung tumours. *Pharm Res*, Volume 28, pp. 2147-2156.

Mariani, G. et al., 2010. A review on the clinical used of SPECT/CT. *Eur J Nucl Med Mol Imaging*, 37(10), pp. 1959-1985.

Martin, J. G. & Tamaoka, M., 2006. Rat models of asthma and chronic obstructive lung disease. *Pulm Pharmacol Ther*, 19(6), pp. 377-385.

Martin, M. G., West, A. P. J., Gan, L. & Bjorkman, P. J., 2001. Crystal structure at 2.8Å of an FcRn/heterodimeric Fc complex: mechanism of pH dependent binding. *Mol Cell*, Volume 7, pp. 867-877.

Martin-Padura, I. et al., 1998. Junctional adhesion molecule, a novel member of the immunoglobulin superfamily that distributes at intracellular tight junctions and modulates monocyte transmigration. *J Cell Biol*, Volume 142, pp. 117-127.

Mather, S. J. & Ellison, D., 1990. Reduction-mediated technetium-99m labeling of monoclonal antibodies. *J Nucl Med*, 31(5), pp. 692-697.

Mayorand, S. & Pagano, R. E., 2005. Pathways of clathrin independent endocytosis. *J Cell Biol*, Volume 161, pp. 673-677.

McMillan, S. J. & Lloyd, C. M., 2004. Prolonged allergen challenge in mice leads to persistent airway remodelling. *Clin Exp Allergy*, 34(3), pp. 497-507.

Moeller, E. H. & Jorgensen, L., 2008. Alternative routes of administration for systemic delivery of protein pharmaceuticals. *Drug Discov Today*, Volume 5, pp. 89-94.

Morjaria, J. B. et al., 2012. Biologic and pharmacologic therapies in clinical development for the inflammatory response in COPD. *Drug Discov Today*, 15(9), pp. 396-405.

Nials, A. T. & Uddin, S., 2008. Mouse models of allergic asthma: acute and chronic allergen challenge. *Dis Model Mech*, 1(4-5), pp. 213-220.

Ober, R. J., Radu, C. G., Ghetie, V. & Ward, E. S., 2001. Differences in promiscuity for antibody-FcRn interactions across species: implications for therapeutic antibodies. *Int Immunol*, 13(12), pp. 1551-1559.

Owens, D. R., Zinman, B. & Bolli, G., 2003. Alternative routes of insulin delivery. *Diabet Med.*, Volume 20, pp. 886-898.

Palaia, G., Vatrella, A., Maselli, R., 2012. The potential of biologics for the treatment of asthma. *Nat Rev Drug Discov*, 11(12), pp. 958-972.

Patil, J. S. & Sarasija, S., 2012. Pulmonary drug delivery strategies: A concise, systematic review. *Lung India*, 29(1), pp. 44-49.

Patton, J. S., 1996. Mechanisms of macromolecule absorption by the lungs. *Adv. Drug Del. Rev.*, Volume 19, pp. 3-36.

Patton, J. S., 1996. Mechanisms of macromolecule absorption from the lung. *Adv Drug Deliv Rev*, Volume 19, pp. 3-36.

Patton, J. S. et al., 2010. The particle has landed- characterising the fate of inhaled pharmaceuticals. *J Aerosol Med Pulm Drug Deliv*, Volume 2, pp. S71-87.

Patton, J. S. & Byron, P. R., 2007. Inhaling medicines: delivering drugs to the body though the lungs. *Nat Rev: Drug Discov*, Volume 6, pp. 67-74.

Plant, J. A., Voulvoulis, N. & Vala-Ragnarsdotir, K., 2012. *Pollutants, human health and the environment: A risk based approach*. Oxford: John Wiley and Sons.

Praetor, A., Ellinger, I. & Hunziker, W., 1999. Intracellular traffic of the MHC I like IgG Fc receptor, FcRn, expressed in epithelial MDCK cells. *J Cell Sci*, Volume 112, pp. 2291-2299.

Proud, D., 2008. *The Pulmonary Epithelium in Health and Disease*. Oxford: John Wiley & Sons.

Pucadyil, T. J. & Schmid, S. L., 2009. Conserved function of membrane active GTPase in coated vesicle formation. *Science*, Volume 325, p. 1217.

Qiagen, 2006. *Qiaprep Miniprep Handbook*. 2nd ed. Qiagen.com: Qiagen.

Rafii, R., Juarez, M. M., Albertson, T. E., Chen, A. L., 2013, A review of current and novel therapies for idiopathic pulmonary fibrosis, *J Thorac Dis.*, 5(1), pp. 48-73.

Raghavan, M., Bonagura, V. R., Morrison, S. L. & Bjorkman, P. J., 1995. Analysis of the pH dependence of the neonatal Fc receptor/immunoglobulin G interaction using antibody and receptor variants. *Biochemistry*, Volume 34, pp. 146-149.

Reichert, J. M., 2012. Marketed therapeutic antibodies compendium. *mAbs*, 4(3), pp. 413-415.

Reichert, J. M., Rosensweig, C. J., Faden, L. B. & Dewitz, M. C., 2005. Monoclonal antibody successes in the clinic. *Nature Biotechnology*, Volume 23, pp. 1073-1078.

Ricciardolo, F. L., Nijkamp, F., Rose, V. D. & Folkerts, G., 2008. The guinea pig as an animal model for asthma. *Curr Drug Targets*, 9(6), pp. 452-465.

Riesenfeld, E. P. et al., 2010. Inhaled salmeterol and/or fluticasone alters structure/function in a mouse model of allergic airways disease. *Resp Res*, 11(22), pp. 1-11.

Roopenian, D. C. & Akilesh, S., 2007. FcRn: The neonatal Fc receptor comes of age. *Nat Rev Immun*, Volume 7, pp. 715-725.

Roopenian, D. C. et al., 2003. The MHC Class I-like receptor controls perinatal IgG transport, IgG homeostasis and fate of IgG-Fc-coupled drugs. *J Immunol*, 170(7), pp. 3528-3533.

Royand, C. L. & Wrana, J. L., 2007. Clathrin and non-clathrin mediated endocytotic regulation of cell signalling. *Nat Rev Mol Cell Biol*, Volume 8, pp. 603-612.

Rubas, W. et al., 1996. Flux measurements across caco-2 monolayers may predict transport in human large intestinal tissue. *J. Pharm Sci*, Volume 85, pp. 165-169.

Rydell-Tormanen, K. et al., 2008. Induction of vascular remodelling in the lung by chronic house dust mite exposure. *Am J Respir Crit Care Med*, 39(1), pp. 61-67.

Saglani, S. et al., 2009. Pathophysiological features of asthma develop in parallel in house dust mite exposed neonatal mice. *Am J Respir Crit Care Med*, 41(3), pp. 281-289.

Sahay, G., Alakhova, D. Y. & Kabanov, A. V., 2010a. Endocytosis of nanomedicines. *J Cont Rel*, Volume 145, p. 182.

Sahay, G., Kim, J. O., Kabanov, A. V. & Bronich, T. K., 2010b. The exploitation of differential endocytotic pathways in normal and tumour cells in the selective targeting of nanoparticle chemotherapeutic agents. *Biomaterials*, Volume 31, p. 923.

Sakagami, M. et al., 2006. Expression and transport functionality of FcRn within rat alveolar epithelium: A study in primary cell culture and in the isolated perfused lung. *Pharm Res*, 23(2), pp. 270-279.

Saltzmann, W. M., Radomsky, M. L., Whaley, K. J. & Cone, R. J., 1994. Antibody diffusion in human cervical mucus. *Biophys J*, Volume 66, pp. 508-515.

Schepens, B. et al., 2011. Nanobodies specific for respiratory Syncytial virus fusion protein protect against infection by inhibition of fusion. *J Infect Dis.*, 204(11), pp. 1692-1701.

Shinagawa, K. & Kojima, M., 2003. Mouse model of airway remodelling: strain differences. *Am J Respir Crit Care Med*, Volume 168, pp. 959-967.

Smith, J. B. & Herschman, H. R., 2004. Targeted identification of glucocorticoid-attenuated response genes: in vitro and in vivo models. *Proc Am Thorac Soc*, 1(3), pp. 275-281.

Smyth, H. D. C. & Hickey, A. J., 2011. *Controlled Pulmonary Delivery: Advances in Delivery Science and Technology*. s.l.:Springer.

Spiekermann, G. M. et al., 2002. Receptor mediated immunoglobulin G transport across mucosal barriers in adult life: Functional expression of FcRn in the mammalian lung. *J Exp Med*, Volume 196, pp. 303-310.

Takeda, K. et al., 2001. Strain dependence of airway hyperresponsiveness reflects differences in eosinophil localisation in the lung. *Am J Physiol Cell Mol Physiol*, Volume 281, pp. 394-402.

Thornton, D. J. & Sheehan, J. K., 2004. From mucins to mucus; toward a more coherent understanding of this essential barrier. *Proc Am Thorac Soc*, Volume 1, pp. 54-61.

Tsukita, S. & Itoh, M. F. a. H., 2001. Multifunctional strands in tight junctions. *Nat Rev Mol Cell Biol*, Volume 2, pp. 285-293.

Tzaban, S. et al., 2009. The recycling and transcytotic pathways for IgG transport by FcRn are distinct and display an inherent polarity. *J Cell Biol*, 185(4), pp. 673-684.

Vaughn, D. E. & Bjorkman, P. J., 1998. Structural basis of pH-dependent antibody binding by the neonatal Fc receptor. *Structure*, 6(1), pp. 63-73.

Wangensteen, O. D. et al., 1993. Tracheal epithelial permeability to non electrolytes; species differences. *J Appl Physiol*, Volume 75, pp. 1009-1018.

Ward, E. S. & Ober, R. J., 2009. Multitasking by exploitation of intracellular transport functions: The many faces of FcRn. In: *Advances in Immunology*. s.l.:Elsevier Inc, pp. 77-115.

Weers, G. J. et al., 2010. Pulmonary formulations: What remains to be done?. *J Aerosol Med Pulm Drug Deliv*, Volume 23, pp. S39-57.

Wegmann, M., 2008. Animal models of chronic experimental asthma - strategies for the identification of new therapeutic targets. *J Occup Med Toxicol*, Volume 3 Suppl, p. S4.

Weibeland, E. R. & Gomez, D. M., 1962. Architecture of the human lung. Use of quantitative methods establishes fundamental relations between size and number of lung structures. *Science*, Volume 137, pp. 577-585.

Yadav, U. C. S. et al., 2009. Inhibition of aldose reductase prevents experimental allergic airway inflammation in mice. *PLoS one*, 4(8), p. e6535.

Zhu, X. et al., 2001. MHC class I-related neonatal Fc receptor for IgG is functionally expressed in monocytes, intestinal macrophages and dendritic cells. *J Immunol*, Volume 166, pp. 3266-3276.

Zosky, G. R. & Sly, P. D., 2007. Animal models of asthma. *Clinical and experimental allergy*, Volume 37, pp. 973-988.